PROCEEDINGS

ORAL PRESENTATIONS

TOPIC 3:
EXTREME VALUE STATISTICS

PAPERS:
COLLECTED AND ARRANGED BY JUDITH DOBMANN AND SIMONE HUNZIKER.
PLEASE NOTE THAT AUTHORS ARE RESPONSIBLE FOR CONSISTENCY IN SPELLING.

BAYESIAN ESTIMATION OF EXTREME RIVER DISCHARGES

Chbab[1] E.H., van Noortwijk[2] J.M., Kalk[2] H.J.

[1] Ministry of Transport, Public Works and Water Management, Institute for Inland Water Management and Waste Water Treatment, RIZA. P.O. Box 17, 8200 AA Lelystad, The Netherlands, h.chbab@riza.rws.minvenw.nl

[2] HKV Consultants, P.O. Box 2120, 8203 AC Lelystad, The Netherlands
j.m.van.noortwijk@hkv.nl, h.j.kalk@hkv.nl

SUMMARY

Understanding and quantifying the behaviour of river floods at extreme discharges has important applications in design of civil structures such as river dikes. For design purposes, one is often interested in return periods that are substantially larger than the observation period. These estimates are often obtained using classical statistical methods. In this paper, a method based on Bayesian statistics is presented. This approach enables us to use all available sources of information, and to take statistical uncertainties into account as well.
Seven predictive probability distributions are considered for determining extreme quantiles of loads: the exponential, Rayleigh, normal, lognormal, gamma, Weibull and Gumbel. The presented method has been successfully applied to estimate extreme quantiles of discharges and their return periods. Prior information based on historical floods is represented in terms of censored data and is then used to determine informative prior distributions of the statistical parameters. This prior information can be updated with actual data to determine the posterior information, and provides a rational basis for extrapolation. As an example, a Bayesian analysis of annual maximum discharges of the river Rhine at Lobith is performed to assess extreme quantiles such as the design discharge.

Keywords: Bayesian analysis, informative prior distribution, non-informative prior distribution, posterior distribution, flood data.

1 INTRODUCTION

Understanding and quantifying the behaviour of river floods at extreme discharges has important applications in design of civil structures such as river dikes. For design purposes, one is often interested in extreme events with larger return periods than the observation period. Extreme discharges with very large return periods can be estimated by fitting various probability distributions to the available observations. See for example DH and EAC-RAND (1993) and Castillo (1988). Probability plots and goodness-of-fit tests, such as chi-square and Kolmogorov-Smirnov are commonly used to select an appropriate distribution.
A major practical difficulty in fitting probability distributions is that there is often a limited amount of observations for determining extreme quantiles and particularly extreme discharges. The associated return period is large compared with the length of the observation period. In the Netherlands, observed flood discharges are available for a period of 98 years only. Consequently, there is a large statistical uncertainty involved in estimating discharges with large return periods when using these observations. The maximum likelihood method has been recognized as one of the best parameter estimation methods (Castillo, 1988; Galambos et al., 1994); but it is especially suitable when there is a large number of observations. Furthermore, the method has the disadvantage that statistical uncertainties cannot be taken into consideration.
One consequence of sparse data is that different probability distributions seem to fit the observations and therefore only a few can be rejected. The different distributions involved usually lead to different extrapolated values and the goodness-of-fit tests for selecting an appropriate distribution are often inconclusive. The tests are more appropriate for the central part of the distribution than for the tail.
Recently, van Gelder (1999) presented an alternative based on a Bayesian approach for estimating extreme quantiles while statistical uncertainties are taken into account. Statistical uncertainty mainly occurs due to a lack of observations. This uncertainty can be subdivided into parameter uncertainty and distribution-type uncertainty. Bayesian estimates and so-called Bayes weights can then be used to account for parameter uncertainty and distribution-type uncertainty, respectively. Using Bayes weights, it is possible to discriminate between different probability distributions and to quantify how well a distribution fits the

observations. The Bayesian approach was successfully applied by van Noortwijk et al. (2001), Chbab et al. (2000) and van Gelder et al. (1999) for estimating extreme river discharges. Different distributions were investigated and therefore weights were determined corresponding to how well they fitted the observed data. In determining Bayes weights, so-called non-informative Jeffreys priors were used. The main disadvantage of non-informative priors is that they are often improper. Although this disadvantage can be overcome, the Bayesian approach is especially useful for combining different sources of information and for using informative priors.
This paper again addresses the Bayesian approach for estimating extreme river discharges. It differs from the results in van Noortwijk et al. (2001) and Chbab et al. (2000) in the sense that informative priors based on historical censored observations are used instead of non-informative priors. In Section 2 we briefly define statistical uncertainties. Bayes estimates of parameters and quantiles associated with large return periods are examined in Section 3. Non-informative Jeffreys priors, as well as informative priors based on historical censored observations are presented in Section 4. Bayes factors and Bayes weights will be treated in Section 5. In Section 6 we examine the river Rhine as a case study, and we end with conclusions in Section 7.

2 STATISTICAL UNCERTAINTIES

According to (amongst others) Slijkhuis et al. (1999) and Siu and Kelly (1998), uncertainties in risk analysis can primarily divided into two categories: inherent uncertainty and epistemic uncertainties; see Figure 2-1. Inherent uncertainties represent randomness or variability in nature. For example, even in the event of sufficient data, one cannot predict the maximum discharge that will occur next year. The two main types of inherent uncertainty are inherent uncertainty in time and inherent uncertainty in space. It is not possible to eliminate inherent uncertainty completely. Epistemic uncertainties represent the lack of knowledge about a (physical) system. The two main types of epistemic uncertainty are statistical uncertainty (due to lack of sufficient data) and model uncertainty (due to lack of understanding the physics). Statistical uncertainty can be parameter uncertainty (when the parameters of the distribution are unknown) and distribution-type uncertainty (when the type of distribution is unknown). In principle, epistemic uncertainties can be reduced as knowledge increases and more data becomes available.

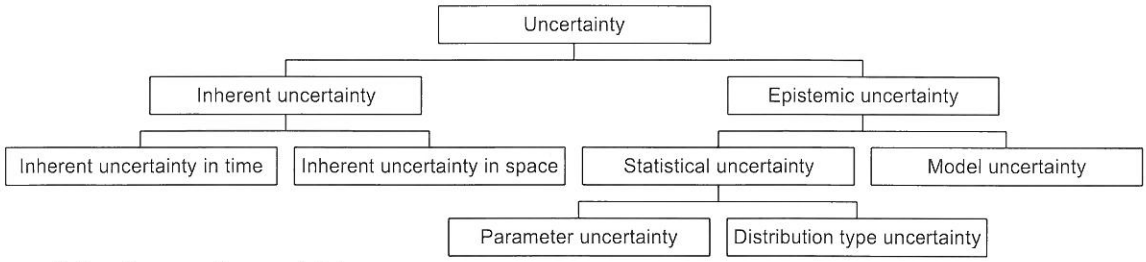

Figure 2-1: Types of uncertainty.

3 BAYESIAN ESTIMATION

The only statistical theory that combines modelling inherent uncertainty and statistical uncertainty is Bayesian statistics. The theorem of Bayes (1763) provides a solution to how to learn from data. In the framework of estimating the parameters $\boldsymbol{\theta} = (\theta_1,...,\theta_d)$ of a given probability distribution, Bayes' theorem can be written as:

$$\pi(\boldsymbol{\theta} \mid \boldsymbol{x}) = \frac{l(\boldsymbol{x} \mid \boldsymbol{\theta})\pi(\boldsymbol{\theta})}{\int_{\theta} l(\boldsymbol{x} \mid \boldsymbol{\theta})\pi(\boldsymbol{\theta})d\boldsymbol{\theta}} = \frac{l(\boldsymbol{x} \mid \boldsymbol{\theta})\pi(\boldsymbol{\theta})}{\pi(\boldsymbol{x})} \tag{1}$$

with

$l(\boldsymbol{x} \mid \boldsymbol{\theta})$ = the likelihood function of the observations $\boldsymbol{x} = (x_1,....,x_n)$ when the parametric vector $\boldsymbol{\theta} = (\theta_1,...,\theta_d)$ is given,
$\pi(\boldsymbol{\theta})$ = the prior density of $\boldsymbol{\theta} = (\theta_1,...,\theta_d)$ before observing data $\boldsymbol{x} = (x_1,....,x_n)$,
$\pi(\boldsymbol{\theta} \mid \boldsymbol{x})$ = the posterior density of $\boldsymbol{\theta} = (\theta_1,...,\theta_d)$ after observing data $\boldsymbol{x} = (x_1,....,x_n)$,
$\pi(\boldsymbol{x})$ = the marginal density of the observations $\boldsymbol{x} = (x_1,....,x_n)$.

The likelihood function $l(\boldsymbol{x} \mid \boldsymbol{\theta})$ represents the inherent uncertainty of a random variable X when $\boldsymbol{\theta}$ is given, whereas the prior density $\pi(\boldsymbol{\theta})$ and the posterior density $\pi(\boldsymbol{\theta} \mid \boldsymbol{x})$ represent the statistical uncertainty in $\boldsymbol{\theta}$. This statistical uncertainty in $\boldsymbol{\theta}$ is parameter uncertainty. Using Bayes' theorem, we can update the prior distribution to the posterior distribution as soon as new observations become available. When more observations become available, the parameter uncertainty gets smaller. If a random variable X has a probability density function $l(\boldsymbol{x} \mid \boldsymbol{\theta})$ dependent on the parametric vector $\boldsymbol{\theta}$, then the likelihood function $l(x_1,...,x_n \mid \boldsymbol{\theta})$ of the independent observations $\boldsymbol{x} = (x_1,....,x_n)$ is given by:

$$l(\boldsymbol{x} \mid \boldsymbol{\theta}) = l(x_1,...,x_n \mid \boldsymbol{\theta}) = \prod_{i=1}^{n} l(x_i \mid \boldsymbol{\theta}) \tag{2}$$

The marginal density $\pi(\boldsymbol{x})$ is obtained by integrating the likelihood $l(\boldsymbol{x} \mid \boldsymbol{\theta})$ over $\boldsymbol{\theta}$. Note that the maximum-likelihood estimate of the parameter vector $\boldsymbol{\theta}$ is defined as the estimate $\hat{\boldsymbol{\theta}}$, which maximizes the likelihood function $l(\boldsymbol{x} \mid \boldsymbol{\theta})$ as a function of $\boldsymbol{\theta}$.
The cumulative distribution function and the survival function of the random variable X are denoted by $F(x \mid \boldsymbol{\theta})$ and $F(x \mid \boldsymbol{\theta}) = 1 - F(x \mid \boldsymbol{\theta})$, respectively. The posterior predictive probability of exceeding a certain x_0 is given by:

$$Pr\{X > x_0 \mid \boldsymbol{x}\} = \int_{\boldsymbol{\theta}} Pr\{X > x_0 \mid \boldsymbol{\theta}\} \pi(\boldsymbol{\theta} \mid \boldsymbol{x})\, d\boldsymbol{\theta} = \int_{\boldsymbol{\theta}} \bar{F}(x_0 \mid \boldsymbol{\theta}) \pi(\boldsymbol{\theta} \mid \boldsymbol{x})\, d\boldsymbol{\theta} \tag{3}$$

Besides representing parameter uncertainty on the basis of Bayesian statistics, distribution-type uncertainty can also be taken into account using so-called Bayes factors or Bayes weights. This will be treated in Section 5.

4 PRIOR CHOICE

To obtain Bayes estimates, a prior distribution of the parameters of the assumed likelihood function and some observations (sample information) are required. The prior distribution and the sample information contained in the likelihood function are then combined using Bayes' theorem to determine the posterior distribution of the parameters. The key question is how to choose the prior distribution.

4.1 Non-informative priors

The Bayesian approach is especially useful for combining prior subjective information with actual observations. Prior information can be represented in terms of a prior distribution, which can be either non-informative or informative. There might be situations in which we would like the observations to 'speak for themselves', especially in comparison to the prior information. This means that the prior distribution should describe a certain 'lack of knowledge' or, in other words, should be as 'vague' as possible. For this purpose, so-called non-informative priors have been developed. An advantage of using non-informative priors is that it provides us with a methodology to perform statistical inference in situations where 'little is known a priori'.
According to (amongst others) Box and Tiao (1973), Kass and Wasserman (1996) and van Noortwijk et al., (2002), the best and most widely used method for determining non-informative priors is that of Jeffreys (1961). This method chooses the non-informative prior to be proportional to the square root of the expected Fisher information measure. In mathematical terms, the non-informative Jeffreys prior is given by:

$$J(\theta) \propto [I(\theta)]^{1/2} \tag{4}$$

where $I(\theta)$ is the expected Fisher information for a single observation of the probability distribution involved; that is:

(5) $$I(\theta) = -E_{X|\theta}\left(\frac{\partial^2}{\partial\theta^2} log\ l(x|\theta)\right)$$

The non-informative Jeffreys priors can be easily extended to the multivariate case. The Jeffreys prior is then taken proportional to the square root of the determinant of the expected Fisher information matrix for a single observation (Box and Tiao, 1973; van Noortwijk et al., 2002). An excellent overview on the selection of non-informative priors is presented by Kass et al. (1996). The main advantage of the Jeffreys prior is that it is always both invariant under transformations and dimensionless.
A disadvantage of most non-informative priors is that they can be improper; that is, they often do not integrate to one. This disadvantage can be resolved by focussing on the posterior distributions rather than on the prior distributions. As a matter of fact, formally carrying out the calculations of Bayes' theorem by combining an improper prior with observations often results in a proper posterior.

4.2 Informative priors

The Jeffreys priors considered in the previous section are useful in situations in which we would like the observations to 'speak for themselves'. This means that a non-informative prior distribution should describe a certain 'lack of knowledge'. On the other hand, an informative prior distribution is one that reflects 'subjective' knowledge concerning the unknown statistical parameters.
For estimating extreme flood quantiles, a useful informative prior is a distribution based on historical floods, which occurred before the period of systematic gauging. For the river Rhine this could be the period 1800-1900. Although the real historical discharges are generally unknown and the river geometry has changed, reference books on storm surges and river floods form a valuable source of additional information. These books mention, for example, whether there was flood damage or even a catastrophe occurred involving drowned people, dike bursts, flooded polders, dislodged houses and collapsed bridges. Their main sources of information are old newspapers, chronicles, letters, diaries, memories, legends, government or business records, and even folk songs (Chen et al., 1975). In addition to these written records, man made high water marks and memorials, as well as geomorphologic and botanical evidence of large and catastrophic floods can be used. As opposed to the systematic gauging records, these floods are generally referred in the hydrological literature as 'historical floods' (see, e.g., Stedinger and Cohn (1986) and Hirsch and Stedinger (1987)). The main aim is to approximately assess the number and magnitudes of the largest pregauge historical floods, which occurred within a period, which is generally larger than the systematic record.
Let the random quantity X be defined as the annual maximum river discharge and let us consider a time period of r years. We propose to quantify historical information as follows: if historical references do not mention any flood damage then $X \le y_1$. If historical references mention flood damage but no catastrophe, then $y_1 \le X \le y_2$. If historical references mention a catastrophe then $y_2 < X$.
On the basis of expert judgement, the number of years falling in each of the above three categories denoted by r_i, $i = 1,2,3$, must be assessed.
The subjective estimates of the proportions of historical flood per discharge category can be regarded as censored observations. An observation x can be censored on the left, doubly censored and censored on the right, when $x \le y_1$, $y_1 < x \le y_2$ and $y_2 < x$ respectively. For more details and examples of data censoring, see Kaczmarek (1977).
When considering historical observations, the censoring is due to the absence of systematic measurements, changes in river and meteorology, as well as unreliable reports of historical floods. Under the assumption of the historical censored observations being independent, the likelihood function can be formulated as:

(6) $$l(r_1,r_2,r_3|\theta) = [Pr\{X \le y_1|\theta\}]^{r_1}[Pr\{y_1 < X \le y_2|\theta\}]^{r_2}[Pr\{y_2 < X|\theta\}]^{r_3} = \\ = [F(y_1|\theta)]^{r_1}[F(y_2|\theta) - F(y_1|\theta)]^{r_2}[1 - F(y_2|\theta)]^{r_3}$$

Given the likelihood function of the historical censored observations $l(r_1,r_2,r_3|\theta)$ and a non-informative Jeffreys prior $\pi(\theta)$, Bayes' theorem (1) can be used to obtain the posterior density $\pi(\theta|r_1,r_2,r_3)$. This posterior can then be considered as the informative prior in a subsequent Bayesian analysis for combining historical information with recent systematic uncensored and reliable observations

$\boldsymbol{x} = (x_1,...,x_n)$. The final result is the posterior density of $\boldsymbol{\theta}$ when both historical censored and systematic uncensored and reliable observations are given: that is, $\pi(\boldsymbol{\theta} \mid r_1, r_2, r_3, \boldsymbol{x})$.
In the absence of doubly censored historical observations, likelihood function (6) reduces to:

$$l(r_1, r_2 \mid \boldsymbol{\theta}) = [F(y_1 \mid \boldsymbol{\theta})]^{r_1} [1 - F(y_1 \mid \boldsymbol{\theta})]^{r_2} \tag{7}$$

According to Stedinger and Cohn (1986), Cohn and Stedinger (1987) and Hirsch and Stedinger (1987), a record of historical flood peaks is generally of this form. To apply Eq. (7), we should be able to define a time period of r years, where $r = r_1 + r_2$, and a threshold level y_1 such that over that period floods greater than y_1 left a record which is still available today. Kaczmarek (1998) used Eq. (7) in a maximum-likelihood analysis to fit a gamma distribution to historical and systematic annual maximum discharges of the Polish river Warta.
When censored observations are used as an informative prior distribution, an important point is how much information is contained in the sample of censored observations. In a Bayesian analysis, the posterior density is formed as a combination of prior information on the one hand and actual observations on the other hand. The more information is contained in the historical censored observations, the more weight they get in comparison with the systematic uncensored observations.

5 BAYES FACTORS AND BAYES WEIGHTS

The Bayesian approach to hypothesis testing originates from the work of Jeffreys (1961). He developed a methodology for quantifying the evidence in favour of a scientific theory using the so-called Bayes factors. This factor is the posterior odds of the null hypothesis when the prior probability on the null is one-half. A recent overview on Bayes factors can be found in Kass and Raftery (1995).
Assume the data $\boldsymbol{x} = (x_1,....,x_n)$ to have arisen under one of the m models H_k, $k = 1,...,m$. These hypotheses represent m marginal probability densities $\pi(\boldsymbol{x} \mid H_k)$, with prior probabilities $p(H_k)$, $k = 1,...,m$, where $\sum_{j=1}^{m} p(H_j) = 1$ and $\sum_{j=1}^{m} p(H_j \mid x) = 1$. These posterior probabilities can be obtained using Bayes' theorem as follows:

$$p(H_k \mid \boldsymbol{x}) = \frac{\pi(\boldsymbol{x} \mid H_k) p(H_k)}{\sum_{j=1}^{m} \pi(\boldsymbol{x} \mid H_j) p(H_j)}, \quad k = 1,...,m \tag{8}$$

where:

$$B_{jk} = \frac{\pi(\boldsymbol{x} \mid H_j)}{\pi(\boldsymbol{x} \mid H_k)}, \quad j,k = 1,...,m \tag{9}$$

is denoted by the Bayes factor. The marginal densities of the data under H_k, $\pi(\boldsymbol{x} \mid H_k)$, can be obtained by integrating with respect to the probability distribution of the uncertain parametric vector $\boldsymbol{\theta}_k = (\theta_{1k},....,\theta_{dk})$ with number of parameters d:

$$\pi(\boldsymbol{x} \mid H_k) = \int l(\boldsymbol{x} \mid \boldsymbol{\theta}_k, H_k)\, \pi(\boldsymbol{\theta}_k \mid H_k)\, d\boldsymbol{\theta}_k \tag{10}$$

where $\pi(\boldsymbol{\theta}_k \mid H_k)$ is the prior density of $\boldsymbol{\theta}_k$ under H_k and $l(\boldsymbol{x} \mid \boldsymbol{\theta}_k, H_k)$ is the likelihood function of the data $\boldsymbol{x}$ given $\boldsymbol{\theta}_k$ and H_k.
A difficulty in using non-informative improper priors for calculating Bayes factors is that the prior odds, and thus the Bayes factors, may be undefined. The reason for this is that strictly speaking, the prior probability $p(H_k)$ is defined as:

$$p(H_k) = w(H_k) \int J(\boldsymbol{\theta}_k \mid H_k)\, d\boldsymbol{\theta}_k \tag{11}$$

where the integral over the non-informative Jeffreys prior $J(\boldsymbol{\theta}_k \mid H_k)$ is often infinite and $w(H_k)$ is the prior weight. However, according to Dawid (1999), this problem can be resolved by redefining the posterior odds as:

$$\frac{p(H_j \mid \boldsymbol{x})}{p(H_k \mid \boldsymbol{x})} = \frac{\pi(\boldsymbol{x} \mid H_j)}{\pi(\boldsymbol{x} \mid H_k)} \times \frac{w(H_j)}{w(H_k)}, \quad j,k = 1,\ldots,m \tag{12}$$

These posterior odds are well defined so long as both integrals in it converge, which will typically be the case so long as the sample size n is large enough. For the seven probability distributions considered in this paper, the marginal densities of the data do indeed converge (Chbab et al., 2000). Using Eqs. (8) and (12), the posterior probability of model H_k being correct can now be rewritten as:

$$p(H_k \mid \boldsymbol{x}) = \frac{\pi(\boldsymbol{x} \mid H_k) w(H_k)}{\sum_{j=1}^{m} \pi(\boldsymbol{x} \mid H_j) w(H_j)}, \quad k = 1,\ldots,m \tag{13}$$

It remains to choose the prior weights $w(H_k)$. For formal model comparison, we propose to use equal prior weights. Using the Bayes weights $p(H_k \mid \boldsymbol{x})$, $k = 1,\ldots,m$, the weighted predictive probability of exceeding x_0 is defined by:

$$Pr\{X > x_0 \mid H_k, \boldsymbol{x}\} = \sum_{k=1}^{m} p(H_k \mid \boldsymbol{x}) Pr\{X > x_0 \mid H_k, \boldsymbol{x}\} \tag{14}$$

where $Pr\{X > x_0 \mid H_k, \boldsymbol{x}\}$ is the predictive probability of exceeding x_0 under likelihood model H_k, $k = 1,\ldots m$.

6 CASE STUDY: THE RIVER RHINE AT LOBITH

Bayesian analysis has been applied to the annual maximum discharges of the river Rhine at Lobith during the period 1901-1998. These observations have been corrected for non-homogeneities as changes in river geometry and suchlike. A non-informative Jeffreys prior as well as an informative prior based on historical censored observations in the period 1800-1900 was used. Statistical analysis of the seven distributions based on the non-informative Jeffreys priors can be found in Chbab et al. (2000) and van Noortwijk et al. (2001). In the former paper an approximate Jeffreys prior for the gamma distribution was used, whereas in the latter paper the exact Jeffreys prior was used. The Bayes weights corresponding to these seven distributions were determined. It was found that the Bayes weights depend largely on the location parameter. For proper model selection we then proposed to use the same location parameter for all seven distributions. On the basis of a statistical analysis the location parameter was chosen to be equal to 2,125 m^3/s for all the seven probability distributions. This location parameter was derived by maximising the weighted marginal density of the observations, where Bayes weights have been attached to the seven individual probability distributions, see Table 6-1. The Rayleigh and Weibull distribution appeared to fit best with Bayes weights of 57% and 32%, respectively. The Bayes estimate of the discharge with an average return period of 1,250 years (the standard in the Netherlands) was 15,860 m^3/s.

Table 6-1: Prior and posterior Bayes weights (van Noortwijk et al., 2001).

Bayes Weights	Exponential	Rayleigh	Normal	lognormal	Gamma	Weibull	Gumbel
Prior	0.1429	0.1429	0.1429	0.1429	0.1429	0.1429	0.1429
Posterior	0.0000	0.5718	0.0481	0.0000	0.0072	0.3173	0.0555

New Bayesian calculations have been made using an informative prior for the parameters of the seven distributions stated above, whereas the location parameter was still chosen to be equal to 2,125 m^3/s. The informative prior is based on historical censored observations in the period 1800-1900. Two methods concerning data censoring, presented in subsection 4.2, have been used. They are indicated as Method 1 and Method 2, respectively. More information about censored observations that was used to define an informative prior is summarised in Table 6-2. The obtained Bayes weights of the

seven probability distributions can be found in Table 6-3. Again the Rayleigh and Weibull distributions appear to fit best when an informative prior has been used. The corresponding Bayes weights are 69% and 19% by Method 1 and 67% and 21% by Method 2, respectively. The Gumbel distribution makes a score of circa 10% by both methods. The Bayes estimates of the discharge with an average return period of 1,250 years are 15,290 m^3/s by method 1 and 15,224 m^3/s by method 2, respectively. The difference is comparatively speaking, small.

Table 6-2: Subjective estimates of the number of historical floods of the Rhine River spread over two or three discharge categories.

	Period	r	r_1	r_2	r_3	y_1 [m^3/s]	y_2 [m^3/s]
Method 1	1800-1900	100	75	20	5	7,000	10,000
Method 2	1800-1900	100	75	25	-	7,000	-

Table 6-3: Prior and posterior Bayes weights with informative prior based on censored observations. (Posterior 1 and Posterior 2 correspond with Method 1 and Method 2, respectively).

Bayes Weights	Exponential	Rayleigh	Normal	lognormal	Gamma	Weibull	Gumbel
Prior	0.1429	0.1429	0.1429	0.1429	0.1429	0.1429	0.1429
Posterior 1	0.0000	0.6929	0.0040	0.0000	0.0148	0.1870	0.1012
Posterior 2	0.0000	0.6688	0.0089	0.0000	0.0144	0.2143	0.0937

Figures 6-1 and 6-2 show both the empirical exceedance probabilities, based on complete and censored observations, and the predictive exceedance probabilities. In these figures asterisks indicate the censored observations.

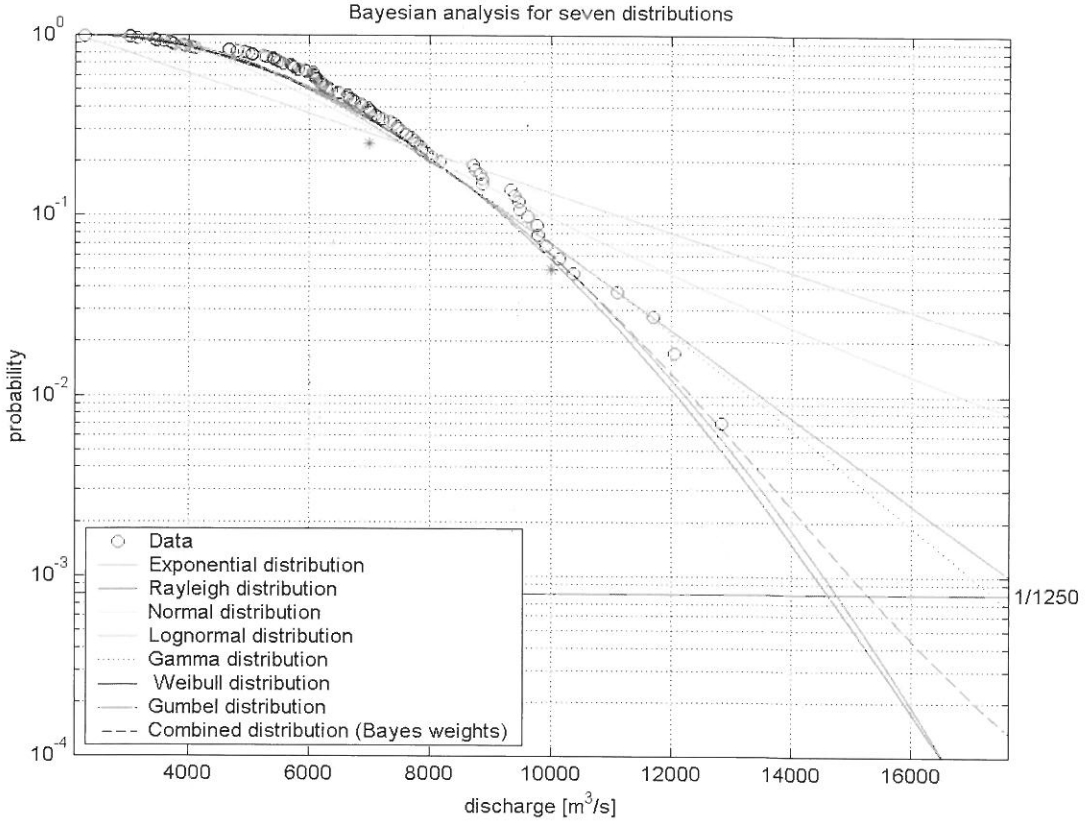

Figure 6-1: Predictive exceedance probability of annual maximum river Rhine discharge using censored observations by Method 1.

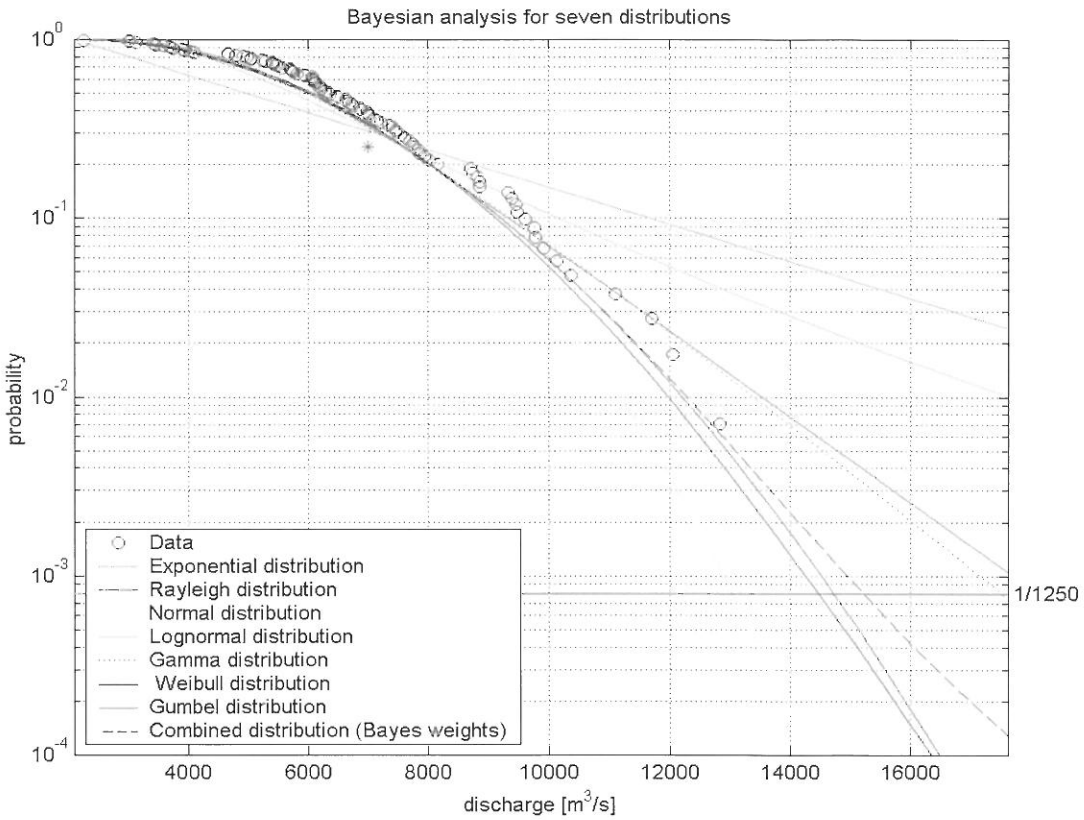

Figure 6-2: Predictive exceedance probability of annual maximum river Rhine discharge using censored observations by Method 2.

7 CONCLUSIONS

A method, based on Bayesian approach, for estimating extreme values of river discharges is presented in this paper. The method deals with inherent uncertainties as well as statistical uncertainties. Bayesian parameter estimates and Bayes weights can be used to account for parameter uncertainty and distribution type uncertainty, respectively. Using Bayes weights, it is possible to discriminate between different probability distributions and to quantify how well a distribution fits the data. For formal distribution comparison, either non-informative or informative priors can be used. Furthermore, the present paper explores the use of informative priors, which are determined using historical censored floods. These floods occurred before the period of systematic gauging.
A Bayesian analysis is carried out on the river Rhine to determine the discharge at station Lobith with an average return period of 1,250 years. From the analysis with both historical floods from the period 1800-1900 and reliable and homogeneous observations from the period 1901-1998, we conclude that a Bayesian approach seems to be very promising. However, we remark that the use of informative priors based on historical floods, instead of non-informative priors results in a lower discharge with a return period of 1,250 years. It is not known yet whether this is due to unreliable information about historical floods, which are generally not homogeneous, or to an actual lower occurrence rate of these floods. Furthermore, it must yet be investigated what perception thresholds can best be chosen in order to classify historical floods.

REFERENCES

Bayes, T. (1763): An essay towards solving a problem in the doctrine of chances. Philosophical Transactions of the Royal Society of London, 53:370-418. London

Box, G.E.P. and Tiao, G.C. (1973): Bayesian Inference in Statistical Analysis. New York: John Wiley & Sons. New York

Castillo, E. (1988): Extreme Value Theory in Engineering. New York: Academic Press. New York

Chbab, E.H. et al. (2000): Bayesian frequency analysis of extreme river discharges. In Frank Toensman and Manfred Koch, editors, River Flood Defence, Proceedings of the international Symposium on Flood Defence, Kassel, Germany, 2000, pages F51-F60. Kassel: Herkules Verlag Kassel. Germany

Chen, J.Q. et al. (1975): The important role of historical flood data in the estimation of spillway design floods. Scientia Sinica, 18(5): 669-680. China

Cohn, T.A., and Stedinger, J.R. (1987): Use of historical information in a maximum-likelihood framework. Journal of Hydrology, 96:215-223. London

Dawid, A.P. (1999): The trouble with Bayes factors. Research Report No. 202, Department of Statistical Science, University College London.

DH and EAC-RAND (1993): Toetsing uitgangspunten rivierdijkversterkingen; deelrapport 2: Maatgevende belastingen [Investigation of basic principles of river dike improvement; Supporting Volume 2: Design loads, Delft Hydraulics (DH) & European American Center (EAC) for Policy Analysis/RAND, Delft, The Netherlands.

Galambos, J. et al. (1994): Extreme Value Theory and Applications. Dordrecht: Kluwer Academic Publishers. The Netherlands

Hirsch, R.M. and Stedinger, J.R. (1987): Plotting positions for historical floods and their precision. Water Resources Research, 23(4):715-725. London

Jeffreys, H.J. (1961): Theory of probability; Third Edition. Oxford Clarendon Press. Oxford

Kaczmarek, Z. (1998): Uwagi krytyczne w sprawie metod oceny zagrożenia powodziowego [Critical remarks on the question of estimating reliable loads]. In L. Starkel and J. Grela, editors. Powódź w dorzeczu górnej Wisły w lipcu 1997 roku [The flood in the upper Wisła river basin in July 1997], pp 219-232. Kraków: Polska Akademia Nauk Oddział w Krakowie.

Kaczmarek, Z. (1977): Statistical Methods in Hydrology and Meteorology. Warszawa: Foreign Scientific Publications Department of the National Center for Scientific, Technical and Economic Information. Warszawa

Kass, R.E. and Raftery, A.E. (1995): Bayes factors. Journal of the American Statistical Association, 90(430):773-795. New York

Kass, R.E. and L. Wasserman (1996): The selection of prior distributions by formal rules.

Journal of the American Statistical Association, 91(435):1343-1370. New York

Siu, N.O. and Kelly, D.L. (1998): Bayesian parameter estimation in probabilistic risk assessment. Reliability Engineering and System Safety, 62:89-116.

Slijkhuis, K.A.H. et al. (1999): On the lack of information in hydraulic engineering models. In G.I. Schuëller and P. Kafka, editors, Safety and Reliability, Proceedings of ESREL '99 – The Tenth European Conference on Safety and Reliability, Munich-Garching, Germany, 1999, pages 713-718. Rotterdam: Balkema

Stedinger, J.R. and Cohn, T.A. (1986): Flood frequency analysis with historical and paleoflood information. Water Resources Research, 22(2):369-375. London

van Gelder, P.H.A.J.M. (1999): Statistical Methods for Risk-Based Design of Civil Structures. PhD Thesis, Delft University of Technoloy, Delft, The Netherlands.

van Gelder, P.H.A.J.M. et al. (1999): Selection of probability distributions with a case study on extreme Oder river discharges. In G.I. Schuëller and P. Kafka, editors, Safety and Reliability, Proceedings of ESREL '99 – The Tenth European Conference On Safety and Reliability, Munich-Garching, Germany, 1999, pages 1475-1480. Rotterdam: Balkema.

van Noortwijk, J.M. et al. (2001): The use of Bayes factors for model selection in structural reliability. 8th International Conference on Structural Safety and Reliability (ICOSSAR), Newport Beach, California, U.S.A., June 17-21, 2001. California

van Noortwijk, J.M. et al. (2002): Bayesian Statistics for Flood Prevention. Institute for Inland Water Management and Wastewater Treatment (RIZA) and HKV Consultants, Lelystad. The Netherlands.

APPENDIX

This appendix contains the probability distributions, which are considered in the statistical analysis of the annual maximum discharges, as well as their non-informative Jeffreys priors.

Distribution	Probability density function	Jeffreys prior
Exponential	$\frac{1}{\theta}exp\left\{\frac{-x}{\theta}\right\}I_{(0,\infty)}(x),\ \theta>0$	$J(\theta)=\frac{1}{\theta}$
Rayleigh	$\frac{2x}{\theta}exp\left\{\frac{-x^2}{\theta}\right\}I_{(0,\infty)}(x),\ \theta>0$	$J(\theta)=\frac{1}{\theta}$
Normal	$\left(\frac{r}{2\pi}\right)^{\frac{1}{2}}exp\left\{\frac{-r}{2}(x-m)^2\right\}I_{(0,\infty)}(x),\quad r>0$	$J(m,r)=\frac{1}{\sqrt{2r}}$
Lognormal	$\left(\frac{r}{2\pi}\right)^{\frac{1}{2}}\frac{1}{x}exp\left\{\frac{-r}{2}(log(x)-m)^2\right\}I_{(0,\infty)}(x),\quad r>0$	$J(m,r)=\frac{1}{\sqrt{2r}}$
Gamma	$\frac{b^a}{\Gamma(a)}x^{a-1}exp\{-bx\}I_{(0,\infty)}(x),\quad a,b>0$	$J(a,b)=\frac{\sqrt{a\psi'(a)-1}}{b}$
Weibull	$\frac{a}{b}\left[\frac{x}{b}\right]^{a-1}exp\left\{-\left[\frac{x}{b}\right]^a\right\}I_{(0,\infty)}(x),\ a,b>0$	$J(a,b)=\frac{1}{b}\frac{\pi}{\sqrt{6}}$
Gumbel	$\frac{1}{b}exp\left\{-\frac{x-a}{b}\right\}exp\left\{-exp\left\{\frac{x-a}{b}\right\}\right\},\quad b>0$	$J(a,b)=\frac{1}{b^2}\frac{\pi}{\sqrt{6}}$

Remark with respect to the Jeffreys prior of the gamma distribution: *The trigamma function $\psi'(a)$ is the first derivative of the digamma function:*

$$\psi'(a)=\frac{\partial\psi(a)}{\partial a}=\frac{\partial^2 log\Gamma(a)}{\partial a^2}$$

for $a>0$, where $\Gamma(a)=\int_{t=0}^{\infty} t^{a-1}e^{-t}dt$ is the gamma function for $a>0$.

FLOOD FREQUENCY ANALYSIS DOWNSTREAM CONFLUENCES. COMPARISON BETWEEN BIVARIATE DENSITIES AND EXPERIMENTAL DATAS

Sandrine LE CLERC, Michel LANG

Cemagref, Hydrology-Hydraulics Research Unit, 3 bis quai Chauveau, 69336 Lyon cedex 09
Leclerc@lyon.cemagref.fr, lang@lyon.cemagref.fr

SUMMARY

Various methods have been used to estimate design flood at ungauged sites, usually in two steps: delineation of homogeneous regions, and use of regional standardised flood frequency curves. When the main river and its tributary exhibit significant differences in flood regime, the assumption of homogeneity is doubtful. Then, an alternative is to combine the probability to have a flood on each branch of the confluence. The dependence between flows in tributaries should be taken into account in the joint probability structure. Some bivariate densities for solving joint probability problems are reviewed : bivariate normal, bivariate Gumbel, Farlie, Hashino... Some of them are tested on experimental sites where data is available on the three branches of the confluence. Then, the theoretical downstream flood distributions, issued from the two upstream flood distributions and different bivariate densities, are compared with the experimental flood distribution.The measure of dependency between flows in tributary is computed, using both concomitant and non concomitant events. The simple correlation coefficient between peak values of concomitant events does not exhibit the total dependency between two river regimes. It is then important to deal with cases when only one river is flooded. We use a correlation coefficient proposed by Bernier and Lencioni (1978), which has been applied on peak-over-threshold data. It allows to analyse the process of both concomitant and non concomitant events. Finally, attention should be paid to the variation of the dependency with the flood intensity. A discussion will provide some guidelines on it.

Keywords: Bivariate density, joint probability, correlation coefficient, confluence, concomitance, frequency

1 INTRODUCTION

The hydraulic analysis of flood consequences is based on the use of hydrological reference scenarios. The estimation of a design flood hydrograph consists on associating the value of one or more flood parameters to its probability of occurrence. One method to estimate all the characteristics of floods at ungauged site is done by the delineation of homogeneous regions, and the use of standardised flood frequency curves. But, if we want to know more precisely the contribution of a tributary catchment on the regime of the main river, we can not accept this assumption of homogeneity if the two flood regimes are too much different. So in this paper, we want to know if it is possible to compose the distribution of flood frequency downstream a confluence only with the use of the upstream floods distributions. This composition could be done by the integration of a joint probability structure. Further bivariate densities for solving joint probability are reviewed here (part 1).
The dependence between flows in tributaries should be taken into account in the joint probability structure. So it is also necessary to estimate the dependence (part 2) between flows in the tributaries, and to take it into account in the joint probability structure.
In the last part of this paper, several models of bivariate densities are verified using observed flood datas from the confluence of the Loire and the Allier rivers. A comparison of those models with the usual ones will be carried out. Finally, attention should be paid to the variation of the dependency with the flood intensity.

2 BIVARIATE DENSITIES

Among the various ideal models of composition of probability laws, we can distinguish the simplified models, the bivariate distributions models using the marginal distributions and those explicitly using the correlation between two variables. The simplified model consists in reasoning on the two extreme cases: independence or total dependence between both variables. These two hypothetical cases, even if they are seldom presented in practice, give the advantage of providing the range of variation in which the general case of two more or less dependent variables is. The models using the marginal

laws deduce the density from probability of the couple of two variables of a function of each density of the variables. Finally, there are also models revealing explicitly the coefficient of correlation between the two variables.
Let X1, X2 denote the discharge of two tributaries and X = X1 + X2 the downstream discharge. The general formulation of the bivariate distribution (Finch et Groblicki, 1984) can be expressed by:

$$F(x) = \text{Prob}[X < x] = \iint f(x_1, x_2)\, dx_1\, dx_2 \tag{1}$$

with:

$$f(x_1, x_2) = f_1(x_1)\, f_2(x_2) \left\{1 + \rho\, [F_1(x_1); F_2(x_2)]\right\} \tag{2}$$

where f_1 and f_2 denote the marginal densities of X_1 and X_2, and ρ is a correlation function linking the two distributions.

2.1 Simple models

Hawkes and Hague (1994) suggest it is better to test extreme cases before using sophisticated bivariate distributions. It is a way to consider the independent and dependent cases for downstream design flood hydrograph to determine the maximum range of uncertainty in downstream design flood hydrograph with any given upstream design flood hydrograph.
The two trivial cases, i.e.,
- complete dependence between the flood regimes of the two tributaries ($\rho = 1$):

$$X(T) = X_1(T) + X_2(T) \tag{3}$$

- strict independence ($\rho = 0$):

$$f(x_1, x_2) = f_1(x_1)\, f_2(x_2) \tag{4}$$

These extreme cases give respectively the higher and lower boundaries of the distribution of two partially correlated variates. If the difference between the two extreme cases is not significant, equation (3) provides a good estimate of the downstream flood distribution because it gives the most unfavourable case to be taken for the flood prevention.

2.2 Bivariate models derived from marginals

A wide range of bivariate distributions derived from the marginals has been proposed by many authors for solving hydrological problems. Singh and Singh (1991) proposed the Farlie density, which has the following correlation function (see equation 2) which is a 0-marginal function (Finch and Groblicki, 1984):

$$\rho\,(u;v) = \left[(n+1)u^n - 1\right]\left[(m+1)v^m - 1\right] \tag{5}$$

where n, m > 0. The Farlie density is expressed by:

$$f(x_1, x_2) = f_1(x_1) \cdot f_2(x_2) \cdot \left\{1 + c\left[(n+1) \cdot F_1^n(x_1) - 1\right] \cdot \left[(m+1) \cdot F_2^m(x_2)\right] - 1\right\} \tag{6}$$

where c is a constant to be chosen in the interval:

$$-\frac{1}{nm} \le c \le \frac{1}{\max(n,m)} \tag{7}$$

The well-known Farlie-Gumbel-Morgenstern (FGM) density is a special case of Farlie density, with n = m = 1. Long and Krzysztofowicz (1992) have derived the value of the correlation coefficient:

(8) $$R_{1,2} = Cov(X_1, X_2) = \iint \left[x_1 - E(x_1)\right]\left[x_2 - E(x_2)\right] f(x_1, x_2)\, dx_1\, dx_2$$

for various marginals f1 and f2. The FGM and Farlie densities can model only weakly correlated variables, because the correlation coefficient $R_{1,2}$ is respectively in the range 1/3,1/2.
The bivariate models using the correlation coefficient are more flexible and allow any positive correlation in [0; 1].

2.3 Bivariate models using the correlation coefficient

The bivariate standardised normal density of probability has the following expression:

(9) $$n^*(x_1, x_2) = \frac{1}{2\pi\sqrt{1-\rho_{12}{}^2}} \exp\left[-\frac{x_1^2 - 2\rho_{12}x_1x_2 + x_2^2}{2(1-\rho_{12}{}^2)}\right]$$

It requires transformation for modelling non-Gaussian marginals. Kelly and Krzysztofowicz (1997) proposed the meta-Gaussian distribution:

(10) $$F(x_1, x_2) = \text{Prob}(X_1 \le x_1, X_2 \le x_2) = N^*\left[\Phi^{-1}(F_1(x_1)); \Phi^{-1}(F_2(x_2)\right]$$

N * is related to the bivariate standardised normal distribution (pdF: $n^*(x_1,x_2)$)
$\phi^{-1}[F_i(x)]$ is the normal quantile transformation, where ϕ^{-1} denotes the inverse of the standard normal distribution.
Hashino et al. (1993) suggested the following bivariate density:

(11) $$f(x_1, x_2) = f_1(x_1) f_2(x_2)(C_0 + C_1x_1 + C_2x_2 + C_{11}x_1x_2)$$

The coefficients C_i are expressed according to the average and the standard deviation of the variables X1 and X2. Finaly, we get the following density :

(12) $$f(x_1, x_2) = f_1(x_1) f_2(x_2)\left\{1 + \rho_{12}\frac{x_1 - E(x_1)}{\sigma_1}\frac{x_2 - E(x_2)}{\sigma_2}\right\}$$

Mousavi (1997), had tested the abilities of bivariates models using the correlation coefficient to solve river confluence joint probability problems. The Hashino distribution has been compared with FGM and Farlie distributions, which are limited to weak dependencies. The Hashino model offered the advantage of accepting any marginal and type of dependence.

3 CORRELATION COEFFICIENT

Several statistics have been proposed to measure the association between two variables (Farlie, 1960). The Pearson correlation coefficient is recommended for linear stochastic relations. The non-parametric Spearman or Kendall rank correlation coefficients are more general. When dealing with confluence problems, the Pearson correlation coefficient is taken to be a good measure of the dependence between the flood regimes of the two tributaries. Those classical correlation coefficients are only relative to concomitant values, with an event recorded on the two stations. This approach introduces a bias into estimations. Bernier and Lencioni (1978) proposed analysing the processes of both concomitant and non-concomitant events. Their method consists to estimate the correlation coefficient such as the likelihood function of the given sample is maximum
Let Z_1, Z_2 denote the peak-over threshold (POT) values on two stations, with cumulative distribution functions F_1 and F_2. Standardised Normal variables V_1 and V_2 are related to the original variates Z_1 and Z_2 through the normal quantile transform, $v_i = \phi^{-1}[F_i(z_i)]$, and define an event when $V_i > S_i$ (S_i

represents the threshold of each sample chosen for the variables V_i). Let us consider three kinds of events downstream of the confluence (figure 3-1):

- (V_{i1}) set of $V_1 \rangle S_1$ with $V_2 < S_2$, is the sample in which there is only an event on the first tributary
- (V_{i2}) set of $V_2 \rangle S_2$ with $V_1 < S_1$, is the sample in which there is only an event on the second tributary
- (V_{i1}^*, V_{i2}^*): set of concomitant (V_1, V_2) events, $V_1 \rangle S_1$ and $V_2 \rangle S_2$, the discharges are over their respective threshold on each station.

The case with $V_2 < S_2$ and $V_1 < S_2$ have to be eliminated because only the flood events are considered.

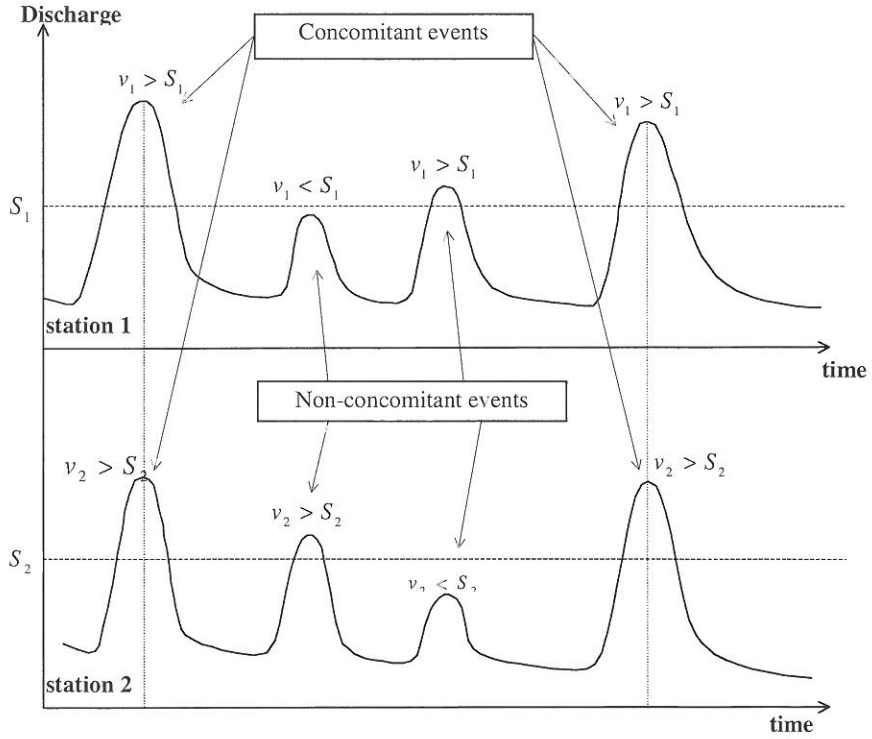

Figure 3-1: Concomitant and non-concomitant events (from Bernier and Lencioni, 1978).

- Likelihood function of (V_{i1}): set of $V_1 \rangle S_1$ with $V_2 < S_2$

The probability of a flood V_{i1} at the first tributary and no flood at the second one is given by:

(13) $$\text{Prob}(V_1 = V_{i1}, V_2 < S_2) = \int_{-\infty}^{S_2} n^*(V_{i1}, y)dy$$

n^* is the Normal bivariate density given by equation (7)
Using the following equation:

(14) $$V_{i1}^2 - 2\rho_{12}V_{i1}y + y^2 = (y - \rho_{12}V_{i1})^2 + V_{i1}^2(1 - \rho_{12}{}^2)$$

and combining equations (9) and (13) gives:

$$\text{Prob}(V_1 = V_{i1}, V_2 < S_2) = \frac{1}{2\pi\sqrt{1-\rho_{12}{}^2}} \exp(-V_{i1}^2/2) \int_{-\infty}^{S_1} \exp\left[-\tfrac{1}{2}\left(\frac{y-\rho_{12}V_{i1}}{\sqrt{1-\rho_{12}{}^2}}\right)^2\right] dy$$

(15) $$= \frac{1}{2\pi\sqrt{1-\rho_{12}{}^2}} \exp(-V_{i1}^2/2) \int_{-\infty}^{\frac{S_1-\rho_{12}V_{i1}}{\sqrt{1-\rho_{12}{}^2}}} \exp(\tfrac{1}{2}u^2)\sqrt{1-\rho_{12}{}^2}\,du$$

By integrating equation (15) with the variable $u = (y - \rho_{12}V_{i1})/(\sqrt{1-\rho_{12}{}^2})$, we obtain:

(16) $$\text{Prob}(V_1 = V_{i1}, V_2 < S_2) = \frac{1}{\sqrt{2\pi}} \exp(-V_{i1}^2/2)\, \phi\left(\frac{S_2 - R_{1,2}V_{i1}}{\sqrt{1-R_{1,2}{}^2}}\right)$$

The likelihood function of the first set of value is:

(17) $$L_1 = \frac{1}{\sqrt{2\pi}} \prod_i \left[\exp\left(-\tfrac{1}{2}V_{i1}^2\right)\right]\phi\left(\frac{S_2 - R_{1,2}V_{i1}}{\sqrt{1-R_{1,2}{}^2}}\right)$$

- Likelihood function of (V_{i2}): set of $V_2 \rangle S_2$ with $V_1 < S_1$

(19) $$L_2 = \frac{1}{\sqrt{2\pi}} \prod_i \left[\exp\left(-\tfrac{1}{2}V_{i2}^2\right)\right]\phi\left(\frac{S_1 - R_{1,2}V_{i2}}{\sqrt{1-R_{1,2}{}^2}}\right)$$

- Likelihood function of (V_{i1}^*, V_{i2}^*)

(20) $$L_3 = \prod_i \mathrm{n}^*(\mathrm{V}_{i1}^*, \mathrm{V}_{i2}^*)$$

The correlation coefficient ρ_{12} is chosen such that $\frac{\partial}{\partial\rho_{12}}(\ln L) = 0$, with $L = L_1\, L_2\, L_3$.

As the correlation coefficient belongs to the range [0 ;1], we prefer to compute the total likelihood L($\rho_{12} = i/1000$), for i = 0 to 1000, and select the value ρ_{12} which gives the maximum likelihood.

4 APPLICATION

4.1 Description of the study basin

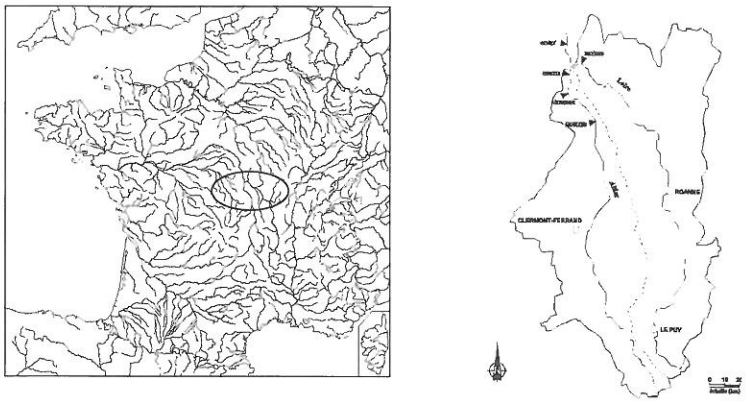

Figure 4-1: Study Basin: Loire – Allier confluence.

The Loire basin at Givry downstream the confluence has an area of 32610 km^2. The sub-basins cover an area of 17600 km^2 for the Loire at Nevers and 14400 km^2 for the Allier at Veurdre. These basins are subject to Mediterranean climatic influences which causes strong rains on the Cevennes regions, and also to phenomena of oceanic origin caracterised by big durations of raining.The discharges time-series cover the period from the year 1982 to the year 1996.

4.2 Study of flood regime

The flood regime study consists of the estimation of the discharges quantiles for different return periods in order to determine the discharges frequency distribution. The time step of the study was fixed to 4 days (according to the gradex study done by Menez and Bontron (1997)). The selected technique of sampling is the POT (Peak Over Threshold) technique. It consists on a selection of all the floods over a fixed threshold according to the stationarity, homogeneity and independence assumptions of events and Poisson law (Lang & al., 1999).

4.2.1 Distribution fitted with the discharge observation (T<20 years)

Exponential laws are fitted on the three discharges time-series. They have the following expression:

(21)
$$G_s(x) = 1 - e^{-\frac{(x-x_0)}{a}} = 1 - \frac{1}{\mu T_s} = p$$
$$x_p(T) = x_0 + a\ln(\mu T_s)$$

with μ the mean number of events per year (here, μ =2)
Law parameters and their first moments are given in the table 1, according to the results of Maniguet (1998).

4.2.2 Distribution extrapolated with the rainfall information

Extrapolation for events of rare frequency was carried out by the methods of the gradex (Guillot & Duband,1967) and the aesthetic gradex (Michel, 1982; CFBG,1994) which respectively following equations (22) and (23). The gradex method represents a simplified rainfall-runoff model which provides estimates of flood magnitudes of given probabilities. It is based on the hypotheses that beyond a given rainfall threshold (known as the pivot point), all water is transformed into runoff, and that a rainfall event of a given duration generates runoff for the same length of time. The aesthetic gradex is a generalisation of the gradex method. The main parts of the model are the fitting of rainfall and discharge distribution. The use of a simple mathematical formulation allows a progressive extrapolation of the discharge distribution.

(22) $$VCXd(T) = VCXd(Tg) + a_p \ln (T/Tg)$$

(23) $$VCXd(T) = VCXd(Tg) + a_p \ln[(a_q/a_p)(T/Tg - 1) + 1)$$

The extrapolation begins at the return period 20 years, with Tg corresponding to the pivot point (Tg=20 years). To estimate the extrapolated quantiles, one needs the quantile of the pivot point and the gradex value $\mathbf{a_p}$ in order to insert rain information

4.2.3 Parameters and graphical distributions

Table 4-1: parameters of distribution.

		GIVRY	NEVERS	VEURDRE
POSITION:	x_0	1053	585.1	334.4
SCALE:	a_q	382.2	381.1	243.4
MEAN:	$E(X_i)$	1538.7	966.2	577.8
ST. DEVIATION:	σ_i	609.1	381.1	243.4
Rainfall gradex:	a_p	1132 m^3/s	615 m^3/s	495m^3/s

We get the graphical distributions on figure 4-3.

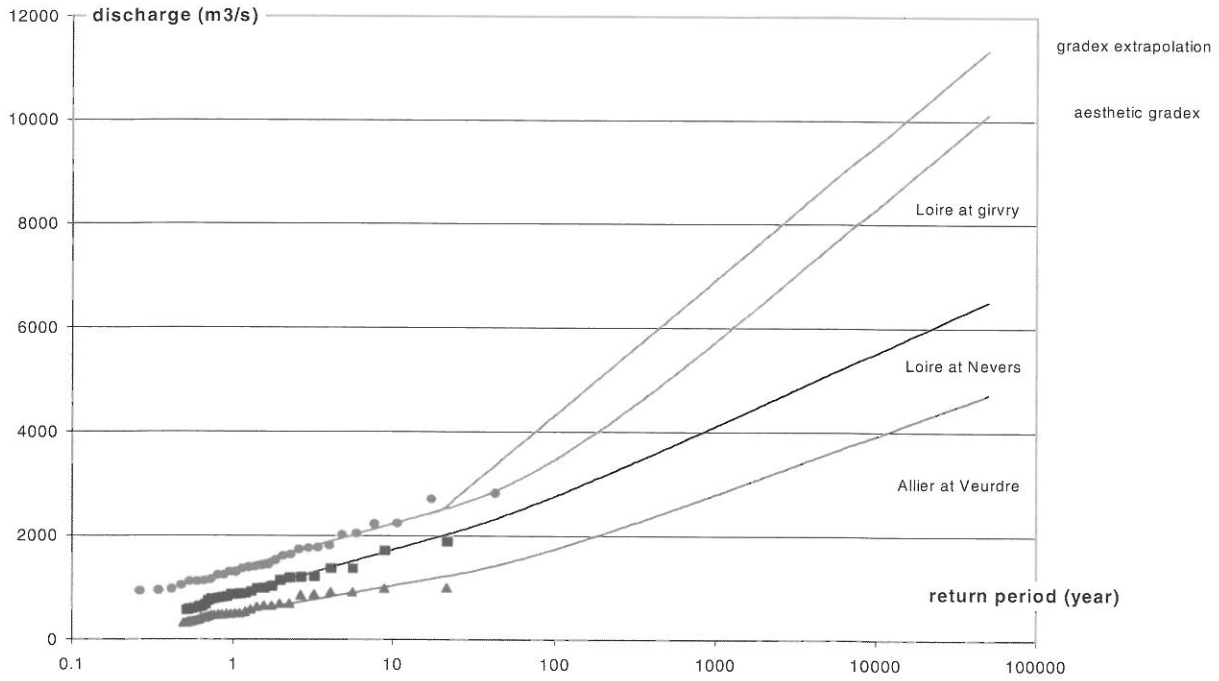

Figure 4-3: Theoretical distribution laws.

4.3 Estimation of correlation coefficient between floods

The correlation coefficient ρ_{12} .is given by the estimation of the maximum likelihood method. The figure 3 presents the evolution of the likelihood function (14) and the function $\frac{\partial}{\partial \rho_{12}}(\ln L)=0$ in the interval [0,1].

The evaluation of the correlation coefficient depends on the duration fixed to define concomitance between events. Several durations were tested to determine the best coefficient (Table 4-2).

Table 4-2: Evaluation of the correlation coefficient according to the duration.

Duration	1	2	3	4	5	6	10
ρ_{12}	0.36	0.52	0.52	0.52	0.52	0.52	0.52
$R_{Pearson}$	0.61	0.58	0.57	0.57	0.57	0.57	0.59

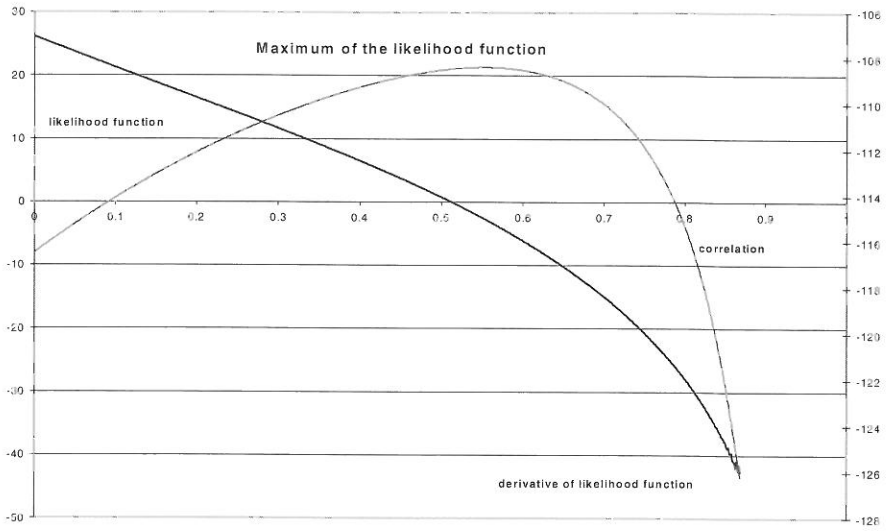

Figure 4-4: Evaluation of the correlation coefficient.

The correlation of both concomitant and non concomitant floods is stable as from two days. The Pearson correlation is higher and less stable. For this study, the correlation of both concomitant and non concomitant floods is ρ_{12}=0.52.The Pearson correlation is also estimated, the value is $R_{Pearson}$ = 0.67

4.4 Composition of flood regimes of Loire and Allier

Using the adjustment parameters of the upstream rivers and the correlation coefficient, the downstream regime can be calculated thanks to the Hashino density. Furthermore, we can compare those results with the results obtained for the gradex and the aesthetic gradex extrapolation. The results are reported on figure 4-5.
We can notice that the Hashino model gives a good estimation of the flood regimes until the return period of 1000 years. From 70 to 1000 years of return period, the Hashino model is between the gradex and aesthetic gradex curves. This model doesn't seem to be sensitive to the rainfall information. The gradex method is very close to the independent distribution until 20 years of return period and develops then towards the full dependent distribution as from the return period of 70 years. The aesthetic gradex is close to the independent case longer, until the return period of 70 years. After that, it is situated between the extreme cases.

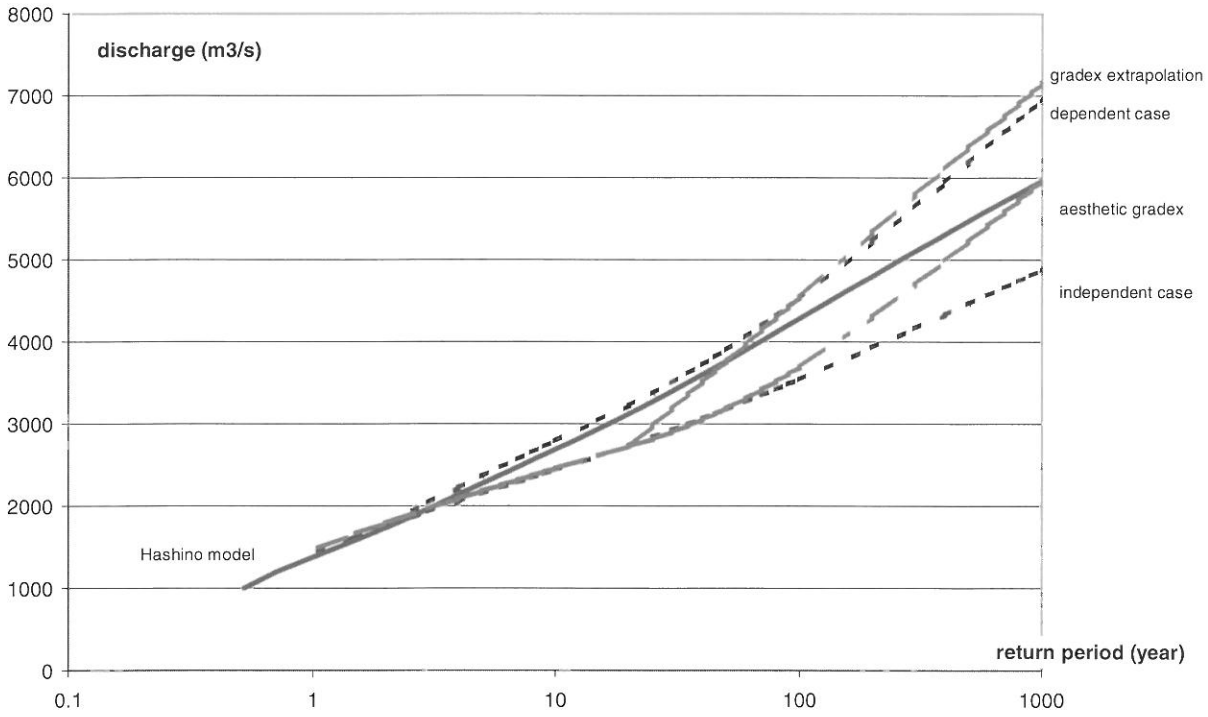

Figure 4-5: Composition of flood regime.

The differences between the composition model and usual extrapolations can be explained with the non stationarity of the correlation coefficient at high return periods. We put in decreasing order all the flood events of each branch of the confluence and notice the ones which are concomitant. We can notice on the following figure 4-6, that the strongest events are concomitant.

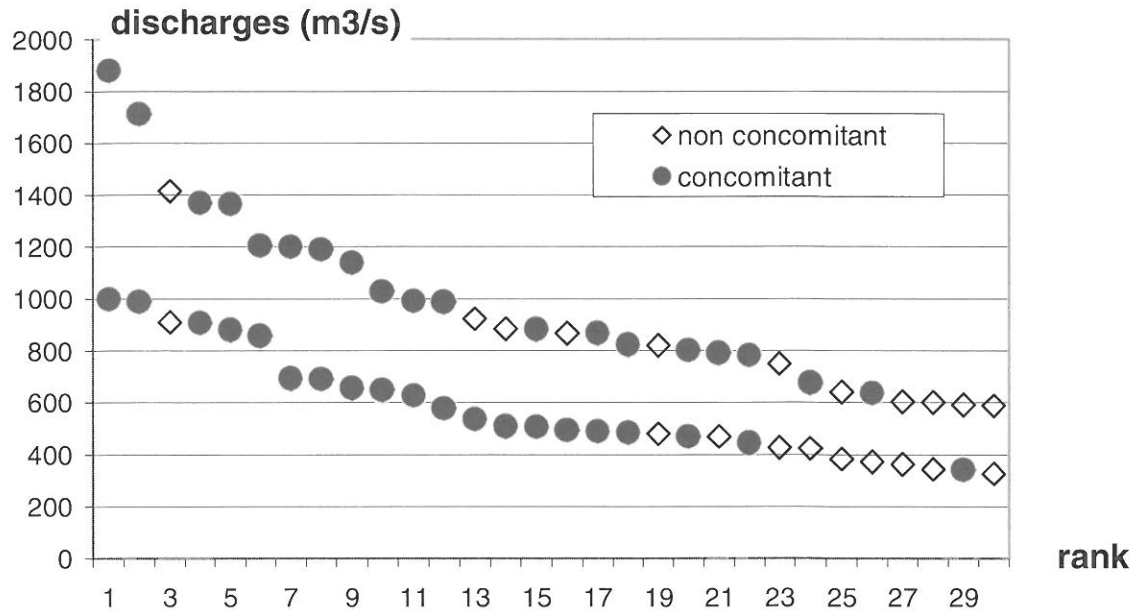

Figure 4-6: Link between discharge and concomitance

So it seems possible that the correlation coefficient is not the same for all the return periods. Using this feeling, we try to compose the downstream regime for several correlation coefficients from [0 to 1] (figure 4-7).

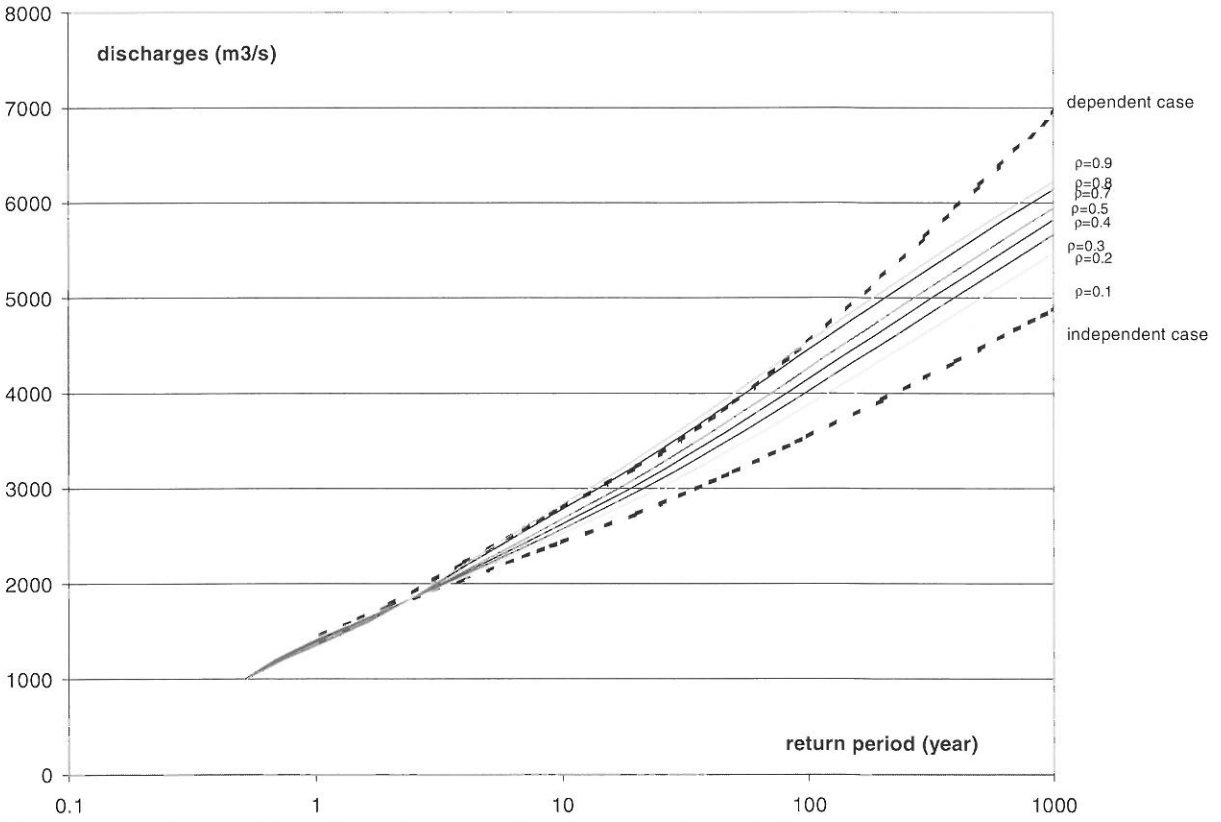

Figure 4-7: Composition of bivariate densities for several correlations.

According to the composed distributions with several correlation coefficients on figure 6, the Hashino model does not seem to be well adapted to high correlation coefficients because it does not gather the distribution of total dependence.

5 CONCLUSION

The control of the dependence between flows is possible only if a very large number of data is obtained. A way to avoid this lack of data is to simulate a continuous flow on a basin in order make the frequential analysis on a long continuous discharge time-serie. These approaches are used to increase the chronicles of flow available. Furthermore, in that case, that will allow to control the degree of connection better between the flows of both tributaries and to analyse more precisely the performances of each model of composition. In that case, the use of a stochastic model with a correlated rainfall generator and a rainfall-runoff model should be interesting in order to make classes of floods according to their magnitude and compose flood regimes using bivariate models of highest performances according to the correlation.

REFERENCES

Bernier, J. and P. Lencioni (1978): Un modèle probabiliste multidimensionnel applicable à la description des processus hydrométéorologique à l'échelle fine (Modèle de renouvellement à plusieurs dimensions), La Houille Blanche, 6, 401-410, France.

CFBG (1994): Design flood determination by the gradex method. 18° Congrès CIBG-ICOLD N°2, Nov., Bulletin du Comité Français des Grands Barrages, 96p. France.

Farlie, D.J.G. (1960): The performance of some correlation coefficients for a general bivariate distribution, Biometrika 47(3), 307-323.

Finch, P.D. and R., Groblicki (1984): Bivariate probability densities with given margins, Foundations of physics 14 (6), 549-552.

Guillot, P., Duband, D. (1967): La méthode du gradex pour le calcul de la probabilité des crues à partir des pluies.Journées, SHF, question 1, rapport 7, Paris.

Hashino et al. (1993): Determination of design storm pattern by a probability model with multi-local peaks, IAHS Publ. n°213, 315-323.

Hawkes, P. and R. Hague (1994): Validation of joint probability methods for large waves and high water levels, Report No. SR 347 to MAFF. Hydraulic Research, 60p., Wallingford.

Kelly, K.S. and R. Krzysztofowicz (1997): A bivariate meta-Gaussian density for use in hydrology, Stochastic Hydrol. Hydraul., 11, 17-31.

Lang, M. et al. (1993): Towards operational guidelines for over-threshold modelling, Journal of Hydrology, 225, 103-117.France.

Long, D. and R. Krzysztofowicz (1992): Farlie-Gumbel-Morgenstern bivariate densities: Are they applicable in hydrology, Stochastic Hydrol. Hydraul., 6, 47-54.

Maniguet F. (1998) : Composition des régimes de crue de la Loire et de l'Allier, au Bec d'Allier., HORIZON S.A,. 25 p. CEMAGREF LYON HHLY.

Menez G., Bontron G. (1997): Analyse de la structure spatiale des précipitations sur le bassin versant de la Loire et de l'Allier à l'amont du bec d'Allier. Application de la méthode du gradex pour la prédétermination des débits de crues extrêmes. ENSHMG-INPG, 42p.+annexes.Grenoble.

Michel, C. (1982): Extrapolation par la méthode du gradex. Note du 03-05. Cemagref Anthony.

Mousavi Nadoshani, S. (1997): Composition des lois élémentaires en hydrologie régionale: application à l'étude des régimes de crue, Ph.D. thesis, Univ. Joseph Fourier Grenoble I, France, Cemagref Lyon, Sept., 164p. Grenoble.

Singh, K. and V.P. Singh (1991): Derivation of bivariate probability density functions with exponential marginals, Stochastic Hydrol. Hydraul., 5 (1), 55-68.

SHIFTS IN FLOOD FREQUENCY DUE TO CLIMATE VARIABILITY

Alistair McKerchar

National Institute for Water and Atmospheric Research (NIWA), PO Box 8602, Christchurch, New Zealand, a.mckerchar@niwa.co.nz

SUMMARY

Almost invariably, frequency analysis methods presume that the expected frequency of hydrological extremes (floods, drought) is unchanged from year to year: in statistical terms the series are said to be stationary. With increasing lengths of archived records and better knowledge of broadscale long-term coupled oceanic-atmosphere oscillations, better scrutiny of the stationarity assumption is possible.
The longest flood records available in New Zealand show that in the northeast of the country, the period from 1947-1977 was "flood rich", whereas the period since 1978 has been "flood poor". Opposite behaviour occurred in the south and west of the country: compared with the period 1947-1977, more floods have occurred since 1978. Substantial changes in design flood quantiles occur when data from the two periods are compared.
The shifts in flood frequency are also evident in relevant rainfall series. In the south and west, increases in mean rainfall of up to 15% have occurred. While the rainfalls are affected to a limited extent by the state of the El Niño Southern Oscillation (ENSO) phenomenon, the mechanism driving the shifts appears to be a change in the relative frequency of El Niño and La Niña episodes since 1978. This change of frequency of the ENSO phenomenon is attributed to a change in the state of the Interdecadal Pacific Oscillation, a broadscale feature that affects much of the Pacific Ocean.

Keywords: Flood frequency, stationarity, climate shift, El Niño Southern Oscillation, Interdecadal Pacific Oscillation, New Zealand

1 INTRODUCTION

Design flood estimates underpin large capital investments in bridges, flood protection works, and dam spillways as well as providing the basis for flood-plain hazard zoning.
Typically, design flood estimates are determined from frequency analysis of flood records collected over the last few decades. The most common method is to apply frequency analysis to the series of peak flows for each year of record – the so-called annual maximum method. The method assumes that the expected frequency of flooding is unchanged from year to year: in statistical terms the series is said to be stationary.
Recent climatological studies (Salinger and Mullan, 1999) have demonstrated that the assumption of stationarity may not be valid for annual rainfall in New Zealand. Compared with the period 1951-1975, consistent decreases of up to 8% were shown for the period 1976-1994 in the north and east of the North Island, and increases of more than 8% were shown in the west and south of the South Island.
These shifts in rainfall were attributed to shifts in the phase of a decadal scale oscillation in broad regions of the Pacific Ocean, the so-called Interdecadal Pacific Oscillation (IPO), described by Mantua et al., (1997) as a "...coherent, interdecadal time scale ocean-atmosphere covariability". Mantua et al. (1997) use the leading eigen vector of North Pacific sea surface temperatures as an index for the state of the IPO. The oscillation shifted phase in 1947, in 1977, and is thought to have shifted again in 1999 (Salinger, pers. com.). Although the index is defined from North Pacific sea surface temperature series, the oscillation affects temperatures across the whole of the Pacific Ocean, including the southwest where New Zealand is located.
The shifts in the IPO coincide with altered frequencies of occurrence of El Niño and La Niña phases of the El Niño Southern Oscillation (ENSO) phenomenon: more El Niño episodes and fewer La Niña episodes have occurred since 1978. In New Zealand El Niño episodes tend to give more rain in the south and west of the country and drier conditions in the northeast; La Niña episodes tend to give less rain in the south and west, and more rain in the northeast.
Because streamflow is the residue of rainfall after losses to evaporation, transpiration and groundwater, changes in flows can be much larger than changes in rainfall. For example, if annual rainfall increases by 10% from 1000 mm to 1100 mm, and losses to evaporation, transpiration and groundwater remain constant at 700 mm, the corresponding annual runoff is expected to change from 300 mm to 400 mm, a 33 % increase!

As more storms accompany an increased annual rainfall, increased storm intensity and more severe floods might be expected. Conversely, where annual rainfall is reduced, reductions in storm rainfall intensity and flood magnitude are possible.
This study assembles a set of long streamflow records to examine whether systematic shifts in flood magnitudes have occurred. Annual maxima are extracted and parametric and non-parametric statistical tests are applied to identify regions of the country where shifts appear to have occurred. The apparent shifts are also evident in representative rainfall series.

2 METHODS

2.1 Details of data and catchments

Streamflow data were sought for rivers where continuous records were available for at least 40 years. In practice this target was not always achieved, but 32 records were assembled with lengths between 33 and 53 years. As the study was confined to investigating the differences between flood records for 1947-1977 and 1978-1999, data for before 1947 for some of the stations, notably from the Manawatu River in the North Island and several South Island lakes, were not used.
The peak flows are estimated by applying stage-discharge rating curves to measured water levels. Peak discharges are prone to error because frequently the rating curves must be extrapolated beyond the range of calibration gaugings. Standard procedures developed for this process (Mosley and McKerchar, 1993) ensure that extrapolation is undertaken systematically. In most cases it is anticipated that the standard error of measurement of individual flood peaks will not exceed 10 – 20 percent. An exception discussed later applies for a river where there is substantial uncertainty about the magnitude of the largest flood in the record.
Peak inflows for six South Island lakes are included. These inflow series are unaffected by hydroelectric operations. As it is not possible to measure lake inflows directly, the inflows are calculated from records of lake levels and outflows. The calculations use the differences in lake levels at successive time steps to estimate change in lake volume. Average inflow over a time interval (e.g. 6 h) is given by the average outflow plus the rate of change of lake volume. Because wind, barometric pressure gradients and seiching affect lake levels, the estimates of lake volume changes, and the resulting inflows over short intervals, are prone to error. In this study, the error is reduced substantially by using peak inflow averaged over 72 hours (3 days). In contrast, the peak flows for rivers are the maxima of measurements made typically at 15 minute intervals. Inflows for the lakes were not available after 1994.
The drainage areas for the records used are shown in Figure 2-1. The site numbers in this figure are a key to the details of the records in Table 2-1.
Very large variations of rainfall occur across New Zealand, especially in the South Island. This island, which extends from latitudes 40° to 46° south is in the Southern Hemisphere zone of persistent westerly wind. It is divided by the Southern Alps, a northeast-southwest oriented chain of mountains more than 600 km long and typically 1500-2500 m high. These Alps intercept moist maritime westerly wind. Heavy precipitation, in places exceeding 10 000 mm/year, occurs where these air flows ascend the western slopes of the Alps (Henderson and Thompson, 1999). In contrast, in the eastern rain-shadow areas, annual rainfalls of less than 400 mm occur. Consequently, the rainfall distribution in river basins is very uneven and difficult to quantify. The headwaters of the east and southeast draining rivers receive most of the precipitation that is recorded at the streamgauges: for example, at station 68526 (Rakaia River) in Figure 2-1, 80 percent of the runoff is received as rainfall within 20 km of the northwest boundary. Thus the flows of the larger rivers draining to the east coast of the South Island reflect a response to rainfall near the main divide of the Southern Alps.

2.2 Graphical presentation

The data for before and after 1978 are presented are pairs of boxplots in Figure 2-2 for six North Island records, and in Figure 2-3 for six South Island records. These plots provide summaries of the annual maxima data. For each series, the plots present the minimum, the 75 percentile value (the value that is exceeded in 75% of years), the 50 percentile (median), the 25 percentile, and the maximum. The interquartile range (IQR) is the range between the 25 and 75 percentile values.

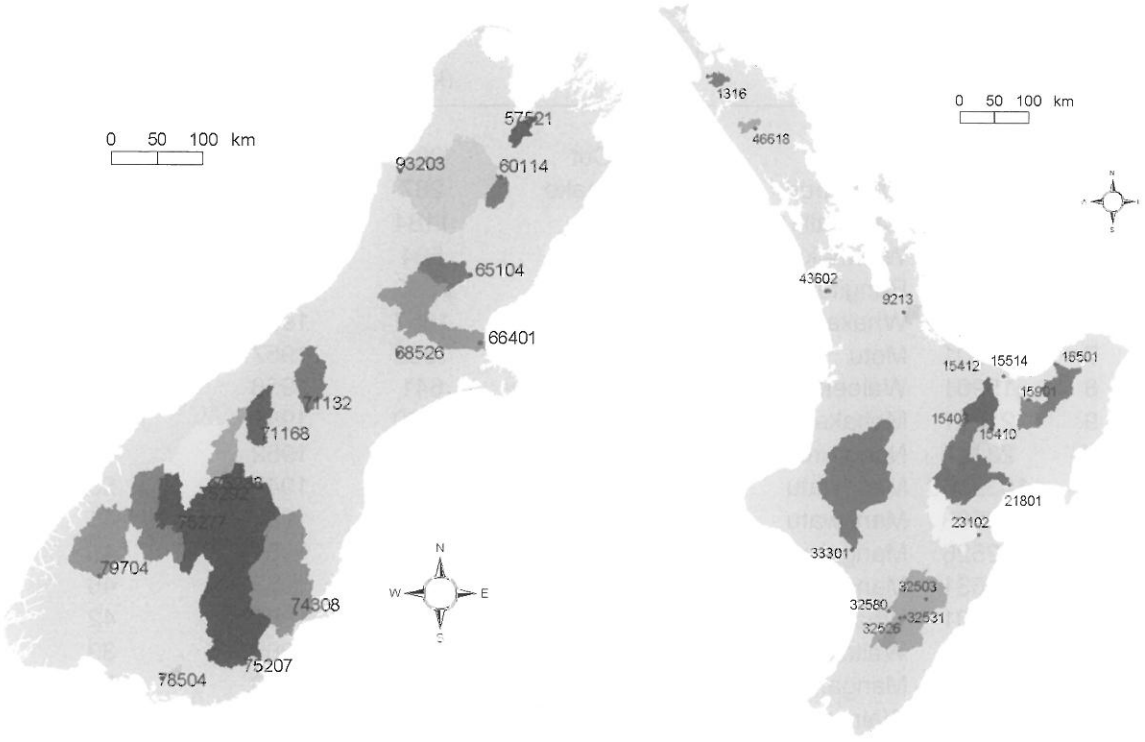

Figure 2-1: Maps of North and South Island showing locations of catchments used in the study. Details for each streamgauge are given in Table 2-1.

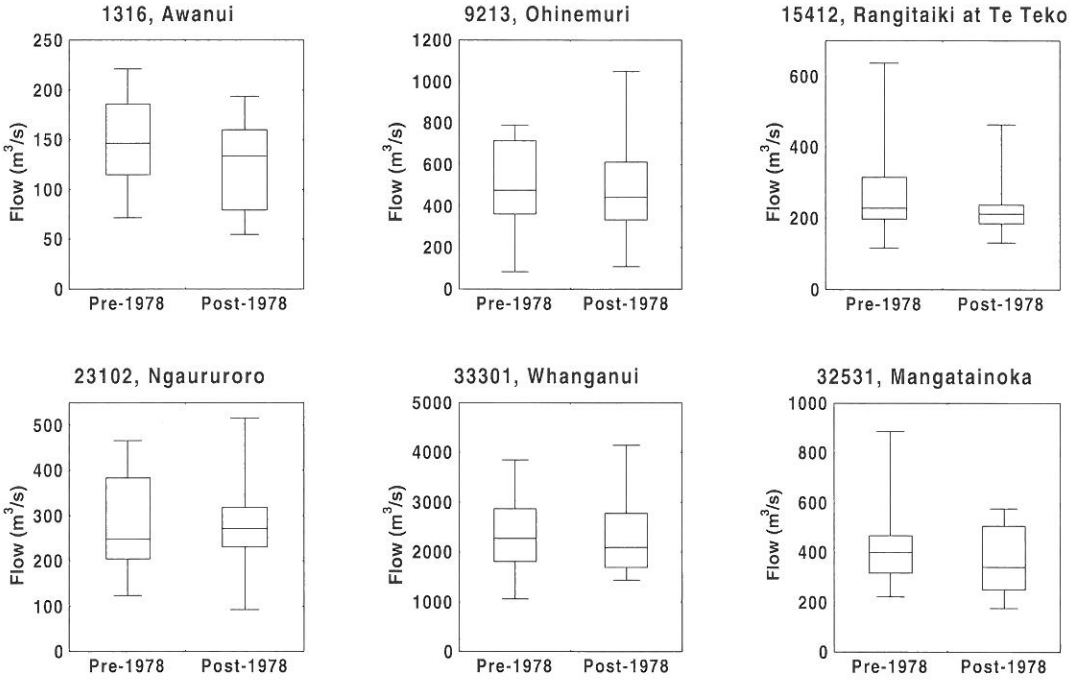

Figure 2-2: Box plots of data for six North Island catchments.

Table 2-1: Details of flood records used (Walter, 2000).

No.	Station number	River	Location	Area (km^2)	Systematic record starts	Full years of record to 1999	Note
1	1316	Awanui	School Cut	222	1958	42	
2	9213	Ohinemuri	Karangahake	287	1956	43	
3	15408	Rangitaiki	Murupara	1184	1952	47	
4	15410	Whirinaki	Galatea	534	1952	47	
5	15412	Rangitaiki	Te Teko	2893	1952	47	
6	15514	Whakatane	Whakatane	1557	1952	47	
7	16501	Motu	Houpoto	1393	1957	42	
8	15901	Waioeka	Gorge Cableway	641	1958	40	
9	21801	Mohaka	Raupunga	2370	1957	42	
10	23102	Ngaururoro	Fernhill	1930	1952	47	
11	1032560	Manawatu	Teachers College	3900	1947	53	5
12	32503	Manawatu	Weber Rd	713	1954	45	
13	32526	Mangahao	Ballance	266	1954	45	
14	32531	Mangatainoka	Suspension Br.	404	1953	46	
15	33301	Whanganui	Paetawa	6643	1957	42	8
16	43602	Waitangi	SHBr	17.6	1966	33	
17	46618	Mangahakia	Gorge	246	1960	39	
18	57521	Wairoa	Irvines	462	1957	42	7
19	60114	Wairau	Dip Flat	505	1951	48	
20	65104	Hurunui	Mandamus	1060	1956	43	
21	66401	Waimakariri	Old Highway Br.	3120	1947	53	
22	68526	Rakaia	Fighting Hill	2560	1957	42	6
23	71132	Lake Tekapo	Inflow	1420	1947	48	1,2
24	71168	Lake Ohau	Inflow	1190	1947	48	1,2
25	74308	Taieri	Outram	4705	1968	43	3
26	75207	Clutha	Balclutha	20582	1954	45	
27	75277	Lake Wakatipu	Inflow	3133	1947	48	1,2
28	75288	Lake Hawea	Inflow	1384	1947	48	1,2
29	75292	Lake Wanaka	Inflow	2628	1947	48	1,2
30	78504	Waihopai	Above Scour	157	1958	41	4
31	79704	Lake Te Anau	Inflow	3124	1947	48	1,2
32	93203	Buller	Te Kuha	6350	1963	36	

Notes
1 Data since 1995 not available.
2 72 h averages used.
3 Annual maxima since 1957
4 Early data from 78503, at Kennington.
5 Early data from 32502 Fitzherbert Br., & 32580 Ruahine St.
6 Early data from 68502, Gorge.
7 Early data from 57502, Gorge.
8 Recorded flows since 1972 increased by 45 m^3/s to allow for upstream abstractions by Tongariro Power Development

2.3 Tests applied

Statistical tests are used to test whether the pre-1978 data differed from the post-1978 data. The tests used are the *t* test for differences between means, the variance ratio (*F*) test, and a range of non-parametric tests.

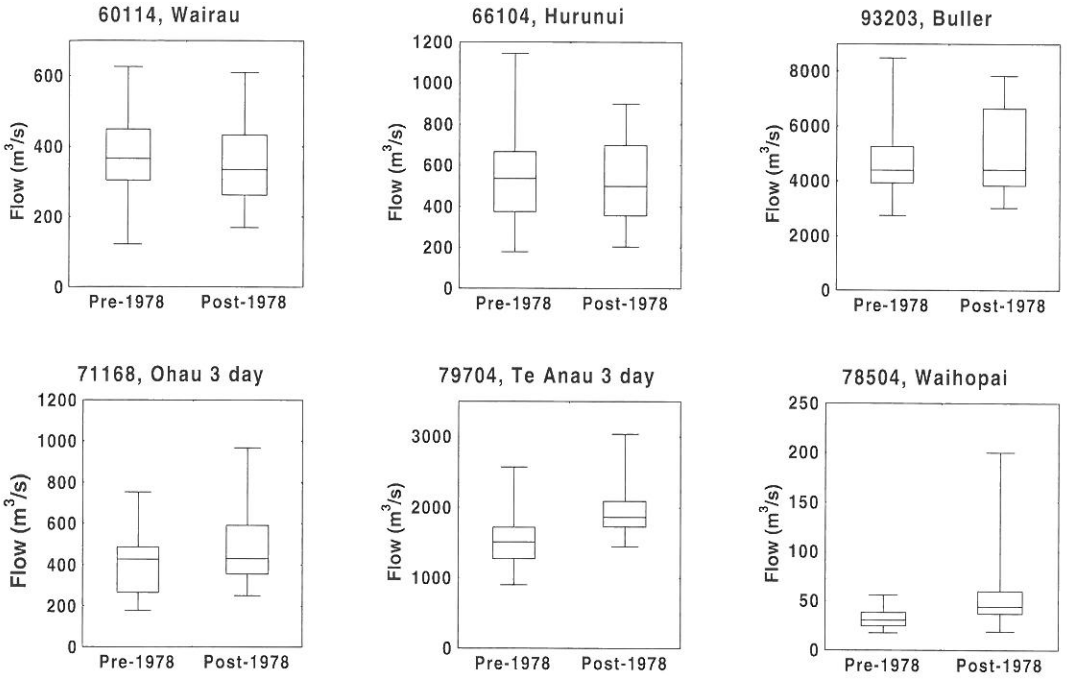

Figure 2-3: Box plots of data for six South Island catchments.

The *t* test and the *F* test are parametric tests that require that the mean of each set of data be normally distributed, and this is assured by the central limit theorem for relatively small samples, except for the most perverse data. The *t* test used includes an adjustment for differing variances between the two samples.
The *t* test is applicable to non-normal data, but it lacks power – that is, it is less likely to detect differences which are truly present than the equivalent non-parametric test (Helsel and Hirsch, 1992).
One way to handle the non-normal data is to transform them. Experience has indicated that in many cases the logarithmic transform is a reasonable normalising transform for NZ flood data. A second problem with the *t* test is that it assumes that the mean is a good measure of central tendency. This is not the case with severely skewed data.
Non-parametric tests are another way to test for differences between non-normal data. Following the recommendation of Robson et al. (2000), the Mann-Witney *U* test and the Kruskal-Wallis test are used to test for a step change when the time of change is assumed known. The Mann-Witney (MW) test is a non-parametric alternative to the *t* test. It is the most powerful of the non-parametric alternatives to the *t* test. The Kruskal-Wallis (KW) ANOVA test assesses the hypothesis that the different samples are drawn from the same distribution or from distributions with the same median. The interpretation is basically identical to that of the parametric ANOVA, except that it based on ranks rather than values.

3 RESULTS

Box plots display the annual maxima for samples of the North Island (Figure 2-2) and South Island (Figure 2-3) records.
For the North Island, the boxplots for the three series in the upper row of Figure 2-2 show lower quantile values, and with the exception of the Ohinemuri maximum, lower maxima and minima. These catchments are located in the north and east of the North Island. The boxplots series in the lower row are for catchments in the southern half of the North Island. They indicate no consistent pattern of differences between the two periods.
For the South Island (Figure 2-3), the first two boxplots, for catchments in the northeast third of the island, indicate little difference between the two periods. The remaining four boxplots indicate generally increased quantile values, and higher maxima and minima, most notably for those in the south and southwest.
The *t* test for log transformed data, the MW test and the KW tests all rejected, at the 5% level, the null hypothesis of no significant difference for the South Island catchments indicated in Figure 3-1.

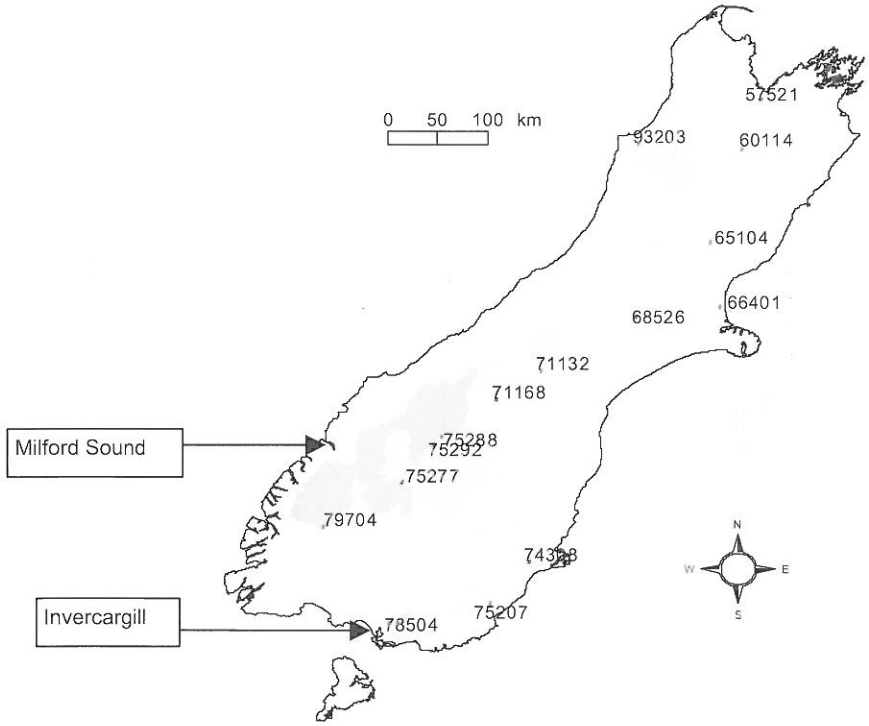

Figure 3-1: South Island catchments (shaded diagonally) for which the Mann-Witney *U* test, the Kruschel Wallis ANOVA and the two-sided *t* test for the log-transformed series were all significant at the five percent level. Milford Sound and Invercargill are locations of two raingauges referred to in the text.

4 DISCUSSION

The box plots convey an overall impression of each series and the changes, if any, of their distributions before and after 1978.
The rivers that drain catchments in the northeast of the North Island (Figure 2-3) show some shifts. The IQR for the post 1978 data is tighter than for the pre-1978 plot and the range of the data tends to be less. This is most pronounced for station 15412 (Rangitaiki at Te Teko), but there is little change in the median. The *F* tests for both natural and log-transformed data suggested that the differences between the variances for the two periods for these series are significant. On the other hand, none of the non-parametric tests indicated any reason to reject the null hypothesis of no difference between the two periods. As longer streamflow records are sparse in the northern half of the North Island, the extent to which the apparent shift extends over the north and northeast is not well defined by the river flow data.
The statistical tests flag the shifts in the south and southwest as being significant at the 5% level. The shifts are most severe for 79704 (Lake Te Anau) and 78504 (Waihopai), the southern-most catchments.
Examination of relevant daily rainfall records supports the apparent shift in the hydrological regime. For example, a rainfall record for Invercargill (see Figure 3-1 for location) is a good proxy indicator for flows in the Waihopai River. The mean annual rainfall for 1947-1977 was 1046 mm, whereas the mean annual rainfall for 1978-1999 was 1138 mm, a 92 mm (9 percent) increase. (This is consistent with the increase in mean runoff for the Waihopai which is 126 mm, or 31 percent.) The number of days per year with rainfalls exceeding various thresholds of extreme daily rainfalls for Invercargill for two periods is illustrated in Figure 4-1. This shows that there were many more occurrences of extreme daily rainfalls in the later period. For example, there was one day in the 31 year period 1947-1977 when the daily rainfall exceeded 50 mm, but ten days in the 1978-1999 period. (The largest flood in the record 200 m^3/s, in January 1984, was due to a daily rainfall of 134 mm, more than twice the maximum of the 1947-1977 daily rainfalls. In terms of insurance claims, this was the most damaging flood that has occurred in New Zealand.)

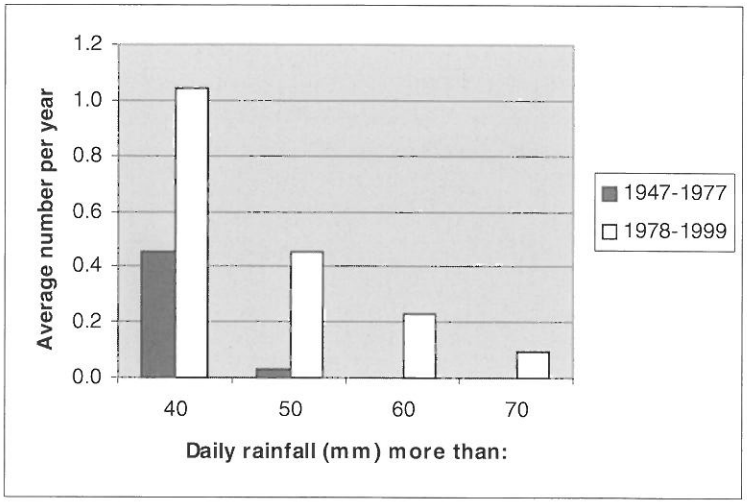

Figure 4-1: Occurrences of extreme daily rainfall at Invercargill, for 1947-1977, and 1978-1999.

The Milford Sound (see Figure 3-1 for location) rainfall is a good proxy indicator for inflows into Lake Te Anau and other South Island lakes. The apparent increase in the mean annual Milford Sound rainfall is from 6060 to 6920 mm/yr, an increase of 860 mm/yr (14%). The number of days per year with rainfalls exceeding various thresholds has also increased (Figure 4-2).

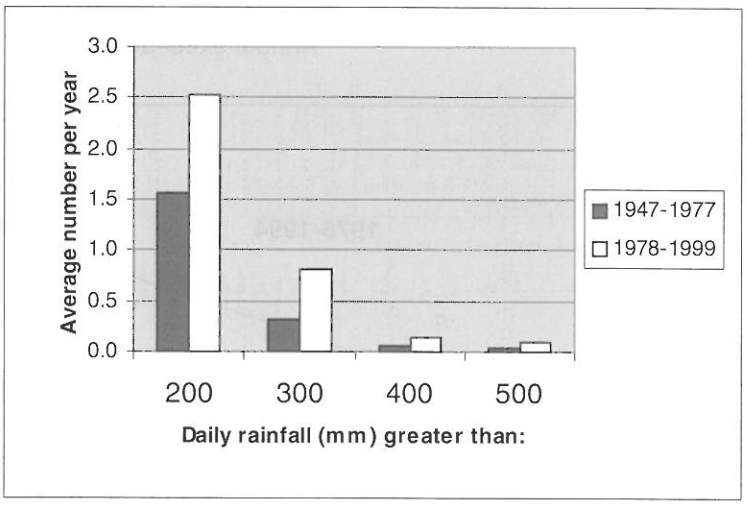

Figure 4-2: Occurrences of extreme daily rainfall at Milford Sound for 1947-1977, and 1978-1999 (No data Oct 70-Dec 71).

The consequences of the shifts for design flood estimates are illustrated in Figure 4-3, which presents the frequency analysis of the pre-and post-1978 data for Waihopai and Te Anau using the Gumbel (Extreme Value type 1) distribution fitted using the method of Probability Weighted Moments (McKerchar and Pearson, 1990). The Waihopai 1 in 100 AEP estimate is almost doubled, from 64 to 119 m^3/s: this is much more than the 95% confidence limits for the estimates. The Te Anau increase is from 2780 to 3560 m^3/s, a 28% increase. The 95% confidence limits for the Te Anau estimates overlap, but probably would not, if the next five years of the Te Anau data (1995-1999), which include several notable floods, were available.
Finally, the result is consistent with the conclusions in Salinger and Mullan (1999) that rainfall in the northeast of the North Island has decreased and rainfall in the west and south of the South Island has increased since 1978 as a consequence of a shift in the IPO.

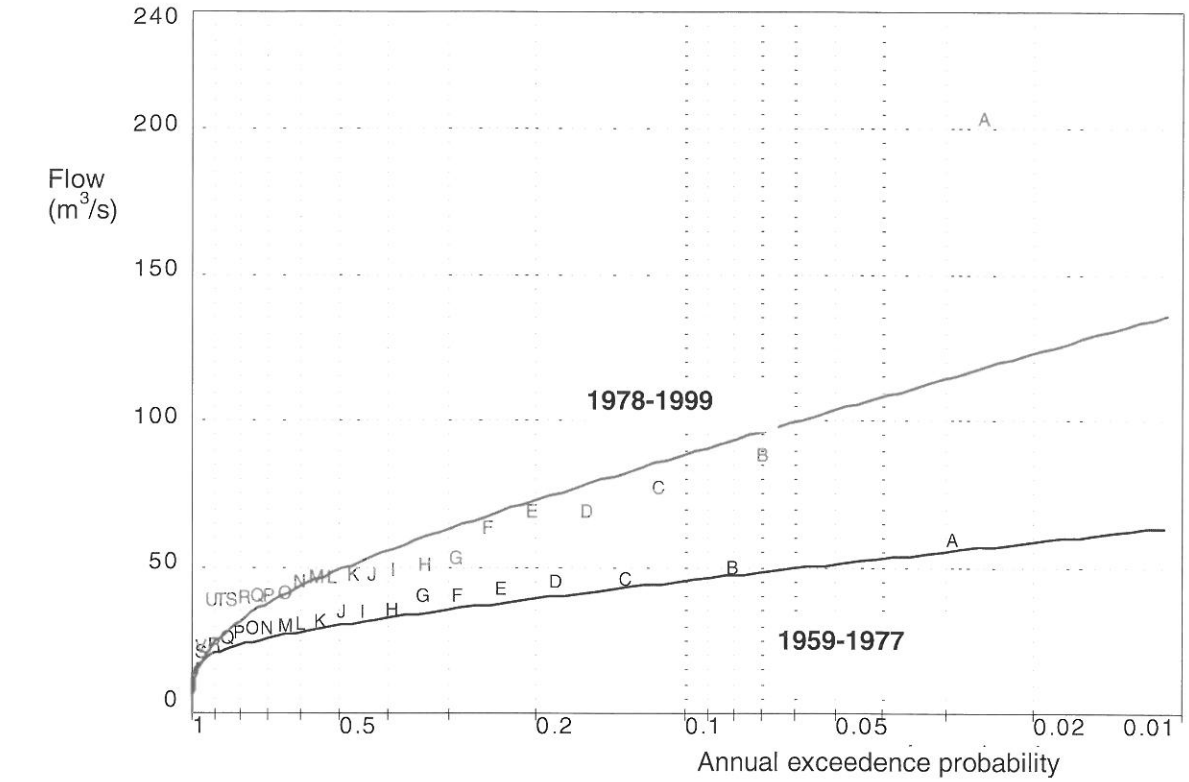

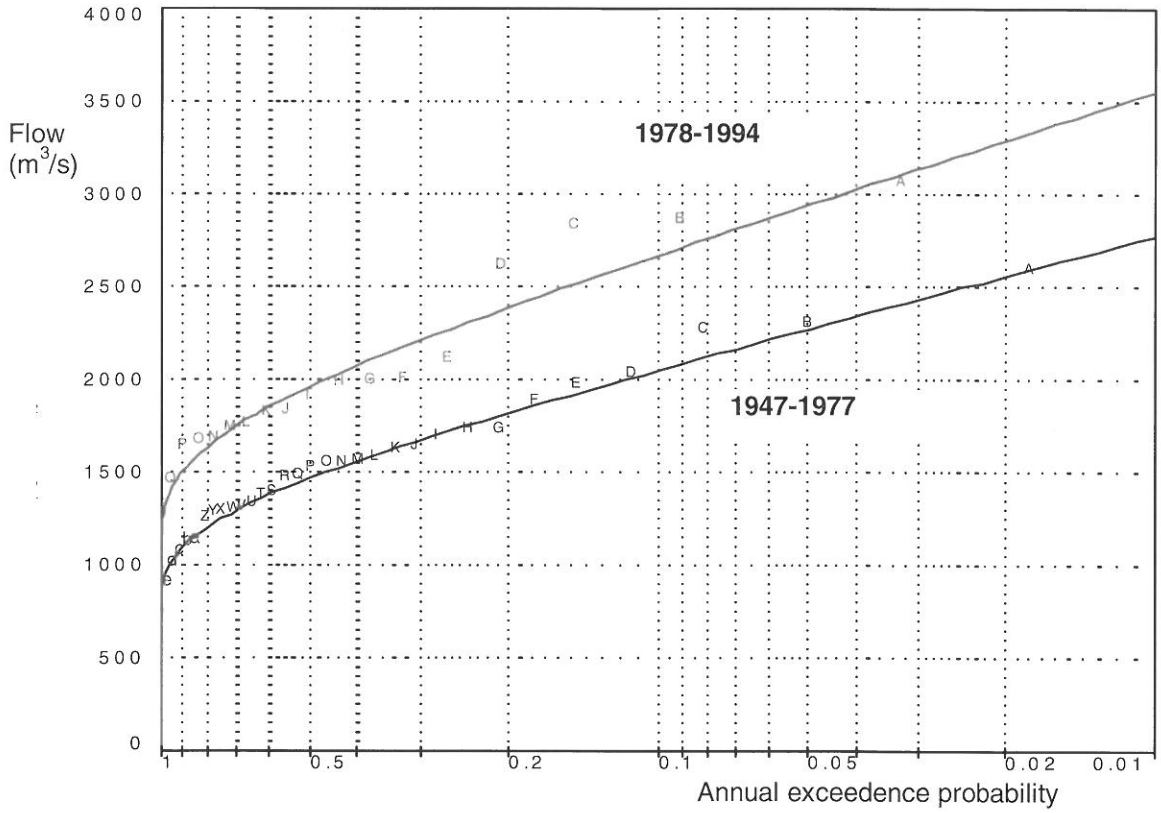

Figure 4-3: Flood frequency analysis for the Waihopai River (upper) and Lake Te Anau (lower) 3 day annual maxima for 1947-1977 and 1978-1999. The lines are Gumbel (Extreme Value type 1) distributions fitted using Probability Weighted Moments.

5 CONCLUSIONS

Less severe floods have occurred since 1978 in the northeast of the North Island. The areal extent of this shift has not been well defined.
More severe floods have occurred since 1978 in the southern two thirds of the South Island, and changes are most pronounced in the south and west of the South Island. Statistical tests indicate that the increases are unlikely to be a chance occurrence.
The shifts in hydrological regime are consistent with changes observed in rainfalls and are attributed to changes in the frequencies in ENSO extremes, due to a shift in the IPO in 1977/1978.
The increases are large enough to justify reassessing flood frequency in this region.
No significant consistent changes are evident elsewhere in the country.

ACKNOWLEDGEMENT

Regional Councils (Environment Bay of Plenty, Environment Waikato, Horizons Manawatu, Environment Canterbury, Environment Southland) are thanked for contributing data. Kathy Walter organised assembly of the data. The work is funded by the Foundation for Research Science and Technology under contract no. CO1X0014.

REFERENCES

Helsel, D.R., Hirsch, R.M. (1992): Statistical methods in water resources. Elsevier Science, Amsterdam, 522p.

Henderson, R.D., Thompson, S.M. (1999): Extreme rainfalls in the Southern Alps of New Zealand. Journal of Hydrology (New Zealand) 38(2): 309-330.

McKerchar, A.I., Pearson, C.P. (1990): Flood estimation maps for New Zealand. Hydrological Sciences Journal 35(6): 609-621.

Mantua, N.J. et al. (1997): "A Pacific interdecadal climate oscillation with impacts on salmon production" Bulletin of the American Meteorological Society 78: 1069-1079.

Mosley, M.P., McKerchar, A.I. (1993): Streamflow. Chapter 8 in: Handbook of Hydrology (Maidment, D.R., Editor-in-chief). McGraw-Hill.

Robson, A. et al. (2000): "Statistical methods for testing for climate change". Chapter 5 in: "Detecting trend and others changes in hydrological data". (Z.W. Kundzewicz and A. Robson, Editors), World Climate Data and Monitoring Programme. World Meteorological Organisation. WCDMP - 45, WMO/TD-No.1013, p. 49-67.

Salinger M.J, Mullan, A.B. (1999): New Zealand climate: temperature and precipitation variations and their links with atmospheric circulation 1930-1994. International Journal of Climatology, 19: 1049-1071.

Walter, K.M. (2000): Index to hydrological recording stations in New Zealand. NIWA Technical Report 73. NIWA, Wellington, 216p.

ESTIMATING FLOOD PROBABILITIES AT THE REGIONAL SCALE

Ralf Merz, Günter Blöschl

Institute of Hydraulics, Hydrology and Water Resources Management, Vienna University of Technology, Karlsplatz 13/223, A-1040 Vienna, Austria, merz@hydro.tuwien.ac.at

SUMMARY

This paper proposes a geostatistical approach to flood regionalisation which takes into account the uncertainty of flood estimation due to a short sample size and uses regional information on the basis of spatial distance. This method is compared to various extreme value statistical methods based on product moments and L-moments and the Gradex method. The predictive performance of the different methods is examined by a jackknifing approach for flood quantiles of different return periods which allows a realistic assessment of the estimation error for ungauged catchments.

Keywords: Flood regionalisation, Geostatistics, Gradex

1 INTRODUCTION

The statistical estimation of flood quantiles for catchments with observed flood data is limited by two uncertainties. The first uncertainty is due to a relatively short length of the observed flood data series compared to the return period of interest (Gutknecht, 1994). The second uncertainty is due to the choice of distribution function and parameter estimation method (Schreiber 1970; Hosking and Wallis, 1997). One possibility for reducing these uncertainties, in order to improve the estimation of floods associated with large return periods, is the use of regional information from nearby catchments (e.g. Kirnbauer, 1981). If 5 catchments with 30 years of observation each are pooled into a group, the available sample size is extended to 150 years under the assumption of statistical independence and regional homogeneity. In ungauged catchments where no observed flood data are available, regional information can be used in a similar manner for estimating flood frequencies. In this case, an additional source of uncertainty comes in as a result of the regional transposition (Blöschl, 1999). Hydrological similarity is a measure that is inversely related to the degree of uncertainty due to the regional transposition of hydrological information. When hydrologically similar catchments are used for the transposition, little uncertainty is introduced. There are two main types of methods for the regionalisation of flood frequencies to gauged and ungauged catchments. The first type applies geographical distance as a similarity measure or uses geographically contiguous regions (Dalrymple 1960). The second type uses catchment characteristics (or attributes) as, for example, in regressions of flood data with catchment area, annual rainfall, and combinations thereof (e.g. Fill and Stedinger 1998), which implies regions that are not necessarily geographically contiguous.
The aim of this study is to assess the predictive performance of various methods of regional flood frequency estimation. What is clearly of utmost interest to any practitioner is the optimum choice of methods and data as a function of purpose, hydrological conditions of the region under study, and data constraints. As data availability is often a limiting factor in practical projects, we focus in this paper on geostatistical methods using only the time series of flood data and the location of the catchments. Additionally we examine the Gradex method which uses rainfall data as additional information. The predictive performance of estimating flood quantiles in ungauged catchments by these methods is assessed using a jackknifing approach.

2 DATA BASE

The analysis is based on (a) the series of the observed maximum annual flood peaks of Austrian catchments with an area from 10 to 1000 km^2 and (b) the coordinates of the centroids of these catchments.
(a) In a first step, we screened the maximum annual flood peaks for data errors and removed all anthropogenically affected stations from the data set (Piock-Ellena & Blöschl, 1998). This resulted in flood series for 597 catchments with observation periods from 15 to 44 years, which were used in the further analysis. To reduce the effects that differences in catchment area might have on the regional patterns of flood frequency the specific flood discharges were standardised to represent specific discharges of a hypothetical catchment area of 100 km^2 according to

(1) $$q_{100} = q_A \cdot A^{0.25} \cdot 100^{-0.25}$$

where q_{100} is the specific discharge for a 100 km^2 catchment and q_A is the observed specific discharge of a catchment of area A (km^2).
(b) The coordinates of the centroids for the 597 catchments were derived from digital catchment boundaries. Two data sets were used. Most of the catchment boundaries were derived from a digital database of catchment boundaries digitised from the Austrian 1:50000 scale map (ÖK 50) (Behr et al., 1998). The remaining boundaries were derived from a digital elevation model (Rieger, 1992a,b; Rieger 1999). All catchment boundaries were checked manually using the ÖK 50.

3 ESTIMATION OF UNCERTAINTY AND GEOSTATISTICAL ANALYSIS

A first spatial analysis of mean annual flood discharges (1st moment) calculated from the flood data revealed pronounced spatial patterns with high values in the western part and small values in the eastern part of Austria. The patterns of the coefficient of variation (2nd moment) are more erratic, i.e. there is a larger degree of randomness. The spatial variability of the skewness (3rd moment) is mainly erratic with essentially no coherent patterns. It is clear that this spatial variability is a result of two sources, natural hydrological heterogeneity and random variability due to a relatively short period of observation. The increasing scatter with the order of the moment is due to the increasing random variability in calculating the flood moments for short periods of observation. To examine what is the variability due to short observation periods and what is hydrological variability in Austria we used Monte Carlo simulations. Samples of different sizes were drawn randomly from a Gumbel (EV1) distribution (mean annual flood = 0.3 m^3/(s*km^2), CV=0.5), which, on average, fits well the Austrian flood data. The moments for each of the samples as well as the variance of the moments between the samples were calculated and have been plotted against sample size in Figure 3-1. As expected, the Monte Carlo simulations give a decreasing variance with increasing sample size for all three moments. The variance of the moments and thus the uncertainty due to a short observation period increases significantly with the order of the moment as shown in Figure 3-1.

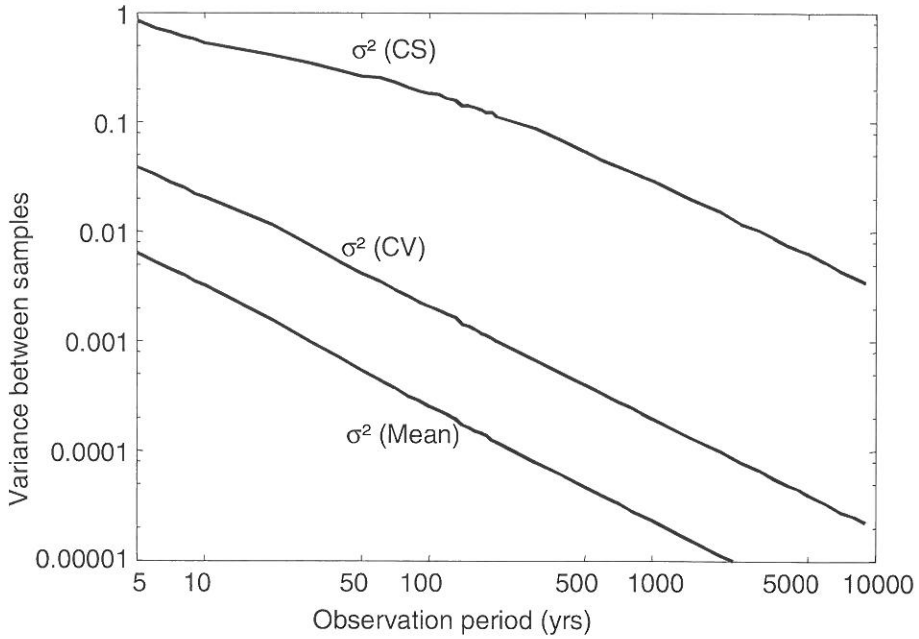

Figure 3-1: Variability between sample moments calculated from Monte Carlo simulations.

In the regionalisation (or spatial interpolation) step of the flood moments, the uncertainty due to short observation periods should be removed, while the hydrological heterogeneity should be retained. In the Ordinary Kriging approach (OK), the nugget of the variogram can be interpreted as the sum of the uncertainty due to short observation periods and the hydrological heterogeneity of adjacent catchments (de Marsily, 1986; Blöschl and Grayson, 2000). As ordinary kriging uses the same variogram throughout the domain, it is not possible to account for differences in record length in different stations. We are proposing here a method which does allow to account for differences in record length. To

consider different uncertainties or errors at different measurement points the kriging equations were *modified. In the case where the errors* ε_i associated with each measurement Z_i are non-systematic, uncorrelated with each other and with Z and have a known variance σ_i^2, the kriging system becomes (de Marsily, 1986),

$$\sum_j \lambda_0^j \gamma(x_i - x_j) - \lambda_0^j \sigma_i^2 + \mu = \gamma(x_i - x_o) \qquad \text{i=1,...,n.}$$

(2)

$$\sum_i \lambda_0^i = 1$$

The function $\gamma(x_i - x_j)$ is the true variogram value of the magnitude Z (without errors) for the measurement points x_i and x_j, λ^i are the weights of the kriging estimator. The estimate Z_0 is a weighted sum of the available measurements Z_i: $Z_0 = \sum_i^n \lambda_0^i Z_i$. To remove the uncertainty due to short observation periods, we used the variance between the sample moments from the Monte Carlo simulations (Figure 3-1) as the variance of the errors:

$$\sigma^2(moment) = a * n^{-b} \qquad (3)$$

where *n* is the number of recorded years in a catchment. Kriging with uncertain data (KUD) allows the spatial interpolation of the flood moments where the sampling variance is taken into account.
To apply the two geostatistical methods (OK and KUD) for flood regionalisation, we performed a variogram analysis of the flood moments. The lags of the variograms are based on the centroids of the catchments. Next, an exponential variogram (de Marsily, 1986) was fitted to the observed variograms, which gave a range of 60 km for the first three moments which was used in all interpolations. The nugget of the variogram was set to zero which implies no natural hydrological spatial variability in the moments at very small scales.
The product moments (mean annual flood, CV, CS) were interpolated using ordinary kriging (OK) and kriging with uncertain data (KUD). The error variance σ_i^2 for each station was taken as (3) which was obtained from a best fit in Figure 3-1. The parameters a and b for traditional product moments (PM) and L-Moments (LM) are shown in Table 3-1. For comparison, an additional scenario was examined where L-moments (Hosking and Wallis, 1997, Stedinger et al., 1993) were calculated and spatially interpolated. The Monte Carlo simulations were repeated for the L-moments.

Table 3-1: Parameters for the error variance σ_i^2 as a result of a short record length.

Moment	Mean – PM	CV – PM	CS - PM	Mean - LM	CV - LM	CS - LM
a	1.3	1.18	10.47	0.03	0.01	0.005
b	-1	-0.96	-1	-10.3	-1.1	-1.1

As the L-moments put more weight on samples that are near the median than on extreme values, the variances between samples are smaller than the variances between samples based on product moments. Extreme values have a relatively minor effect on the calculated L-moments and thus the estimation of the moments is more robust, particularly for short observation periods. However, L-moments are based on the assumption that the observed values near the median have more predictive power for extreme situations than observed extreme values.

4 DERIVED FLOOD FREQUENCY APPROACH

To examine the value of additional information (i.e. rainfall data) a variant of the Gradex method was applied (Guillot, 1972; Duband et al., 1994). At the heart of the method is the assumption that the average maximum storage capacity of the catchment is reached at a return period T_G. The storage capacity is the difference between catchment rainfall and flood runoff. From this assumption follows that for rainfall events greater than the storage capacity the catchment can be assumed to be completely saturated and additional rainfall produces a corresponding increase in runoff, i.e.

$$Qm_T - Qm_{Tg} = \left(N_T{}^{Geb} - N_{Tg}{}^{Geb}\right) \cdot A \tag{4}$$

where Qm_T is the average flood runoff over the time interval H with a return period $T > T_G$ and Qm_{Tg} is the corresponding runoff with a return period T_G (i.e. where saturation occurs). $N_T{}^{Geb}$ and $N_{Tg}{}^{Geb}$ are catchment rainfall for return periods T and T_G, respectively. Both rainfalls are associated with a duration H. A is catchment area. The assumption (4) is a statistically weak point of the method, because rainfall of a given probability does not necessarily cause a runoff of the same probability (Blöschl and Sivapalan, 1997; see also Figure 3-2 in Vol. 4 of Institute of Hydrology, 1999). The flood peak Qs is then calculated by

$$Qs_T = r \cdot Qm_T \quad \text{and} \quad Qs_{Tg} = r \cdot Qm_{Tg} \tag{5}$$

The r-value in Eq. 5 is the ratio of the flood peak to the mean runoff over a time interval H and is a measure of both the runoff dynamics of the catchment and the temporal distribution of rainfall. Flashy catchment response and spiky temporal rainfall patterns are both associated with large r-values.
When plotted in a graph, these assumptions imply that beyond the return period T_G the flood probability function Q_T is parallel to the transformed extreme rainfall probability function Q_N. The extreme rainfall N is transformed into the units of runoff [m³/s] by

$$Q_N = N \cdot A \cdot ARF \cdot r \tag{6}$$

where ARF is the areal reduction factor for rainfall. Flood probabilities with a return period $T \leq T_G$ are obtained from a frequency analysis of the observed floods while floods with $T > T_G$ are obtained from a parallel line to the transformed extreme rainfall probability function.
To apply the Gradex method in Austria, annual maximum daily precipitation for 922 stations was used as rainfall input and the curve I of Hershfield (1968) was used as the areal reduction factor to calculate catchment rainfall. To determine extreme rainfall in a catchment, the statistical moments of the series of the annual maximum daily precipitation (mean and standard deviation) were estimated and spatially interpolated by the kriging method. By overlaying the spatial interpolation of the moments and the digital catchment boundaries, the moments of the areal rainfall were derived. The probability of rainfall was assumed to be Gumbel distributed. The r-values were calculated from the assumption that the time of concentration is only a function of catchment area, and the following relationship was used (Merz et al. 1999):

$$tc = 2 \cdot A^{0.35} \tag{7}$$

where t_c is the time of concentration (hrs) and A is catchment area (km²). For a better comparison of catchments of different size, discharges were standardised to a catchment size of 100 km² by

$$Q_{red} = Q(A) \cdot \frac{ARF(100km^2) \cdot r(100km^2)}{ARF(A) \cdot r(A)} \tag{8}$$

where Q_{red} is the flood discharge for a catchment size of 100 km² and $Q(A)$ is the flood discharge for a catchment size of A. For return periods $T \leq Tg$ = 10 years, flood probabilities were calculated from the flood moments based on a Gumbel distribution, while for probabilities $T > Tg$ the flood probabilities were calculated from rainfall by the Gradex method.

5 INTERCOMPARISON AND PREDICTIVE PERFORMANCE

The predictive performance of the three methods has been assessed in this intercomparison by a jackknifing approach. It is important to note that this approach only examines the error due to the regionalisation to ungauged catchments. Other error sources such as the extrapolation to large return periods are not considered in this approach. However, the regionalisation error is usually significantly larger than other error sources as long as the return period is not much larger than the observation period. In the jackknifing approach we assumed that no flood data are available for a particular gauged catchment. We then estimated the T-year flood from neighbouring catchments only. Next we compared the regional estimate so obtained with the estimate derived from local extreme value analysis using the flood data and a GEV distribution. We repeated this procedure for every catchment in turn. This allowed us to obtain a regional estimate for each gauged catchment from which an error estimate could be derived for each catchment.
For a visual appreciation of the spatial patterns as produced by the various regionalisation methods, we have interpolated the spatial Jackknifing estimates (i.e. estimates with only regional information) to obtain spatial flood frequency patterns of the study area. Figure 5-1 shows the local estimates using local flood data (left) and the Jackknifing estimates (without using local flood data) (left) in terms of the specific 100 year floods (m³/s/km²) standardised to a catchment area of 100 km^2 .

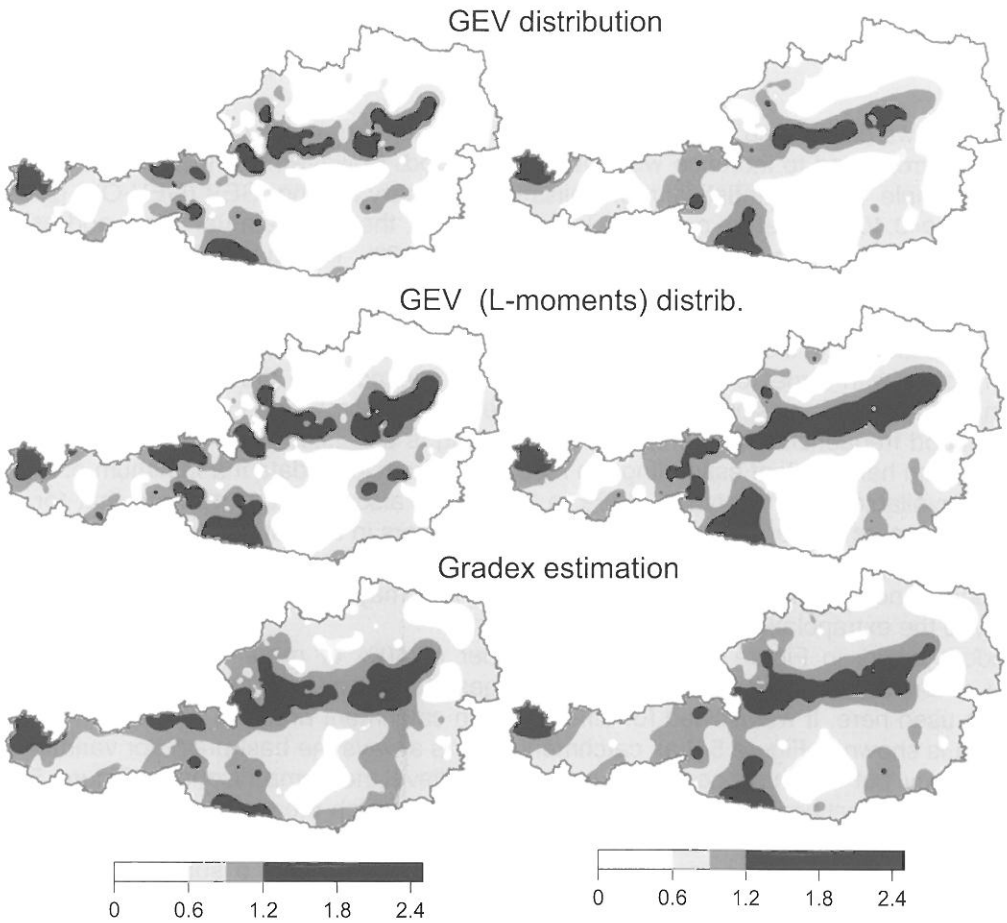

Figure 5-1: Specific floods (m^3/s/km^2) standardised to a catchment area of 100 km^2 for a return period of 100 years. Geostatistical (top: GEV product moments, centre: GEV - L-Moments) and derived flood frequency (Gradex) (bottom) local estimates (left) and regionalisation results using Jackknifing (without using local flood data) (right).

The patterns of the specific 100 year floods estimated by the GEV distribution with product moments and L-Moments are similar with high values at the northern part of the central Alps and low values in the lowlands of eastern Austria. The patterns of the regional estimation (left) using jackknifing are smoother than the patterns of the local estimation. This is because the spatial heterogeneity of adjacent catchments due to short observation periods has been removed.
The patterns of the Gradex derived flood frequencies (bottom) are a combination of the rainfall and discharge patterns. Due to the assumption of saturation for high return periods the Gradex values are significantly higher than the results of the geostatistical approaches.
To compare the predictive performance of the different approaches we performed a detailed error analysis. Specifically, we examined bias and random error of the regional estimates. The bias *nme* was defined as the normalised mean error:

$$nme = \frac{1}{n}\sum_{n}(\hat{q}_{100} - q_{100}) \Big/ \frac{1}{n}\sum_{n} q_{100} \tag{9}$$

where q_{100} is the observed T-year flood discharge $\hat{q}_{100}$ is the regionally estimated T-year flood discharge and n is the number of catchments. Note that q_{100} and $\hat{q}_{100}$ are specific discharges standardised to a nominal catchment area of 100 km^2 according to equation (1) in order to give equal weights to small and large catchments. The subscript 100 relates to the nominal catchments area. The random error *nsdve* was defined as the normalised standard deviation of the error:

$$nsdve = \sqrt{\frac{1}{n}\sum_{n}\left[(\hat{q}_{100} - q_{100}) - \frac{1}{n}\sum_{n}(\hat{q}_{100} - q_{100})\right]^2} \Big/ \frac{1}{n}\sum_{n} q_{100} \tag{10}$$

Figure 5-2 shows biases and random errors plotted versus the return period. As would be expected, the random errors tend to increase with the return period. However, this increase is relatively moderate. For example, the geostatistical regionalisation (Ordinary Kriging, GEV (GEV-OK) gives a random error of *nsdve*=0.40 for a return period of T=2.3 years (i.e. the mean annual flood) and *nsdve*=0.41 for a return period of T=100 years. This is an increase of only 3%. This means that by far the largest error source in flood regionalisation is the regional transposition of the mean annual flood and the extrapolation to larger return periods introduces relatively little error. From a practical perspective it will therefore be essential to also use flood data from stations with very short record lengths (e.g. 5 years). Although floods with large return periods cannot be derived from these stations, the estimation of mean annual floods is possible with relatively little uncertainty, which can improve the regional estimation of flood frequencies tremendously. This finding is consistent with the suggestions in the UK-flood estimation handbook of estimating the index flood from local data if a minimum of 2 years of run-off data is available (Inst. of Hydrol. 1999, p.1/18). It is also important to note that for large return periods (>100 years) the errors cannot be considered errors in a strict sense as the local estimate will also be associated with some uncertainty. Rather these errors should be considered as differences between local and regional estimates and the differences may be partly due to the regional estimation and partly to the extrapolation to large return periods.
The random errors in Figure 5-2 are on the order of 40% or more, which is a significant error. However, it should be noted that specific discharges (standardises to a catchment size of 100 km^2) have been used here. If we allowed for differences in catchment area the errors would be only about half of what is shown in Figure 5-2 as catchment area is always the best predictor variable for regional flood frequency but has not been used here. We believe the comparisons in Figure 5-2 are more meaningful than direct comparisons of flood discharges in which the errors tend to be dominated by a few large catchments that are often of less interest than small catchments. The biases in Figure 5-2 are smaller than the random errors although some methods do give a substantial bias. Root mean square errors will therefore be similar to the random errors.

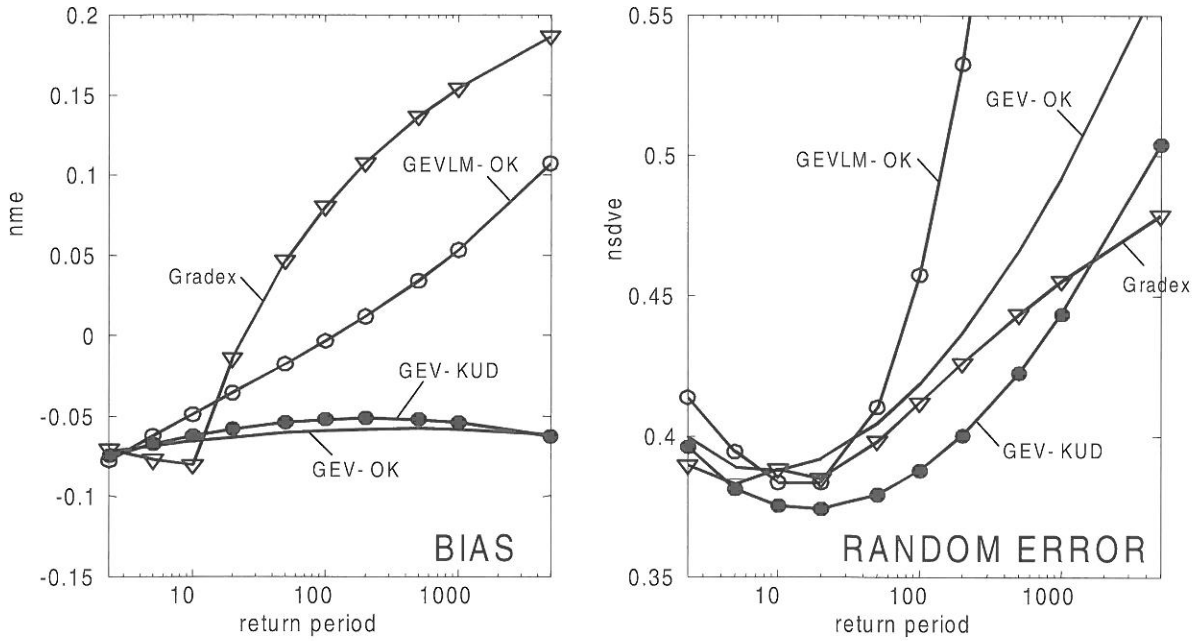

Figure 5-2: Errors of regional flood frequency estimates for ungauged catchments evaluated by jackknifing. Ordinary kriging (OK) (without markers: GEV product moments, open circles: GEV L-Moments), Kriging with uncertain data (KUD) using GEV (full circles), derived flood frequency (Gradex) method (Triangles).

The predictive performance of the various regionalisation methods as assessed by jackknifing gives the following results (Figure 5-2): The geostatistical regionalisation method kriging with uncertain data (KUD) has the smallest bias and the smallest random error. This is likely due to the declustering properties of geostatistics and the method accounting for record length. Ordinary Kriging (OK) has a similar small bias, but the random error is considerably higher. This suggest that OK sometimes over- and sometimes underestimates the flood quantiles which gives on average a small bias. GEV with linear moments (GEV-LM) gives larger errors at high return periods than GEV with product moments. In some catchments the specific shape of the flood frequency curve with a positive curvature around the median of observed floods causes a high skewness due to the emphasis on the median observed floods of the L-moment approach. The high skewness in turn tends to give higher flood quantiles for large return periods than an estimate based on product moments.

The derived flood frequency (Gradex type) method combines flood data and rainfall information. For small return periods the regional Gradex approach is a simple geostatistical approach using a Gumbel distribution, while as one moves to more extreme events, rainfall dominance tends to take over from catchment dominance. In the jackknifing approach we do not use local flood data but local rainfall information. Thus the local and regional estimates at high return periods are dominated by the same rainfall information and the error analysis gives a small bias and a small random error. As this analysis is not very meaningful, we compared the regional Gradex estimates with local extreme value statistics using a Gumbel distribution in Figure 5-2. The results of the error analyis can now be interpreted as a difference between a method based only on flood data and a method using additional information. The Gradex method shows some bias and a small random error. The bias is positive, so the method gives estimates that are 'on the safe side' which is a result of the assumption of saturation.

To asses the value of an approach that accounts for record length, we compared the reduction of the random error of the methods compared to an ordinary kriging method using only stations with records longer than 20 years. The jacknifing analysis was performed for those catchments that can be assumed to be not affected by a short flood data sample and compared with the KUD results. Figure 5-3 shows the reduction in the random error when including stations with short record lengths as compared to OK with long series only. For return periods lower than 40 years OK with short and long series will reduce the random error. For a return period of 2 years, for example, the random error is 10% smaller than when using long series only. However, for longer return periods the random error is higher (hence a negative reduction in Figure 5-3). This means that for the regionalisation of flood quantiles associated with a return period of less than 40 years with ordinary kriging, all stations should be used. For quantiles higher than 40 years only stations with longer observation records should be used in the kriging procedure. However, the kriging with uncertain data (KUD) approach proposed

here reduces the random error for all return periods. For regionalising flood quantiles the latter method is therefore recommended.

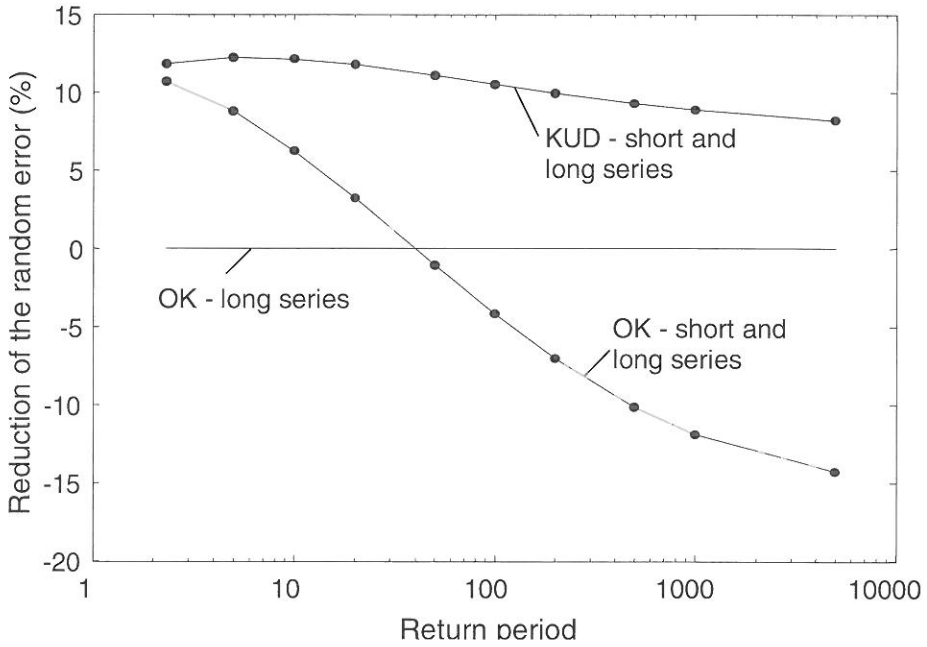

Figure 5-3: Importance of the use of stations with short record length for regionalisation. Reduction of the random error (%) of ordinary kriging (OK) with station of short and long observation periods and kriging with uncertain data (KUD) as compared to OK with stations of long observation periods only.

6 CONCLUSIONS

This intercomparison has examined the predictive performance of geostatistical regionalisation methods based on jackknifing techniques which assesses the errors due to regionalisation only. The kriging with uncertain data (KUD) approach proposed here takes the uncertainty due to short record lengths into account. The jackknifing analysis showed that the proposed method has a smaller random error than the traditional geostatistical methods and a similar bias. Additionally the Gradex method was examined which gives reasonable results in Austria although it has a bias towards overestimating flood quantiles. The geostatistical methods analysed in this paper are simple and only need minimum data. However we anticipate that more complex methods based on process understanding and more extensive data will allow more accurate regional flood estimates. Work on these more complex methods is in progress.

REFERENCES

Behr, O., Blöschl, G., Piock-Ellena, U. (1998): "A digital data base of catchment characteristics for assessing anthropogenic effects on flood processes". Annales Geophysicae. European Geophysical Society., Katkenburg-Lindau, Supplement II to Vol. 16, p. C507.

Blöschl, G. (1999): Scaling issues in snow hydrology. Invited Keynote paper at the International Conference on Snow Hydrology, Brownsville, Vermont, organised by the CRREL, Hanover, NH, Oct. 6-9, 1998, Hydrol.Processes,Chichester, 13,149-2175.

Blöschl, G. & Grayson, R. (2000): Spatial observations and interpolation. Chapter 2 in R. Grayson and G. Blöschl (Eds.) Spatial Patterns in Catchment Hydrology: Observations and Modelling. Cambridge University Press, Cambridge, pp. 17-50.

Blöschl, G. & Sivapalan, M. (1997): Process controls on regional flood frequency: Coefficient of variation and basin scale. Wat. Resour. Res., Washington, D. C., 12, 2967-2980.

Dalrymple, T. (1960): Flood frequency methods. U.S. Geol. Surv., Washington D.C., Water Supply Pap. 1543-A, 11-51.

de Marsily, G. (1986): Quantitative Hydrogeology. Academic Press Inc., San Diego, 440 pp.

Duband, D. et al. (1994): Design flood determination by the Gradex method, CIGB, ICOLD; Paris, 96 pp.

Guillot, P. (1992): Application of the Method of Gradex, in: Schulz E.F., Koelzer V.A. and Mahmood K. (Ed.), Floods and Droughts, Proceedings of the Second International Symposium in Hydrology, Fort Collins, Colorado, USA, Water Resources Publications, 44-49.

Fill H. D. and Stedinger J. R. (1998): Using regional regression within index flood procedures and an empirical Bayesian estimator. J. Hydrology, Amsterdam, 210, pp. 128-145.

Gutknecht, D. (1994): Extremhochwässer in kleinen Einzugsgebieten. Österr. Wasser- und Abfallwirtschaft, Wien, 46, 50-57.

Hershfield, D.M. (1968): Rainfall inputs for hydrological models. Proc. Bern Symp., Gentbrugge, IUGG No 78, 177-188.

Hosking, J. R. M. and Wallis J. R. (1997): Regional Frequency Analysis. Cambridge University Press, Cambridge, 224 pp.

Institute of Hydrology (IH) (1999): Flood Estimation Handbook. Institute of Hydrology, Wallingford.

Kirnbauer, R. (1981): Zur Ermittlung von Bemessungshochwässern im Wasserbau. Wiener Mitteilungen, Wasser-Abwasser-Gewässer. Band 42, TU-Wien, Wien.

Merz, R., Blöschl, G., Piock-Ellena, U. (1999): Zur Anwendbarkeit des Gradex-Verfahrens in Österreich. Österr. Wasser- und Abfallwirtschaft, Wien, 51, 291-305.

Piock-Ellena U., Blöschl, G. (1998): Abflußtypen-Klassifizierung als Basis für die Regionalisierung von Hochwässern. Zwischenbericht 1998, Österreichische Akademie der Wissenschaften (HÖ-12/97). Institut für Hydraulik, TU-Wien, Wien.

Rieger, W. (1992a): Hydrologische Anwendungen des digitalen Geländemodelles. Dissertation, TU-Wien, pp 97.

Rieger, W. (1992b): Automated River Line and Catchment Area Extraction from DEM Data. Proc. des 17. ISPRS-Kongreß, Washington, D. C., IAPRS, 28 (B4), 642- 649.

Schreiber, H. (1970): Über Methoden zur Berechnung der n-Jährlichkeit von Hochwässern. Österr. Wasserwirtschaft, Wien, 22, 138-153.

Stedinger, J. R., Vogel, R. M., Foufoula-Georgiou, E. (1993): Frequency analysis of extreme events. In: Maidment, D. R. (Ed.) Handbook of Hydrology. McGraw-Hill, New York.

SEASONAL FLOOD PROBABILITY FOR SOUTH CANTERBURY NEW ZEALAND RIVERS

David J. Painter

Department of Civil Engineering, University of Canterbury, Private Bag 4800, Christchurch, New Zealand,
painter@civil.canterbury.ac.nz

SUMMARY

It is common practice to estimate flood probabilities on an annual basis. If flood magnitude probabilities vary within a year, such results could be misleading. These differences need not necessarily arise from obvious flood process differences, such as snowmelt versus rainfall. And they might be operationally important: when expected damage varies within years (e.g. for cropped land); or when the particular time period of interest for flooding to occur is less than a year (e.g. a dam or bridge project construction site).
For the first time in New Zealand, a preliminary examination has been made of seasonal flood probabilities for four rivers in a region previously characterised by annual data best fitted by an annual maxima/EV2 approach. A peak-over-threshold/Generalised Pareto parametric approach was most promising for the seasonal data, and suggested within-year probability variation for some rivers.

Keywords: floods, flood estimation, seasonal floods, partial duration, Pareto

1 INTRODUCTION

In NZ, regional flood estimation techniques for operational purposes have been refined in a series of quasi-official publications, leading to the most recent, published in 1989. (Beable, McKerchar, 1982, McKerchar, Pearson, 1989). For most of New Zealand, the parametric approach used in these techniques to estimate annual flood probabilities led to Extreme Value Type 1 (EV1 or Gumbel) as the preferred probability distribution for extrapolating observed flood event data from rated river discharge sites to smaller annual exceedance probabilities than the data range. A quite small minority of gauging sites in particular regions provided data not well fitted by EV1, but apparently better fitted by EV2 distributions. One such area was South Canterbury, on the East Coast of South Island (Figure 2-1).
It is most common to estimate flood magnitude probabilities with the 'conditioning event' being the passage of one year (calendar year or hydrological year). Useful statistical techniques derived from extreme value theory do not proscribe the choice in this way; the conditioning event could also be the passage of one summer, one spring, or one January, for example. In principle, a month or a week could be the conditioning event, but the likelihood of threshold and independence difficulties, and non-occurrence of "floods", becomes greater as the chosen time period becomes shorter.
An underlying problem with many parametric approaches to flood magnitude probability estimation is too few data points to provide confidence in parameter estimates. The problem is neither better nor worse when a season, rather than a year, is the conditioning event. Gauged data periods for New Zealand rivers are short in comparison to some in Europe. There are now periods greater than 30 years available at some sites, sufficient to conduct preliminary analyses of the kind described in this paper.
Hydrological and catchment management reasons for considering seasonal flood magnitude probabilities include:

- Expected flood damage variation during a year e.g. land in agricultural or horticultural crops. This can affect benefit:cost analyses and priorities for flood control works.
- Vulnerability to flood damage during part only of a year e.g. a dam or bridge construction site. This can affect the choice of construction start time and duration.
- Flood probability variation within years complicates the results of annual maxima analyses.

If any of these reasons exist for a site or area, and there is some *a priori* reason to believe that within-year flood magnitude probability variation might be occurring, a seasonal analysis could be useful. The first two reasons were present for the study location, and the third was suspected.

2 LOCATION

Canterbury is one of the six regional government areas of South Island, New Zealand. South Canterbury is East of the main NE-SW mountain divide (the Southern Alps), and between approximately latitudes 44° S and 45° S (Figure 2-1). There were seven rivers studied, indicated by name in Figure 2-2, in which the dot symbols are approximately at the location of the discharge recording sites. Only data from the four rivers having the longest periods of record are presented here.
Some information about the rivers and their catchments is given in Table 2-1. Hydrographic information is summarised in Table 2-2 (in which dates are given as yymmdd). For this study, the two Orari River records from closely adjacent sites, with 69505 replacing 69506, were combined using changeover date 821231.

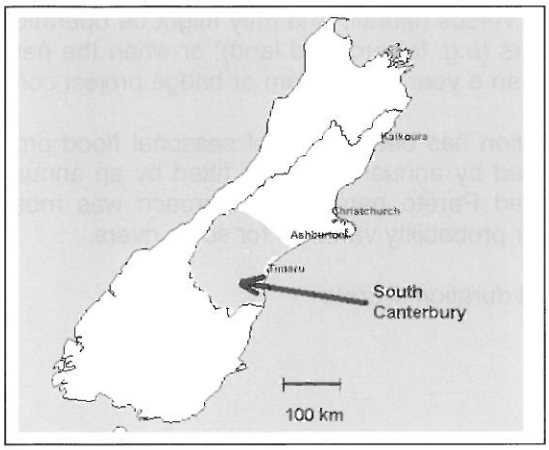

Figure 2-1: South Island, New Zealand, with Canterbury region boundary marked, and South Canterbury shown shaded.

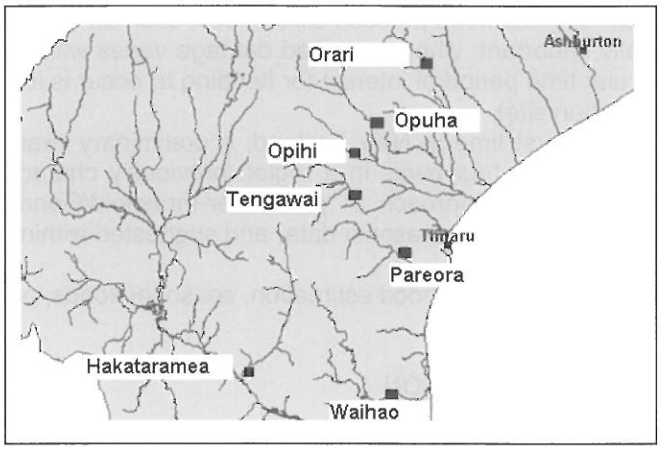

Figure 2-2: Approximate gauging site locations for seven rivers in South Canterbury.

Table 2-1: Catchment and flow data for four rivers; total length of record used 33 years 1966-98.

River	Catchment km^2	Mean Flow m^3/s	Mean Ann. Flood m^3/s
Hakataramea	896	6.1	191
Opihi	406	5.5	165
Opuha	458	9.7	204
Orari	520	10.6	215

Table 2-2: Hydrographic data for four rivers.

River	Site #	Levels Start	Levels End	First Rating	Last Rating	Gap Days
Hakataramea	71103	631231	990118	631126	981204	74
Opihi	69618	630701	990125	640511	970912	384
Opuha	69614	620301	990115	640801	980116	268
Orari	69506	650812	830613	640504		-
Orari	69505	820908	990107		981014	55

The climate in South Canterbury is temperate, with mean annual rainfall about 600 mm at Timaru (Figure 2-1), and much higher along the western mountain boundary. It is about 4000 mm at The Hermitage tourist hotel at Mt Cook, and up to about 8000 mm at high elevations in the mountains. Yellow-brown and yellow-grey earths and rendzina soils on plains areas (Cutler, 1968) overlie moderately indurated greywacke (quartzite), non-foliated schist and tertiary rocks (Mutch, 1963).

3 ANNUAL ANALYSES

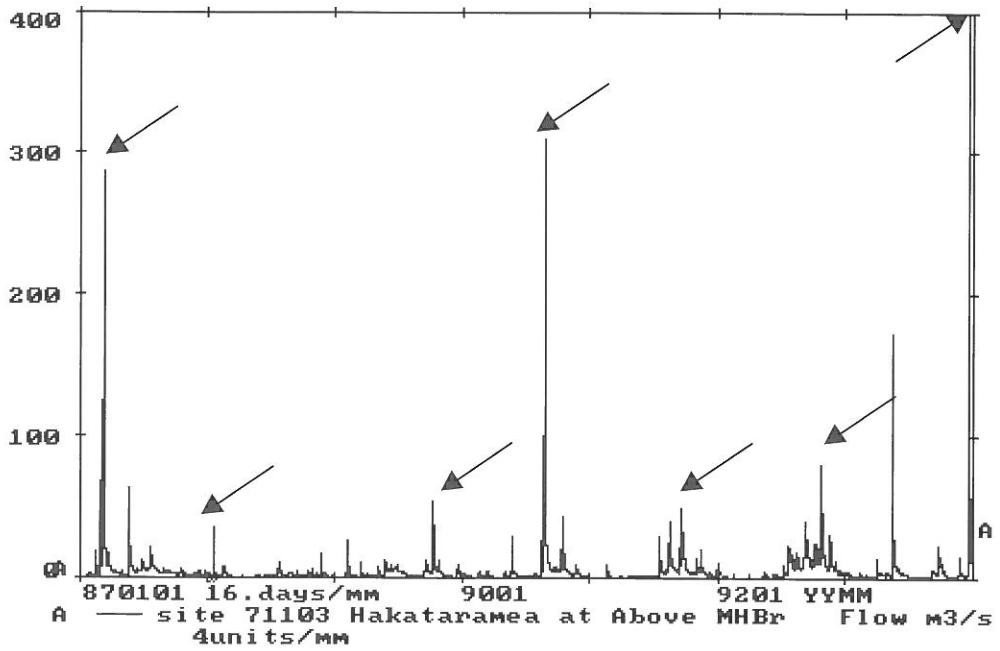

Figure 3-1: Discharge hydrograph 1987 to 1993, Hakataramea River, annual maxima arrowed.

Figure 3-1 shows part (7 years) of a record of discharge, converted from recorded stage heights using current meter ratings, for the Hakataramea River. Annual maximum flows are indicated by the arrows. Provided that a multi-peaked flood does not occur through a year change, in which case the last maximum in one year might not be independent of the first maximum in the next year, there is no particular difficulty in identifying the series of annual maxima.
An appropriate probability distribution for maxima of flood events is the General Extreme Value (GEV). The well-known and often used EV1, or Gumbel, distribution is the special case of GEV when the shape parameter, κ, is zero (Stedinger et al., 1993).

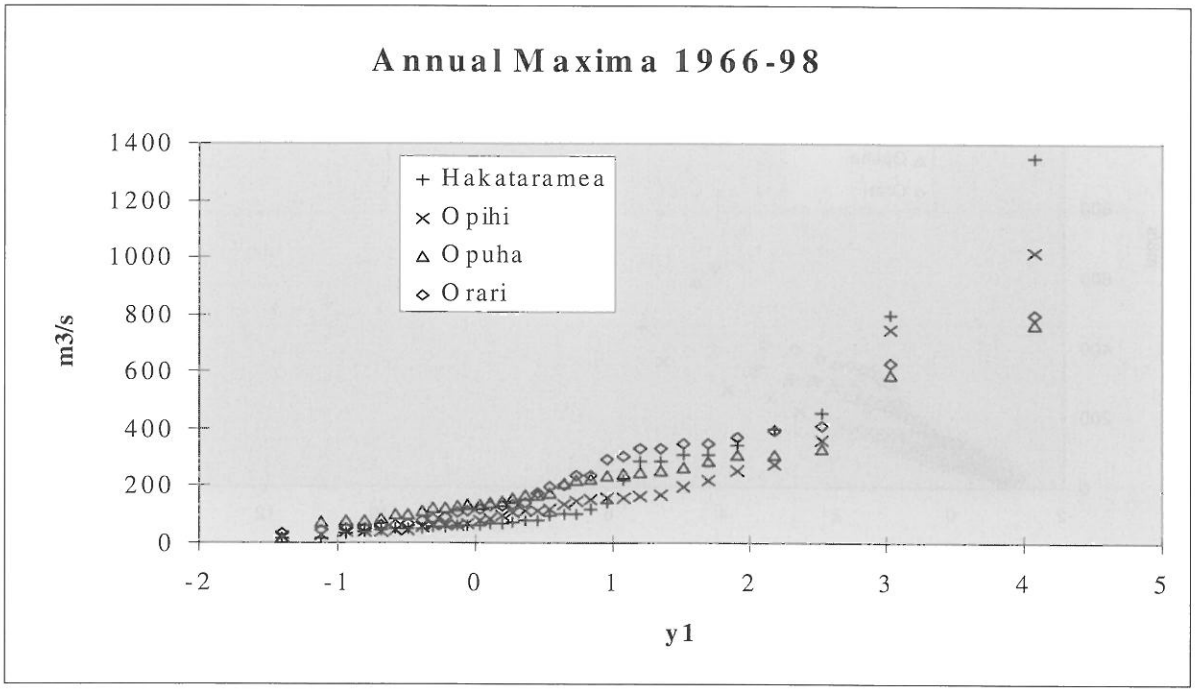

Figure 3-2: Annual maxima 1966-1988 for four rivers, against EV1 reduced variate, y_1.

Figure 3-1 also indicates that in this (complete duration series) approach, some floods of greater magnitude than those included are left out because they occur in a year containing a flood of higher magnitude (e.g. May 1987, May 1993).
The annual maxima for four rivers 1966-1998 are plotted in Figure 3-2 against the EV1 reduced variate, y_1. The Gringorten (1963) plotting position formula relating rank to probability has been used. y_1 is

(1) $$y_1 = \frac{x-u}{\alpha}$$

and the cumulative probability distribution, F_1, of x is

(2) $$F_1(x) = e^{-e^{-\left(\frac{x-u}{\alpha}\right)}}$$

in which:

x flood discharge magnitude
u location parameter
α scale parameter

As cumulative probability is the complement of exceedance,

(3) $$y_1 = - \ln (- \ln (1 - AEP))$$

where AEP is the annual exceedance probability $p(x \geq x_{reference})$. Values for u and α were obtained in this study using linear moments (Hosking, 1988; 1990) to fit equation (2) to the data.
From equations (1) and (3), flood magnitude data conforming to equation (2) would plot linearly against y_1, which is a measure of probability. The data in Figure 3-2 clearly do not plot linearly.

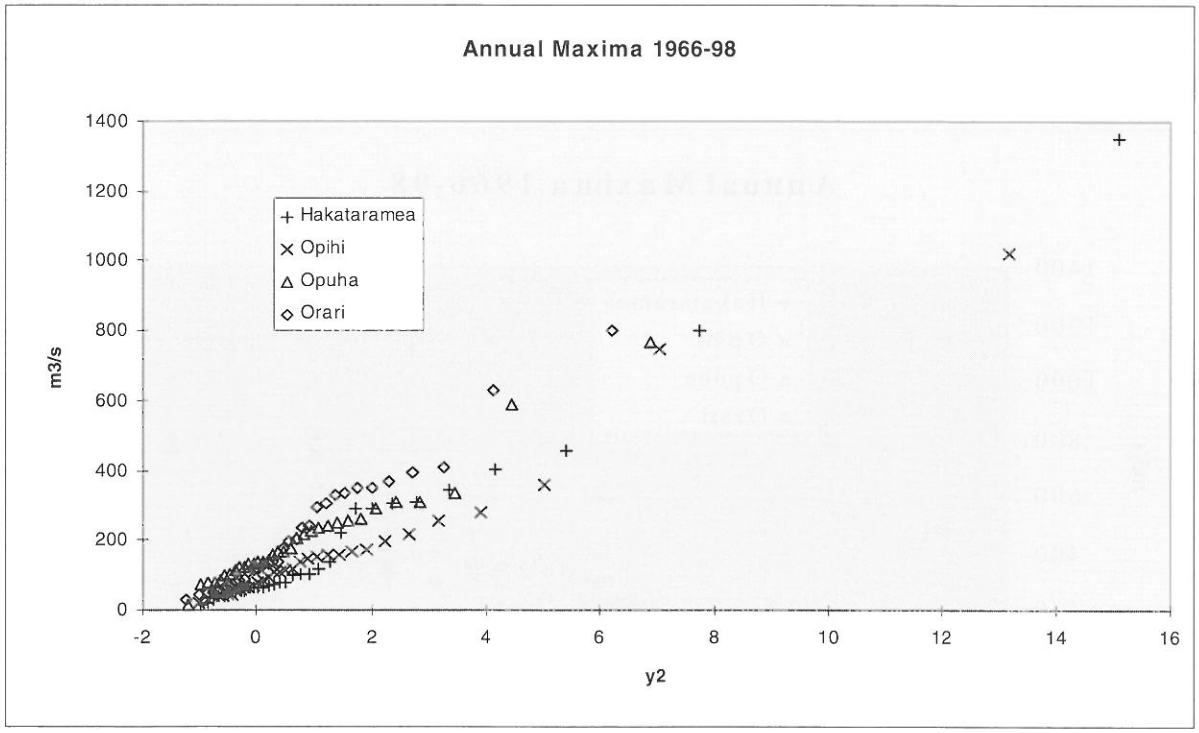

Figure 3-3: Annual maxima 1966-1988 for four rivers, against EV2 reduced variate, y_2.

In Figure 3-3 the same flood magnitude data are shown plotted against the EV2 reduced variate, y_2. y_2 has the same linear relationship with x, but the cumulative probability distribution is

(4) $$F_2(x) = e^{-\left[1-\frac{\kappa(x-u)}{\alpha}\right]^{\frac{1}{\kappa}}} \qquad \kappa < 0$$

and the relationship with AEP is

(5) $$y_2 = \frac{1}{\kappa}\left\{1-\left[-\ln(1-AEP)\right]^{\kappa}\right\}$$

The additional parameter introduced is

κ shape parameter

Flood magnitudes conforming to equation (4) would plot linearly against y_2, which is a measure of probability. The fit shown in Figure 3-3 (also shown by the three rivers of shorter total period of record in Figure 2-2) is why this region has been previously said to be "EV2" rather than the "EV1" regions typical of most of New Zealand (McKerchar, Pearson, 1989). But clearly the linearity is far from perfect.
A censored partial duration series, of independent flood magnitudes greater than a specified threshold, is an alternative to the complete duration series formed from one flood magnitude maximum for each conditioning event, such as a year.

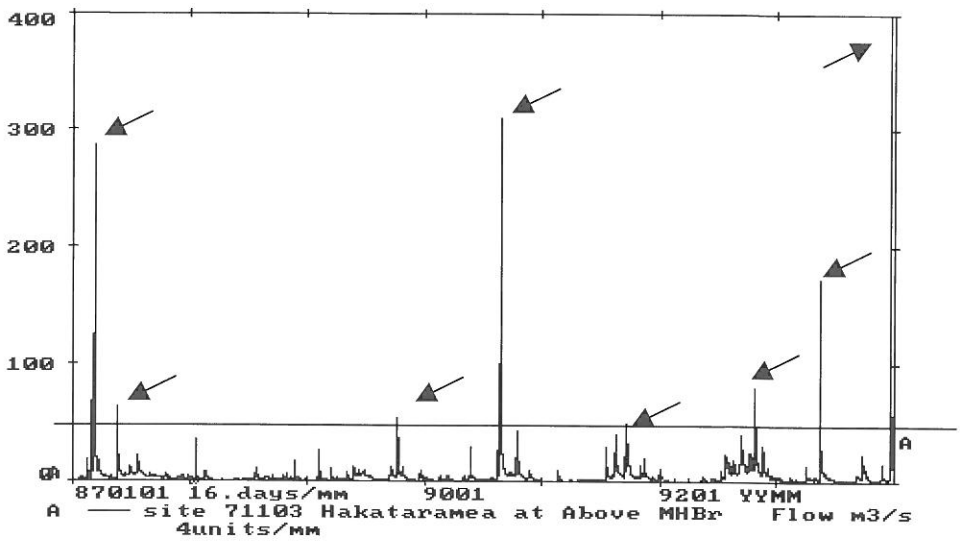

Figure 3-4: Discharge hydrograph 1987 to 1993, Hakataramea River, independent peaks > 50 m^3/s arrowed.

Figure 3-4 shows the same period of record as Figure 3-1, but the magnitudes indicated by arrows are all "independent" peaks greater than a "threshold" of 50 m^3/s. These can be used to form a whole-record peak-over-threshold (POT) series.
The multiple flood peaks visible in March 1987 and August 1990 do not arise from independent "events", but it is not a trivial matter to decide on "independence" in general. The eight peaks indicated here exceed a threshold discharge equal to mean discharge plus three standard deviations (rounded to nearest 5 m^3/s). This gives a similar number of flood events to the complete duration series (seven in Figure 3-1), but again, it is not a trivial matter to decide on a threshold value in general.
Lang et al. (1999) have reviewed POT modelling practice and offered guidelines, based on accumulated international experience, for setting independence criteria and selecting threshold values in circumstances like these.
An appropriate probability distribution for independent POT flood events is the Generalised Pareto (GPa). A special case of GPa when the shape parameter, δ, is zero is the 2-parameter exponential distribution (Stedinger et al., 1993).

The POT magnitudes for 1966-1998 for the same four rivers as in Figure 3-2 are plotted in Figure 3-5 against the GPa reduced variate, y_p. Again, the Gringorten (1963) plotting position formula relating rank to probability has been used. y_p is

(6) $$y_p = \frac{x - \nu}{\beta}$$

and the cumulative probability distribution, F_p, of x is

(7) $$F_p(x) = 1 - \left[1 - \delta \frac{x - \nu}{\beta}\right]^{\frac{1}{\delta}}$$

in which:

x flood discharge magnitude
ν location parameter
β scale parameter
δ shape parameter

As cumulative probability is the complement of exceedance,

(8) $$y_p = \frac{1}{\delta}\left[1 - (AEP)^{\delta}\right]$$

where AEP is the annual exceedance probability $p(x \geq x_{reference})$. As for GEV, linear moments (Hosking, 1988,1990) were used to evaluate ν, β and δ.

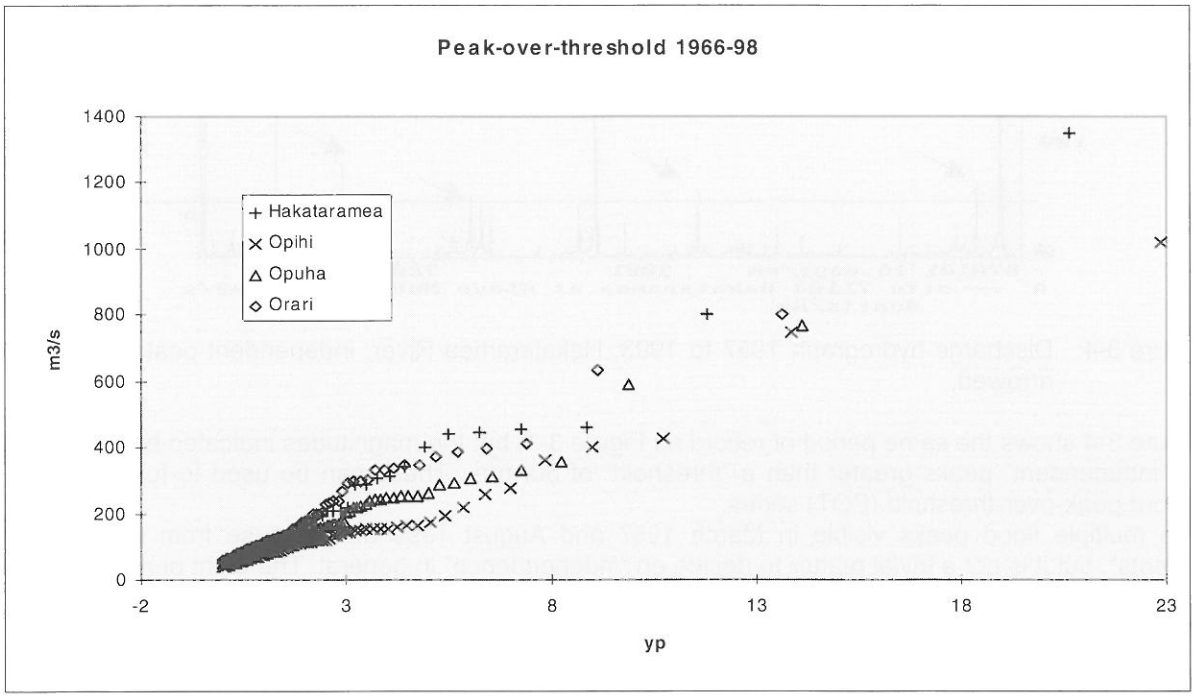

Figure 3-5: Annual peaks-over-threshold 1966-1988 for four rivers, against GPa reduced variate, y_p.

From equations (6) and (8), flood magnitude data conforming to equation (7) would plot linearly against y_p, which is a measure of probability. Comparing Figures 3-2 and 3-5 does not immediately suggest superiority of either approach in terms of conformity of the data to a linear model.

4 SEASONAL ANALYSES

A previous investigation of Hakataramea River data (Painter, Larsen, 1995) suggested that flood magnitude probabilities varying within years could be affecting interpretation of annual probabilities. That preliminary study investigated weather pattern effects on flood magnitude probability, but without clear relationships being established. Instead, mixtures of distributions were apparent, with seasonality of probabilities suspected.
South Canterbury rivers are short and steep (Figure 2-2), rising in mountain and foothill areas, and flowing in predominantly rural floodplains to the Pacific Ocean. Most have some degree of river control imposed by stopbanks (levees) to prevent flooding of highways, towns and agricultural land for livestock and cropping. The flooding which does occur (Connell et al., 2001) thus has different costs depending on the state of the agricultural land at the time of flooding. In 1997, a dam under construction on the Opuha River to provide irrigation water supply and hydro-electricity failed when a flood exceeded the capacity of the diversion works in place at the time. The flood probability determination was controversial, and the legal and financial implications were important (Anon, 2001).
The three hydrological and catchment management reasons for considering seasonal flood magnitude probabilities listed in the Introduction therefore have applied in South Canterbury.
For seasonal, compared to annual, analyses, the same two approaches could be taken: selecting seasonal maxima for a complete duration series, or selecting peaks over a threshold for a partial duration series. Some of the difficulties with each approach described for annual analyses are exacerbated with the reduced length of record which follows from extracting seasonal data from a total record. In addition, there is now the problem of deciding what are "seasons" in order to most appropriately select the "conditioning event". Ideally, the most relevant seasons would be "flood behaviour" seasons. But in the present context, for the study region climate, geology and land use, this flood behaviour seasonality is unknown, and whether it exists is unknown.
The simplest rational approach is to adopt the conventional (austral) seasons: December-February (DJF) summer; March-May (MAM) autumn; June-August (JJA) winter; September-November (SON) spring. Once databases and algorithms are appropriately established, varying the season boundaries only implies extra computational effort.

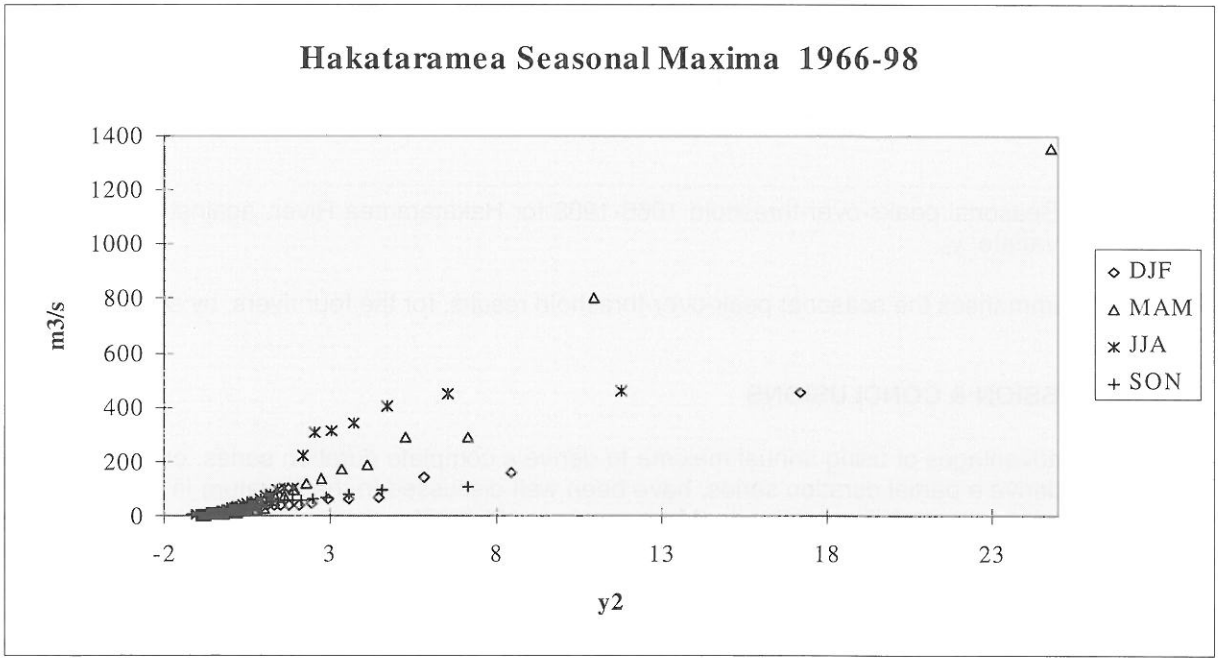

Figure 4-1: Seasonal maxima 1966-1988 for the Hakataramea River, against EV2 reduced variate, y_2.

Seasonal maxima selection, and seasonal peak-over-threshold selection are as in Figures 3-1 and 3-4, respectively, but in each case the time axis is discontinuous, comprising the sequence of 3 months from each year in the total record appropriate to the chosen season.
Comparing the results from all seasons for each river indicates whether or not flood probability variation within years is occurring. Comparing the results from all rivers for each season indicates (as for annual analyses) whether or not regional analysis is likely to be useful.

Figure 4-1 shows the seasonal maxima for the Hakataramea River, plotted against the EV2 variate, y_2. The implication from Figure 4-1 is that spring and summer plot with similar flood probability, and that this differs from each of autumn and winter. It is also noticeable that there is a magnitude gap from about 100-200 m^3/s in the winter (JJA) data. Summer and winter maxima plot differently for the Opihi and Orari Rivers, as for the Hakataramea River, but autumn and spring behaviour is not consistent for all four rivers. Seasonal data are not clearly different for the Opuha River.
Figure 4-2 shows seasonal peak-over-threshold data for the Hakataramea River, plotted against the GPa variate, y_p. The implication from Figure 4-2 is that autumn and summer plot with similar flood probability, and that this differs from each of spring and winter. Both approaches suggest that summer and winter are different, but are not consistent about autumn and spring. Only summer plots differently for the Opihi River, only autumn for the Orari River. In contrast to the seasonal maxima data, the peak-over-threshold data for the Opuha River show summer and autumn data together, but different from each of spring and winter.

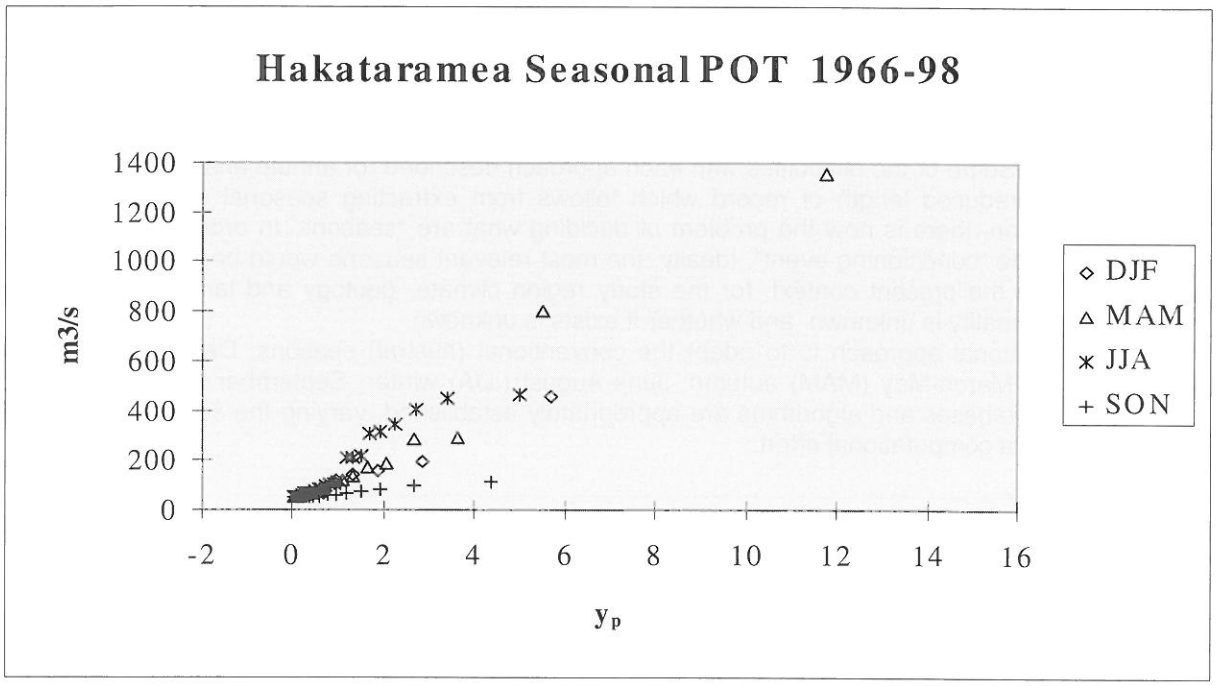

Figure 4-2: Seasonal peaks-over-threshold 1966-1988 for Hakataramea River, against GPa reduced variate, y_p.

Figure 5-1 summarises the seasonal peak-over-threshold results, for the four rivers, by season.

5 DISCUSSION & CONCLUSIONS

The relative advantages of using annual maxima to derive a complete duration series, or peaks over a threshold to derive a partial duration series, have been well discussed in the literature in the context of annual exceedance probabilities of floods (Madsen et al., 1997). The occurrence of floods in mixtures of distributions, due to differing rainfall or catchment processes, has also been reported and discussed (Arnell, Gabriele, 1988). Seasonal occurrence of floods is well understood in many climatic contexts, from monsoonal to arid (Meigh et al., 1997) and when spring snowmelt contrasts with rainfall events in other seasons (Stoddart, Watt, 1970). This study draws on all three of these contexts, but applies the understanding to seasonal probabilities of flood magnitudes in a climatic and geological setting where the reasons for within-year variation in probability, if any, are not obvious.
The preliminary results for seasonal flood magnitude probabilities reported here for four rivers in South Canterbury, New Zealand, indicate the likelihood that probabilities do differ in some seasons from others, and therefore differ from the usual annual probabilities. Seasonal maxima complete duration series and GEV fitting by linear moments, leads to "EV2" values for the shape parameter, κ. The requirement that the maxima be chosen from among an "asymptotically large" number of "floods" in the conditioning event (Leadbetter et al., 1983) is not well met, and this approach is not preferred.

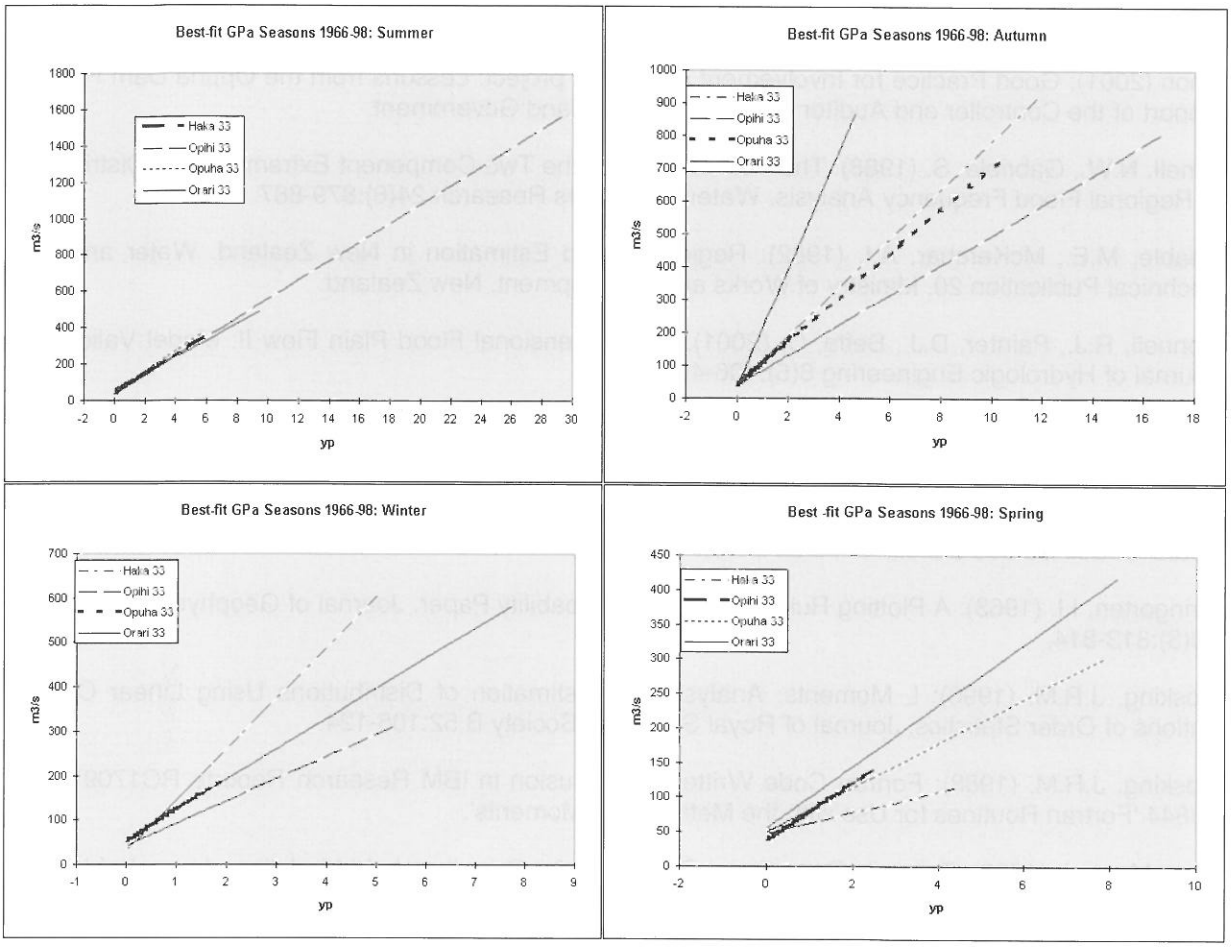

Figure 5-1: Best-fit GPa to seasonal POT series for four rivers 1966-1998.

An approach using partial duration series of independent peaks over a threshold, and GPa fitting by linear moments, is preferable, providing appropriate choices of criteria for independence and threshold values are made. Such an approach used here showed seasonal differences in flood magnitude probabilities which differed in some river/season cases from the AMS/GEV approach.
The present results were obtained using the following relatively simple criteria:

- Event peaks independent if separated by three days or more
- Threshold discharge equal to mean plus three standard deviations
- Mean arrival rate equivalent to at least 1.6 events per year

A recent review (Lang et al., 1999) has provided "coherent practice-oriented guidelines" which will allow refinement of the methodology for a closer examination of the data for these four rivers, and the three others also shown in Figure 2-2, which now each have 19 years of data available. Another recent paper (Martins, Stedinger, 2001) has provided means of restricting the shape parameter, δ, of the GPa distribution, to a "statistically physically reasonable range". Two of the 16 fitted values of δ in this study (4 rivers, 4 seasons) were "absurd" (Opihi Spring +0.270, Opuha Winter +0.453, Figure 5-1). There are many traps and difficulties in working with small samples of flood data from unknown parent distributions (Cunnane, 1985). Some of these are made worse by choosing to examine seasonal data. But doing so shows promise both for explaining some hitherto mysterious behaviour, and for providing operationally significant information.

6 ACKNOWLEDGEMENTS

Rob Connell and Tony Boyle of Environment Canterbury, New Zealand, arranged data provision and financial support for the work on which this paper is based. George Griffiths of Environment Canterbury approved its conference presentation. Charles Pearson of the National Institute for Water and Atmospheric Research (NIWA) provided technical advice.

REFERENCES

Anon (2001): Good Practice for Involvement in a Major project: Lessons from the Opuha Dam Project. Report of the Controller and Auditor General. New Zealand Government.

Arnell, N.W., Gabriele, S. (1988): The Performance of the Two-Component Extreme Value Distribution in Regional Flood Frequency Analysis. Water Resources Research 24(6):879-887.

Beable, M.E., McKerchar, A.I. (1982): Regional Flood Estimation in New Zealand. Water and Soil Technical Publication 20, Ministry of Works and Development, New Zealand.

Connell, R.J., Painter, D.J., Beffa, C. (2001): Two-dimensional Flood Plain Flow II: Model Validation. Journal of Hydrologic Engineering 6(5):406-415.

Cunnane, C. (1985): Factors Affecting Choice of Distributions for Flood Series. Hydrological Sciences Journal 30(1):25-36.

Cutler, E.J.B. (1968): Map sheet 11 in Gibbs H.S., Raeside J.D. Soil Maps of the South Island, New Zealand. Soil Bureau Bulletin 27, DSIR, New Zealand.

Gringorten, I.I. (1963): A Plotting Rule for Extreme Probability Paper. Journal of Geophysical Research 68(3):813-814.

Hosking, J.R.M. (1990): L Moments: Analysis and Estimation of Distributions Using Linear Combinations of Order Statistics. Journal of Royal Statistical Society B 52:105-124.

Hosking, J.R.M. (1988): Fortran Code Written for Inclusion in IBM Research Reports RC17097, RC 13844 'Fortran Routines for Use with the Method of L-Moments'.

Lang M. et al. (1999): Towards Operational Guidelines for Over-threshold Modeling. Journal of Hydrology 225:103-117.

Leadbetter, M.R. et al. (1983): Extremes and Related Properties of Random Sequences and Processes. Springer-Verlag. New York.

Madsen, H. et al. (1997): Comparison of Annual Maximum Series and Partial Duration Series for Modeling Extreme Hydrologic Events 1: At-site Modeling. Water Resources Research 33(4):747-757.

Martins, E.S., Stedinger, J.R. (2001): Generalized Maximum-Likelihood Pareto-Poisson Estimators for Partial Duration Series. Water Resources Research 37(10):2551-2557.

McKerchar, A.I., Pearson, C.P. Flood Frequency in New Zealand. Publication No. 20 of the Hydrology Centre, Christchurch, DSIR New Zealand.

Meigh, J.R., Farquharson, A.K., Sutcliffe, J.V. (1997): A Worldwide Comparison of Regional Flood Estimation Methods and Climate. Hydrological Sciences Journal 42(2):225-244.

Mutch, D.H. (1963): Sheet 23 Oamaru of the 1:250 000 Geological map of New Zealand, DSIR, New Zealand

Painter, D.J., Larsen, S.H. (1995): Effects of Season and Weather Patterns on Flood Frequency: Hakataramea River New Zealand. Journal of Hydrology (New Zealand): 34(2):111-128.

Stedinger, J.R. et al. (1993): Frequency Analysis of Extreme Events. Chapter 18 in Maidment D.R. (ed.): Handbook of Hydrology, McGraw-Hill.

Stoddart, R.B.L., Watt, W.E. (1970): Flood Frequency Prediction for Intermediate Drainage Basins in Southern Ontario. CE Research Report No. 66, Queens University at Kingston, Ontario, Canada.

AN ESTIMATE OF PROBABLE MAXIMUM FLOOD IN LARGE MOUNTAINOUS BASINS (A CASE OF THE KARUN BASIN IN IRAN)

Hossein Sedghi[1], Jahangir Porhemmat[2]

[1] Chamran University, Ahwaz, Iran, hsedgh@yahoo.com

[2] Soil Conservation and Watershed Management Research Center (SCWMRC), Tehran, Iran, porhemmat@scwmrc.com

SUMMARY

The probable maximum flood (PMF) was estimated in Karun, a large mountainous basin in Iran, in several studies with different results during the three last decades. Four major sources of errors were found in these studies. This is similar as found for other large mountainous PMF studies. These are as follows:

1) There was not considered the continues duration of precipitation for flood events.
2) The use of the annual depth-area-duration (DAD) curves in the basin with mixed condition of snow and rain.
3) The using of the parameters of rainfall-runoff models in simulation of basin in which the optimization conditions were not similar to PMF estimation condition.
4) The errors in snowmelt simulation in critical condition of PMF generation.

An analysis of the sources of errors and development of a procedure corresponding to the large mountainous basins is the aim of this paper.

Keywords: Probable maximum precipitation, PMP, Probable maximum flood, PMF, Mountainous basin, depth-area-duration (DAD), Rainfall runoff models

1 INTRODUCTION

1.1 Definition

Chow et al. (1988) defined the probable maximum flood (PMF) as "the largest flood to be expected assuming complete coincidence of all factors that would produce the heaviest rainfall and maximum runoff. This is derived from a probable maximum precipitation (PMP), and hence its frequency can not be determined". Different authors involved in PMP and PMF determination (Wang and Revell, 1983; Wang, 1984; Wang and Jawed, 1986; Mutreja, 1986) have used this definition.

1.2 Geography of the Karun River Basin

The Karun river basin as a mountainous region is located in southwest of Zagross, Iran. As shown in Figure 1-1 the entire Karun river basin is about 32500 km^2 in Gotvand or 24000 km^2 in Pol-e -shalu hydrometery stations. The main sub basins of Karun are Khersan, upper Karun (Armand basin) and Bazoft, which are jointed to each other and form the Pol-e -shalu basin (Table 1-1).

1.3 Previous PMF studies in the Karun

Several studies have been carried out for the estimation of the Probable Maximum Flood (PMF) of the Karun basin in order to develop the design flood criteria for a set of dam construction project planned along the Karun River. Among the studies concerning hydrological analysis of the Karun basin a number of reports have been dealt whit the verification of the magnitude of the PMF's components evaluated, all, for a common section of the River.

The resulting components of design floods are compared with real hydrological characteristics of the region based on observations during almost a century, possibly a record of several thousands of years of nob-exceedance can be constructed on the bases of undamaged ancient monuments in the lower parts of the Karun basin. The degree of conservatism in the estimation of the PMF has to be clarified

by comparison whit these proxy observation. The PMF components of the Karun basin in the common section of Pol-e -shalu (24,200 km^2) are shown in Table 1-2.

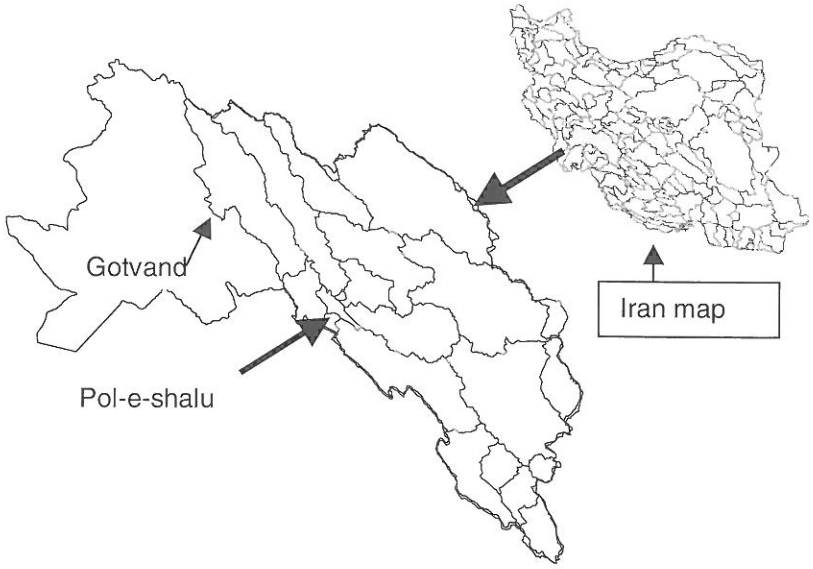

Figure 1-1: Karun basin in Iran map

Table 1-1: The main sub basins of the Karun basin at Pol-e –shalu.

Sub basins	Area (km^2)	Maximum elevation from mean sea level (m)	Maximum elevation from mean sea level (m)
Karun at Gotvand	32500	75	4500
Karun at Pol-e - Shalu	24200	700	4500
Bazoft at Marghak	2175	980	4200
Upper Karun at Armand	10071	1050	4200
Khersan at Barz	9000	815	4500

Table 1-2: Results of PMF studies in the Karun basin at Pol-e –shalu

Institute or Consultant	Peak Discharge (m^3s^{-1})	Volume of the PMF flood ($10^6 m^3$)	Duration of the PMF flood (days)
Harza (1967)	26600	1970	3
LWRD/Acers (1982;1984)	27900	16000	20
Lahmayer Int. Con. And Moshanir (1995)	21100	7920	20
Mahab Ghodss and Acers (1991)	22350	9600	20
Sedghi (1992-a; 1992-b)	11500	6052	15
Moshanir-Caitec (1996)	25200	13050	20

With regarded to the definition of the PMF as a reasonable upper physical limit of flood in a finite basin the following questions could be raised:

- Is it reasonable to expect the occurrence of a flood having a peak discharge of the order of 10000 to 30000 m^3s^{-1} in this geographical location?
- What range would be the best estimate of volume of the PMF flood at the outlet of the Karun basin among the values, which range from $1.97*10^9$ to $16*10^9$ m^3s^{-1}?

It is obvious that in determination of the probable maximum precipitation (PMP), and from further computation for a finite basin with specific characteristics, based upon different methodologies and available data, many assumptions can be considered. The PMF components with a range of discrepancies shall be evaluated depending on the studies.

Since the most important point in hydrological studies concerning evaluation of design criteria is to obtain as realistic and significant values for the design parameters related the major structures, a review of basic concept and hydrological factors could assess the degree of discrepancy in consecutive steps of the PMF determination of the watershed under study.

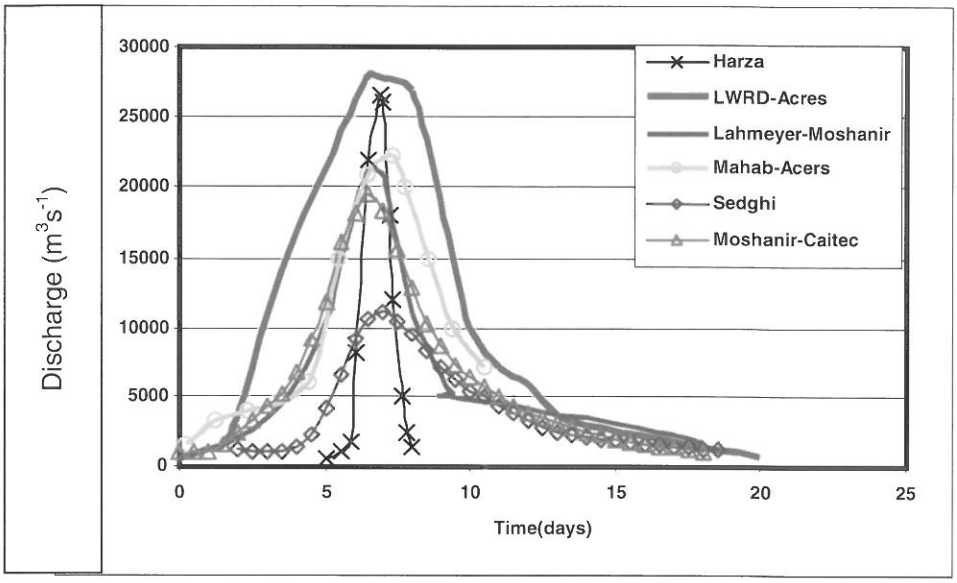

Figure 1-2: PMF hydrographs of Karun Basin at Pol-e-shalu based on different studies shown in table 1-2.

2 COMPARISON OF CASUSAL FACTORS

2.1 Comparison of the PMP and the PMF components

The numerical values of hydrological factors affecting the PMF estimation of the Karun basin for each study are presented in table 2-1. The PMF hydrographs and the appropriate values of the components from the above references are shown in Figure 1-2.

2.2 PMP evaluation

There are some differences in the origin and the methodology in the estimation of PMP in the above studies. The original storm is either selected as "in situ rainfall" or transposed from the adjacent region. The significant difference in selection of duration, depth, time and Arial distribution pattern of the original rain and the maximization factor converting rainfall to PMP cause a large discrepancy affecting the results. Some examples are presented for each of the affected factors:

2.2.1 PMP duration

The runoff is generated by continuous effective rainfall duration. Due to absence of recorded values of rainfall, the 24 hours increment was considered for assessment of observed storms and relevant PMP. A detailed analysis of recorded rainfall in some parts of the Karun basin suggests a significant overestimation concerning initial storms and the PMP 's duration. Figure 2-1 and Figure 2-2 shows the cumulative and incremental values of rain during a historical storm recorded at Pol-e-shalu station. The continuos duration of rain at this station is almost 40 hours. This value has been recorded during the Dec. 1986 storm, which may be the most severe storm observed over a large mountainous area of about 400,000 km^2 in the Zagross range in the southwest part of Iran. The Depth Area Duration curves of this storm are established for 24 hours increment of time (Figure 2-3). This document was considered as a description of the regional characteristic of a heavy storm and has been used as a Standard Project Storm, SPS, used in the estimation of Standard Project Storm, SPF, for some dam construction project in Iran. Figure 2-2 shows the DAD curves of the Dec. 1986 storm over 400,000 km^2 area.

It should be mentioned that the observed values of rain during different duration and over definite area are comparable with the estimated values of the PMP by different references. Figure 2-1 shows that the observed continuous duration of a sever historical storm (40 hours) over a part of the Karun basin is much less than the 7 days (192 hours) duration of generalized PMP which is considered as Continuous rainfall, in Ref. 6. This very high modification of intensity and continuous duration of rainfall seems to be unreasonable. The result of such synthetic temporal pattern of precipitation produces unreasonable volume and peak discharge in a large scale. The Numerical values of DAD of the Dec. 1986 Storm are presented in Table 2-2.

Table 2-1: Numerical values of hydrological factors of the PMP and the PMF in the Karun basin at Pol-e-shalu

Step of Studies	Parameters	References					
		1	2	3	4	5	6
PMP evaluation	Selected depth of rain to be maximized (mm)	220	285	230	285	270	
	Transposed or maximizing factor	0.8	1.51	1.87	1.51	1.4	1.53
	Maximized rainfall (PMP) in mm	176	432	430	430	380	425
	PMP duration in days	1	9	7	4.5	7	7
Snow	Equivalent snowmelt depth (mm)	None	0.15 PMP	Unde-fined	208	Base Flow 40	
Runoff	Runoff coefficient	0.5	1.61	0.8	0.87	0.53	
	Excess rainfall (mm)	86	696	339	402	201	
Time and arial distribution	Point Excess Rain (mm)	-	966	480	-	-	
	Intensity mm/day	86	-	180	-	-	
Unit Hydrograph	Time of concentration (hrs)	16	16	40	17.5	53	
	Unit Peak Discharge (m^3s^{-1})	300	120	63	-		
PMF Hydrograph	Base time in days	4	20	20	20	15	20
	Peak Discharge(m^3s^{-1})	26600	27900	21100	22350	11150	25200
	Volume (10^6 m^3)	1970	16000	7920	9600	6052	13050

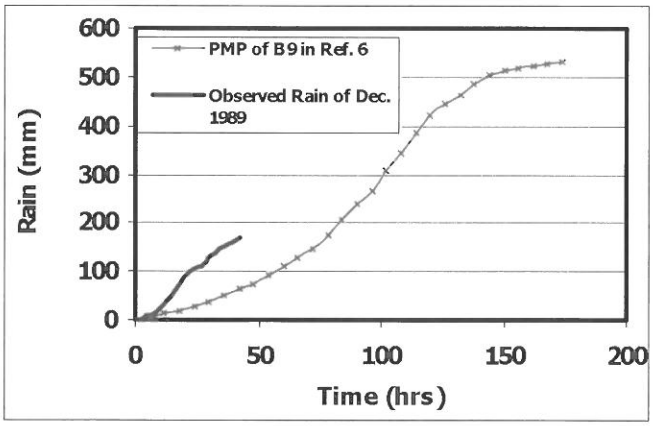

Figure 2-1: Comparison between the cumulative curves of recorded continuous observed rainfall and the PMP of B6 in reference 6.

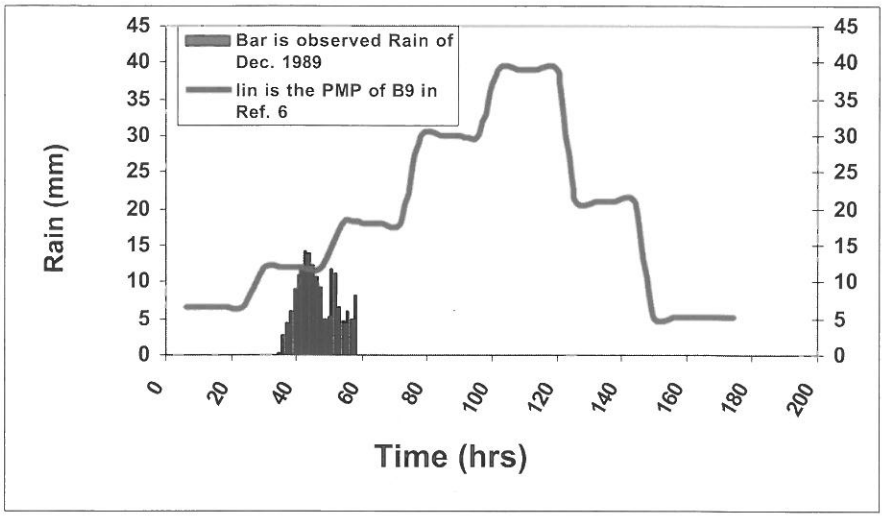

Figure 2-2: Comparison between the hyetograph of a continuous observed rainfall and a 6 hrs Incremental PMP of B6 in reference 6.

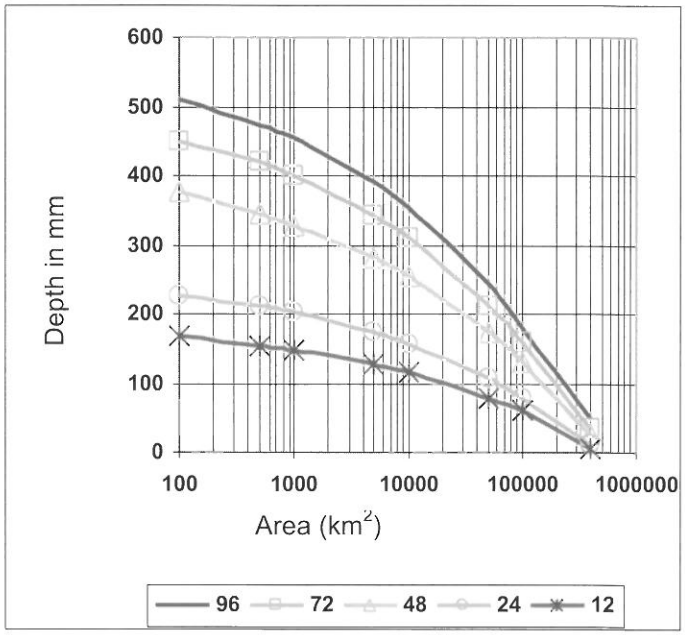

Figure 2-3: DAD curves of Dec. 1986 storm over a 400,000 Km^2 area in southwestern part of Iran.

Table 2-2: Depth area values during Dec. 1986 storm in southwestern part of Iran.

Area (Km^2) / Duration (hrs)	12	24	48	72	96
100	168	226	378	450	510
500	155	212	345	420	472
1000	148	203	328	400	455
5000	128	174	280	342	390
10000	117	157	254	310	354
50000	79	107	175	212	243
100000	60	78	130	160	181
400000	5	12	25	36	48

2.2.2 The PMP temporal pattern

The temporal pattern of the PMP must correspond to the regional condition of a sever storm. Transposition of patterns such as SCS types II III and I are not applicable to Karun climatological conditions.

2.3 Snowmelt Contribution

The snowmelt contribution in flood flow generation was considered in different manner in the studies shown in table 1-2. In Ref. 1 the snowmelt is almost neglected, but this factor is highly important in Ref. 2 and 3.
In Ref. 2 a rough ratio of 18% of the total precipitation was proposed as a snowmelt depth that contributed to floods up to a return period of 10000 years. In this Ref. a HEC1 model application, based on antecedent snowpack water equivalent prior to PMP, a probabilistic critical temperature sequence during the rain and an unrealistic lapse rate resulted in a large overestimation of the PMF with a runoff coefficient of 1.61. The total value of snowmelt of order of 266 mm in the whole basin may causes at least $6*10^9$ m^3 overestimation in volume and about 6000 to 7000 m^3s^{-1} overestimation in peak discharge.

2.4 Rainfall Runoff relationships

In order to carry out the estimation of the size of many rainfall runoff components, a set of flood hydrographs were analyzed based on the sever floods characteristics. Flood hydrograph parameters like peak discharge, total volume, base flow, total runoff, and net runoff were estimated and compared with the storms producing the floods. The coefficient of runoff for the entire basin and the three major sub basins has been evaluated for each flood event. A pattern of SCS runoff curve numbers has been designed to carry out a comparison for the verification of observed runoff-rainfall potential of basins to show the unreasonable reliability of rainfall-runoff relationships for PMP values. Figure 2-4 shows the obvious discordance between rainfall depth as PMP and the relevant values of runoff according to the SCS pattern.

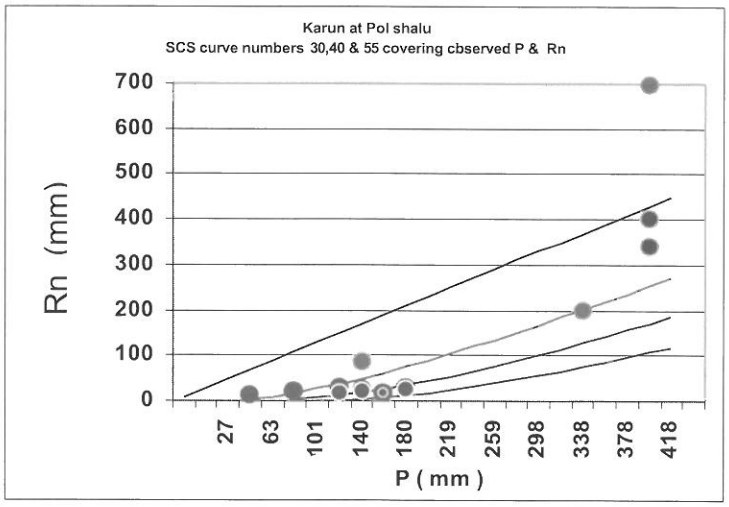

Figure 2-4: Comparison of rainfall runoff relationship in estimated PMF and observed floods in a SCS pattern of runoff (Rn) vs. precipitation (P) at Pol-e-shalu.

The eight most sever floods that have been observed in the Karun basin at Pol-e-shalu were selected and analyzed in order to estimate the hydrological balance parameters. The results are summarized in Table 2-3. Table 2-3 shows that the effective basin area is between 77.2 to 99.7 percent of the total basin area during different storms due to freezing effects. Although this table shows that the net runoff coefficient varies from 1.5 to 18.1 percent based on rain and snowmelt in different season of years that this parameter takes values between at least 50 to 161 percent in PMF studies shown in table 1-2. The annual hydrograph components are computed for the Karun basin at Pol-e-Shalu in 3-index water years (1992-93, 1996-97, and 1997-98) which are the wettest, dry and normal to wet years respectively. The results are summarized in Table 2-4. This values show that the net annual runoff is varying from 41 mm for the dry year (1996-7) to 165 mm for the wettest year (1992-93) of observations.

Table 2-3: Flood hydrograph components during selected severs storms in the Karun basin at Pol-e-shalu (24,200 km^2).

Date of Occurrence	Feb-Mar 1978	Dec 1989	Nov 1994	Mar-Apr 1998	Mar 1998	Nov-Dec 1986	Feb 1993	Jan 1978
Effective Area (%)	77.3	91	98	99	98	83	88	74
Peak Discharge (m^3/sec)	2384	3907	2935	4590	6230	3470	4564	2858
Total Volume ($10^6 m^3$)	568	682	392	681	731	693	1009	338
Base Flow Volume ($10^6 m^3$)	314	280	328	370	345	362	482	193
Net Runoff Volume ($10^6 m^3$)	253	402	64	311	385	332	528	144
Rainfall (mm)	108	150	174	88	112	152	129	199
Snowmelt (mm)	13	7	5	20	30	8	8	37
Rain+ Snowmelt (mm)	121	157	180	108	142	160	137	236
Net runoff (mm)	14	18	3	13	16	17	25	8
Runoff Coef. (%)	11.2	11.7	1.5	11.9	11.4	10.4	18	3.4
Equivalent SCS Curve No.	48	42	28	52	44	42	52	25

Table 2-4: value of runoff components for the annual water balance during three distinguished water years at Pol-e-shalu.

Water year	Annual total flow (mm)	Annual net runoff (mm)	Annual base flow (mm)	Net runoff coef. (%)	Base flow coef. (%)	Ratio of total annual flow to mean annual flow
1992-93	833	165	668	20	80	2.14
1996-97	344	41	303	12	88	0.88
1997-98	494	110	384	22	78	1.27

2.5 Volume and Peak discharge of PMF

Rainfall -runoff models were developed for the evaluation of the PMF hydrographs in the different studies shown in table 1-2. The common model is the HEC-1 model, which was used in order to optimize parameters and to convert PMP to PMF using observed data of many historical sever storm Floods observed in the Karun basin. The shape of unit hydrograph, which affects seriously the volume distribution and the value of peak discharge of the PMF, differ significantly in these studies. In fact, it varies between 60 to 300 m^3s^{-1} per one mm of precipitation in a basin of 24,200 km^2. Consequently, the very large values of peak discharge of the PMF ranging from almost 10^9 to $30*10^9$ m^3s^{-1} for the study Basin are due to partly overestimation of this parameters. A very detailed study was performed to verify the magnitude of peak discharge as related to flood volume of observed events in the region. A series of data containing of more than one hundred flood events was analyzed for three sub basins. These are Armand (10000 km^2), Bazoft (2250 km^2), Khersan (9000 km^2) and the entire Karun basin at Pol-e-shalu (24200 km^2). Variables such as max daily and instantaneous discharge, total volume and corresponding depth, base flow and its depth, runoff volume and depth, time parameters such as time to peak, recession time, and base time were evaluated. Some results of this study are used in order to verify the reasonability of the volume of the PMF and the peak discharge. The results of this study are summarized in Figure 2-5 and Figure 2-6. Figure 2-5 shows the net runoff versus peak discharge (maximum of mean daily values) for the entire flood events at Pol-e-shalu.
Similarly, scattered charts were developed for the different time to peak to demonstrate the effect of flood duration as related to storm duration and to verify the frequency of occurrence of floods with respect to the importance of volume or peak discharge.
Finally the position of different PMF's volume and peak discharge have been compared using the general pattern of the entire observed flood event of the Basin during a long historical period, considering the antiquarian index of the region.

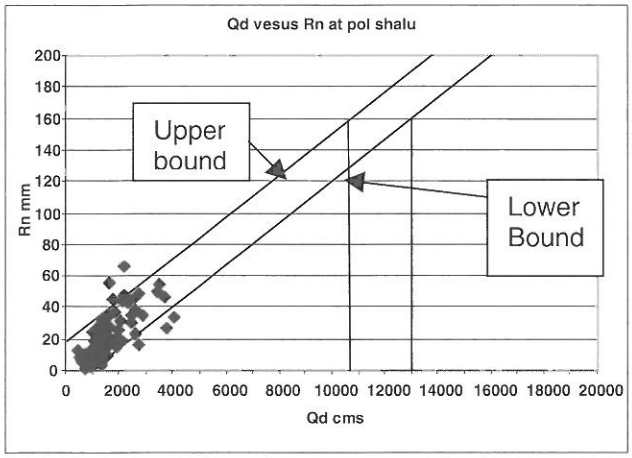

Figure 2-5: Scattered values of net runoff and peak discharge based on more than one hundred flood event in the Karun basin at Pol-e-shalu.

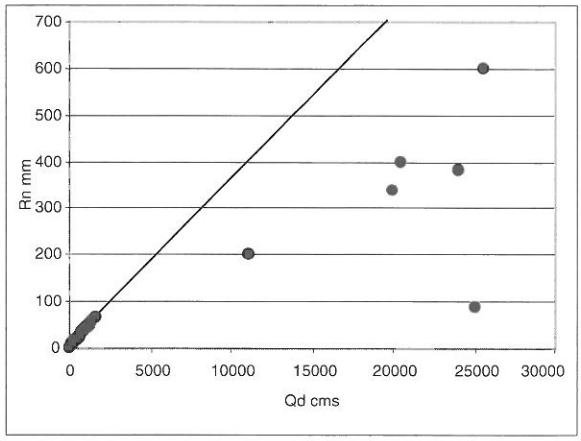

Figure 2-6: Observed daily peak discharge vs. net runoff in the Karun basin at Pol-e-shalu and compared with the position of pervious estimated PMF points.

2.6 Comparison of PMF and observed floods

Two examples are presented in this paper in order to show the degree of increase in key parameters in some studies. Table 2-5 shows the PMF increased values of PMF parameters with respect to maximization factor of PMP in Ref 2. In Table 2-6 the increasing ratios of peak and volume of PMF hydrographs with respect to maximization factor of the PMP is presented for some storm flood events selected PMF evaluation. Generally, according to the above-mentioned ratios, an increment about 35 to 89 percent in rainfall depth over a basin like the Karun at Pol-e-shalu (24,200 km^2) can result in a flood 10 times greater than observed flood by peak and volume.

Table 2-5: Comparison of observed flood and PMF parameters.

Storm flood events	Observed rainfall depth (mm)	Runoff net (mm)	Runoff base (mm)	Runoff coefficient net	Runoff coefficient total
Jan.1968	248	36	11.5	12.7	16.7
Jan.1975	285	29	17.4	10.2	16.3
PMP/PMF	432	629	67	145	161
Of Increase Ratio	1.52	9.7	4.6	12.7	9.8

Table 2-6: Growing ratios of PMF parameters with respect to PMP maximization factor.

Storm-Floods	Ref.	PMP maximization ratio	PMF Peak discharge increased ratio	PMF volume increased ratio
Jan.1968	2	1.35	10.9	10.7
Jan.1968	3	1.89	8.4	8.2
March 1972	2	1.43	6.2	9.9
March 11972	3	2.45	7.0	10.8
Jan.1976	2	1.51	12.9	12.7
Jan.1976	3	1.87	8.2	7.8

3 REVIEW STUDIES

Since 1998 the Iran Water and Power Resources Development recommended a general study of re-evaluation of the PMP/PMF in the Karun Basin. This study was planed to review the Flood Designed Criteria for a number of 10 dams construction projects on the Karun River. The Authors of the present article conducted these studies.
Here we present briefly the methodology of the work and a summary of the results for the Pol-e-shalu station in order to compare the key values with those of previous studies.
Parameter selection;
Based storm flood:

- Selection of most sever flood observed during spring, in order to maximizing rainfall and snowmelt over entire basin
- Selection of continuous duration of storms and analyzing recorded rainfall of some rain gauge stations in view of the DAD curves construction.
- Calculate snowmelt based on snowpack evaluation and real time temperature variation before and during the storms
- Hydrograph analysis of selected flood hydrographs for a number of subbasins based on hourly-recorded data.
- Calibration of the HEC1 model by real times parameters and control of the calibrated parameters e.g. loss coefficient and unit hydrograph components.

The resulting of the PMF parameters concerning the Karun basin at Pol-e-shalu are presented in Table 3-1 and the PMF hydrographs are shown in Figure 3-1.

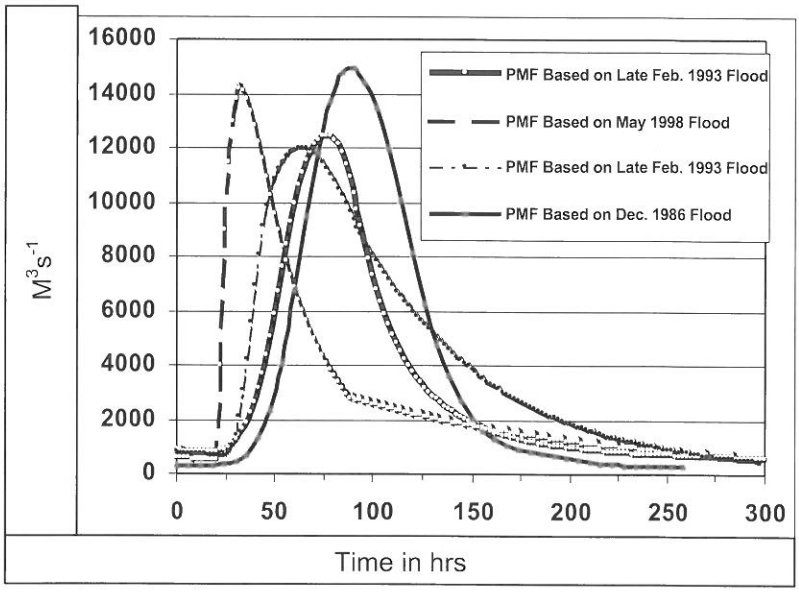

Figure 3-1: 4 Hydrograph computed as the PMF based on the 3 most sever storm and flood in Karun basin at Pol-e-shalu.

Table 3-1: Peak and discharge of PMF in the Karun basin at Pol-e-shalu.

PMF Components	PMF based on late Feb. 1993 flood	PMF based on May 1998 flood	PMF based on late Feb. 1993 flood	PMF based on Dec. 1986 flood
Peak discharge (m^3s^{-1})	12478	14169	12015	14968
Volume in ($10^6 m^3$)	3364	3093	4364	3656

4 CONCLUSION

With respect to preceding description of the six mentioned Studies in table 1-2, and with comparison of parameters used in PMF computation, it is clear that an important degree of conservatism is associated with evaluation of causal factors in producing the PMF of the Karun. The causal factors that can lead to overestimation in the size of the calculated flood in a region like the Zagros mountainous area in Iran could be described as follows:

1- The Zagross Mountain in the northwest to southeast of Iran is a terminal barrier receiving the Mediterranean and Sudanese air masses with a limited potential of humidity and with a relative low quantity of perceptible water. The duration of activity of such systems could be in order of many days during winter and shorter in spring, but the real duration of effective rain producing runoff is of the order of many hours. Thus the first factor affecting the PMP value could be the assumptions of longer discrete duration causing a non-realistic depth-duration of rainfall.
2- Using synthetically time distribution pattern of PMP rain affects seriously the shape of the hyetograph of the PMP having a multiple effects on runoff generation.
3- The use of generalized D-A-D curves in order to evaluate the areal distribution of storm and related PMP in a mountainous region with very cold climate causes a significant overestimation on depth-area relationship of precipitation as rain. It could be mostly due to variable contributing areas due to freezing in parts of the basin.
4- Use of an appropriate method for evaluating the basin retention during rain is very delicate. The SCS curve number method is specially applicable to agricultural conditions of soil, is very far from giving realistic results for large area covered by geological karstic formation which have indeterminable macro porosity as usual by the mentioned method.
5- Finally, the unit hydrograph peak discharge, evaluated normally by HEC1 application or synthesized by empirical methods was mentioned as a key factor affecting the PMF volume distribution and causing a significant increase of peak discharge of the calculated PMF.

REFERENCES

Chow, V.T., Maidment, D. R. and Mays, L. W. (1988): Applied Hydrology. McGraw-Hill International.

Harza Engineering Co. International (1967): Karun River Development, Special Progress Repot, Part 1, Hydrology and River Control. Chicago.

Lahmaeyer International (1995): Karun IV HEPP, Memorandum No.1, Report on Second mission of the Technical Review Consultant.

Lahmaeyer International (1996): Karun IV HEPP, Memorandum No. 2,Report on Second mission of the Technical Review Consultant.

LWRD/Acres, (1982): Karun II and III Development Project, Project Definition Report, Vol. 2, Hydrometeorology.

LWRD/Acres (1984): Karun II and III Development Project, Feasibility Study, Vol. 2, Hydrometeorological Studies.

Mutreja, K.N. (1986): Applied Hydrology. Teta McGraw-Hill Publishing Company Limited.

Mahab Ghods-Acers (1991): Karun III Development project, Miscellaneous Study, 05-600 in: Probable Maximum Flood Review, Revision B.

Moshanir-Lahmaeyer International (1988): Godar-e-Landar Hydroelectric Project, Vol. 2, Hydrological Report.

Moshanir-Caitec (1996): Upper Gotvand Hydroelectric Power project, Feasibility Study, appendix 8, Hydrology, Probable Maximum Precipitation.

Moshanir-Caitec (1996): Upper Gotvand Hydroelectric Power project, Feasibility Study, appendix 9, Hydrology, Probable Maximum Flood.

Sedghi, H. (1992-a): A Survey of Hydrological Studies Concerning the PMF Evaluation of Karun Basin in Iran, Water Research Center-Jihad Ministry, Tehran, Iran.

Sedghi, H. (1992-b): Hydrological Studies of Karun Basin, Design Flood Criteria, *Water* Research Center-Jihad Ministry, Tehran, Iran.

Wang, B. G. and Revell, R. W., (1983): Conservatism of Probable Maximum Flood Estimates. Journal of Hydraulic Engineering, Vol. 109, No. 3.

Wang, B. G. (1984): Estimation of Probable Maximum Precipitation, Case Studies, Journal of Hydraulic Engineering, Vol. 110, No. 10.

Wang, B. G.and Jawed, K. (1986): Transformation of Probable Maximum Precipitation to Probable Maximum Flood. Journal of Hydraulic Engineering, Vol. 112, No. 7.

RELATIVE WORTH OF THE REGRESSION ESTIMATES OF FLOODS – COMPARISON OF THE PROCEDURES

Savithri Senaratne[1], Conleth Cunnane[2]

[1] Department of Engineering Hydrology, National University of Ireland, Galway, Ireland.
savithris@oceanfree.net

[2] Department of Engineering Hydrology, National University of Ireland, Galway, Ireland.
c.cunnane@nuigalway.ie

SUMMARY

Index flood method is one particular approach in flood frequency analysis used to estimate floods at a specific site in which the regional growth curve is used in conjunction with the at-site index flood. The index flood in this case is the at-site mean annual flood, $\overline{Q}$, obtained using flood records at a near-by gauging station. However, instances arise when such data records are not available and $\overline{Q}$ have to be obtained using a regression relationship between mean annual flood and numerically measured catchment characteristics such as catchment area, slope, rainfall etc. The reliability of floods so estimated is of major concern and a number of methods were suggested in the past to estimate the standard error of the flood magnitude. This study, using three data sets, shows that the standard error calculated by these methods differ from one another and these difference are more pronounced when the standard error is high. These differences are also seen in the equivalent number of years calculated using the four different methods.

Keywords: Floods, Flood frequency, Relative worth, Regression, Index flood, Regional Growth Curve, standard error

1 INTRODUCTION

In the index flood method of flood frequency analysis, a regional growth curve along with the at-site mean annual flood is used in estimating an at-site flood Q_T of return period T. The mean annual flood, $\overline{Q}$, at ungauged site is estimated using a regression relationship between $\overline{Q}$ and catchment characteristics. It is important to know how reliable these estimated Q_T values are, relative to those estimated using data records. The reliability is assessed with respect to the standard error of the regression estimate. A number of expressions were suggested (Nash and Shaw, 1965; Hardison, 1975; Hebson and Cunnane, 1987) to estimate the standard error of the estimated flood magnitude. Moreover, Nash and Shaw (1965) defined a quantity termed equivalent length of record to describe the worth of the regression estimate of $\overline{Q}$.

The equivalent length of record (n′) is the length of record of a station when, the standard error of the at-site estimate of $\overline{Q}$ is, equal to the standard error of the regression estimate of $\overline{Q}$.

In this paper, the results of estimating the standard error of the regression estimate of $\overline{Q}$ by the different existing methods are compared over a number of data sets. The corresponding relative worth of the estimates of the $\overline{Q}$ expressed in equivalent number of years is also examined. These results are studied when both Ordinary Least Squares (OLS) method and Weighted Least Squares (WLS) method (Draper and Smith, 1981) are used in calibrating the regression model.

2 BACKGROUND

Nash-Shaw (1965) in their study of 57 British catchments for a regression relationship between $\overline{Q}$ and catchment characteristics examined the relative worth of the estimated $\overline{Q}$. This was accomplished by equating the standard error of the regression estimate to the standard error of the at-site estimate, expressed in terms of the at-site sample size. It was found that the standard error of $\overline{Q}$ estimated using a single year of data record, is less than the standard error estimated from regression

relationship between $\overline{Q}$ and catchment characteristics. Therefore it was concluded that the regression estimate is worth less than even one year of data.
The expression used for the standard error of $\ln \overline{Q}$ was that for a station at the centroid of the data space although it was generally used for any station. In the Flood studies report (NERC, 1975), standard error of $\overline{Q}$ was estimated specifically for a station at the centroid of the data space. This result confirmed the previous conclusion by Nash-Shaw (1965) that the regression estimate of $\overline{Q}$ is worth less than one year of record.
There was a doubt about the accuracy of the expression used in Nash-Shaw method as it is an asymptotic result which may not be quite valid for practical samples sizes. An alternative method is to estimate the standard error of $\overline{Q}$ experimentally in a Monte-Carlo study. Hebson and Cunnane (1987) calculated the standard error of $\overline{Q}$, obtained by a regression relationship, from a simulation experiment for selected stations representing low, medium and high Cvs. Although the high Cv station had a $\overline{Q}$ estimate with lower standard error than the other stations of interest, all three stations indicated that n′ was less than one year.
Kumar (1991) continued the work of the previous two authors examining the standard errors of $\overline{Q}$ estimated by regression models with different combinations of catchment characteristics. He observed that the standard error of $\overline{Q}$ varied with the combination of catchment characteristics in the model, which in turn resulted in improved values for n′ with some combinations of catchment characteristics. It was concluded that a specific high Cv station resulted in an equivalent length of record of 5.97 years using a regression model of $\overline{Q}$ ~ (Area, Stmfrq, SAAR and MSL).
Hardison (1971) used the same argument of equating the standard error of regression estimate to the at-site estimate of the standard error of Q_T. Thus the relative worth of the regression estimate is calculated as equivalent number of years of record as was done by previous authors. The estimator for standard error of $\overline{Q}$ used by Hardison was different from the estimators used by other authors cited above.
He assumed, $ln\overline{Q}$ at the ungauged station obtained from the regression relationship to have a Normal sampling distribution. The standard deviation of this distribution is transformed to the standard deviation of $\overline{Q}$ (standard error of $\overline{Q}$) using a table provided in his paper. This table was based on the relationship given in equation 1.

(1) $$Cv^2_{real\ space} = \exp(\sigma^2_{\log space}) - 1$$

The estimates of standard error of $\overline{Q}$, obtained using the methods suggested by the authors cited thus far are compared in the present study, and their usefulness is discussed.

3 DEFINITIONS

In the present study four estimators of the standard error of $\overline{Q}$, from a regression relationship between $\overline{Q}$ and catchment characteristics are compared. These estimators are given in Table 3-1.
In the introduction it was stated that Nash and Shaw (1965) defined a quantity termed equivalent length of record (n′) with respect to the estimated standard error of $\overline{Q}$. The expression for n′ is, The at-site standard error of $\overline{Q}$, i.e. se_{AS}, is expressed as given by equation 2 as $\overline{Q}$ is considered to have a normal sampling distribution.

(2) $$n' = \frac{\sigma_{AS}^2}{se_{reg}^2}$$

Where, se_{reg} takes the value of one of the four estimators described in Table 3-1 which is the standard error of the regression estimate of $\overline{Q}$ and σ_{AS} is the population standard deviation of the at site annual maximum data .

Table 3-1: Estimators of standard error of $\overline{Q}$.

Estimator	standard error of $\overline{Q}$	standard error of $ln\,\overline{Q}$	Remarks
se1	σ of the sampling distribution of $\overline{Q}$ obtained from the simulation experiment		Used by Hebson and Cunnane (1987)
se2	(3) $\sigma_{\overline{Q}} = \exp(\mu_z + 0.5\sigma_z^2).(\exp\sigma_z^2 - 1)^{1/2}$ where $z = ln(\overline{Q})$ and μ and σ are the mean and standard deviation. σ_z^2 is var($\ln\overline{Q}$) from equation (4).	(4) $\mathrm{var}(\ln\overline{Q}) = \sigma^2\{(x)'(\boldsymbol{X}'\boldsymbol{X})^{-1}x+1\}$ where $\boldsymbol{X}$ is the matrix of independent variables which are ln*A*, ln*S*, ln*G* etc. (A being area, S being slope...). *x* is the vector of independent variables which identify the specific station.	Used by Hardison (1971) although it is not the exact estimator as Hardison used.
ns1	(5) $\mathrm{var}(\overline{Q}) = \overline{Q}^2\,\mathrm{var}(\ln\overline{Q}))$	(6) $\mathrm{var}(\ln\overline{Q}) = \sigma^2\left[1+\frac{1}{n-1}\right]$ n is the sample size.	Used by Nash and Shaw (1965)
ns2	(7) $\mathrm{var}(\overline{Q}) = \overline{Q}^2\,\mathrm{var}(\ln\overline{Q})$	$\mathrm{var}(\ln\overline{Q}) = \sigma^2\{(x)'(\boldsymbol{X}'\boldsymbol{X})^{-1}x+1\}$ where $\boldsymbol{X}$ is the matrix of independent variables which are ln*A*, ln*S*, ln*G* etc. (A being area, S being slope...). *x* is the vector of independent variables at the specific station.	Used by Nash and Shaw (1965) although the expression for the variance of $\ln\overline{Q}$ is not for a station at the centroid as in ns1

4 EXPERIMENTAL PROCEDURE

The experimental procedure followed is as follows:

1. Calculate at-site statistics (mean, standard deviation and coefficient of skewness) and GEV parameters from the AM flood data in m sites in the region. cc_{ij}, i=1,2,...,p; j=1,2,...m, are the catchment characteristics.
2. Calibrate a relationship of the form given by equation 8.

   (8) $$\ln\overline{Q} = a\ln A + s\ln S + r\ln R + ... + \ln c$$

   where $\overline{Q}$ is the dependent variable and A, S and R are catchment characteristics corresponding to cc as noted in step 1. In estimating the parameters (a, s, r and c) of equation 8, the data of (m-1) catchments were used, site j* being excluded (j* is a selected site of immediate interest). The number of variables included depends on the significance of the coefficients *a*,*s*,...,ln*c* at 5% level.
3. Generate m random samples of size N_j, j = 1,2,...M, j≠j*.
4. Calculate sample means $\overline{Q}_j$, j = 1,2,...,M.
5. Calibrate a relation of the form given by equation 9, where the independent variables included are those found significant in step 2. In calibration of the regression model (M-1) catchment were used, j* being excluded.

   (9) $$\overline{Q} = CA^a R^r S^s$$

   Calculate the residual mean square error s_e^2.
6. Obtain the OLS regional regression model estimate of $\overline{Q}$ at the site of interest j*

   (10) $$\hat{\overline{Q}}_{j*} = A^{\hat{a}} R^{\hat{r}} S^s \exp(z)$$

   where z is a $N(0,s_e^2)$ variate where s_e^2 is the regression model variance. The noise term is added in every simulation because individual values are simulated.
7. Calculate $se(\ln \hat{\overline{Q}}_{j*})$ from equations 4 and 6 respectively with σ^2 substituted with s_e^2.
8. Calculate $se(\hat{\overline{Q}}_{j*})$ as follows:

   i) The quantity se_c using the relationship $se_c = se(\hat{\overline{Q}}_{j*}) = \hat{\overline{Q}}_{j*}.se(\ln \hat{\overline{Q}}_{j*})$ where $se(\ln \hat{\overline{Q}}_{j*})$ is obtained from step 8.

   ii) The quantity denoted se_d using the relationship $se_d = se(\hat{\overline{Q}}_{j*}) = \hat{\overline{Q}}_{j*}.se(\ln \hat{\overline{Q}}_{j*})$ where $se(\ln \hat{\overline{Q}}_{j*})$ is obtained from step 8.

   iii) The quantity denoted se_b which is $\sigma_{\overline{Q}}$ from equation 3.
9. Repeat steps 3 to 9, 1000 times.
10. Obtain the sampling distributions of the following using the samples of 1000 values.

    i) $\hat{\overline{Q}}_{j*}$ calculated in step 8.

    ii) se_b calculated in step 10.

    iii) se_c calculated in step 10.

    iv) se_d calculated in step 10.
11. Denote the final quantities obtained as follows:

    i) The standard deviation of the distribution of $\hat{\overline{Q}}_{j*}$ as se_1.

    ii) The mean of se_b as se_2.

    iii) The mean of se_c as se_{NS2}

    iv) The mean of se_d as se_{NS1}.
12. The above simulation experiment was repeated M times with the station of interest j* being selected as j (j=1,2,...M).
13. Repeat steps 7 to 13 using the WLS method to calibrate the model.

5 RESULTS AND DISCUSSION

The experiment outlined in the previous section was carried out with three different data sets. Each data set contained 30 stations. Data set 1 was from Southeast England (record lengths varied from 20 years to 80 years); Data set 2 from Southeast Ireland (record lengths varied from 12 years to 20 years) and Data set 3 from the State of Arkansas in the USA (record lengths varied from19 years to 58 years). The behaviour of the 4 estimators of standard errors of $\hat{Q}_{j^*}$ denoted se_1, se_2, se_{NS1} and se_{NS2} (these estimators were described in table 3-1) are discussed in this section.
se_1 is assumed to estimate the standard error accurately as it is the standard deviation of the sampling distribution of $\overline{Q}$, obtained from the simulation experiment. The differences between se_2, se_{NS1} and se_{NS2} relative to se_1 were examined by plotting the percent se_1, se_2, se_{NS1} and se_{NS2} against se_1. All these quantities were standardised by true $\overline{Q}$ to remove the scale effects (Senaratne, 1998). These plots of the standard errors against se_1 for all data sets are given in Figure 5-1.
It is evident from these figures that when the standard error is low all the estimators are equally efficient whereas, when the standard error is high the estimators behave differently. The variation of this difference with se_1, is consistent across the data sets.
Weighted Least Squares (WLS) method is found to be able to circumvent the heteroscedastic nature of the AM flood data, resulting in better estimates of $\overline{Q}$ (Senaratne and Cunnane, 2002). Hence, in the following section, behaviour of the different estimators is examined when the regression models of real data are calibrated using the WLS method.

5.1 Behaviour of the estimators when the WLS method is used

Figure 5-2 shows the variation of standard error when the WLS method is used to estimate the regression parameters. The same vertical scale is used as in the corresponding OLS plots in Figure 5-1 for easy comparison between the two methods. It is evident from these figures, that the difference between the four estimators are reduced.
It is apparent that the estimates se_1 and se_{NS1} become very close to each other whereas se_{NS2} and se_2 are overestimating mainly in the case of Irish and US data. This phenomenon can be explained by examining the expressions used in obtaining the standard error of $\hat{\overline{Q}}$ (se_b, se_c and se_d) of the estimators se_2, se_{NS1} and se_{NS2}.
The standard error obtained using the residual error of the regression analysis is the standard error of $ln\hat{\overline{Q}}$. In the expressions of the standard error of $\overline{Q}$, $\hat{\overline{Q}}$ is a multiplier as seen in equations 5 and 7. These estimators were termed as se_c and se_d. Since these expressions contain $\hat{\overline{Q}}$ as a multiplier, any underestimation or overestimation of $\overline{Q}$ is reflected in the standard error of $\hat{\overline{Q}}$. In the OLS method, the standard error of $ln\hat{\overline{Q}}$ was underestimated and in most cases $\hat{\overline{Q}}$ was overestimated. The net result is that the underestimation of standard error of $\hat{\overline{Q}}$ is reduced. In the WLS method $\hat{\overline{Q}}$ is efficiently estimated, in which case the overestimation of $\hat{\overline{Q}}$ tends to result in an overall overestimation of standard error of $\hat{\overline{Q}}$.
Moreover it appears that se_2 and se_{NS2} are behaving in a similar manner. The common characteristic between se_2 and se_{NS2} is taking account of the location of the station relative to the centroid of the data space in their respective expressions. Hence, the standard error obtained using se_2 and se_{NS2} result in higher values than se_{NS1} at stations further from the centroid.

5.2 Comparison of the estimated equivalent number of years from the 4 estimators

The standard error is used in calculating the equivalent number of years (n′) using equation 2, to estimate the relative worth of the regression estimate of $\overline{Q}$. Therefore it is important to examine the values of n′ estimated by the four different estimators. The variation of n′ with se_1 is shown in Figure 5-3, for Irish data using the OLS method. The corresponding figure for the WLS method is shown in Figure 5-4.
It is important to note that the estimators of n′ have the maximum difference between them when the standard error is high and this difference is reduced when the standard error is low.

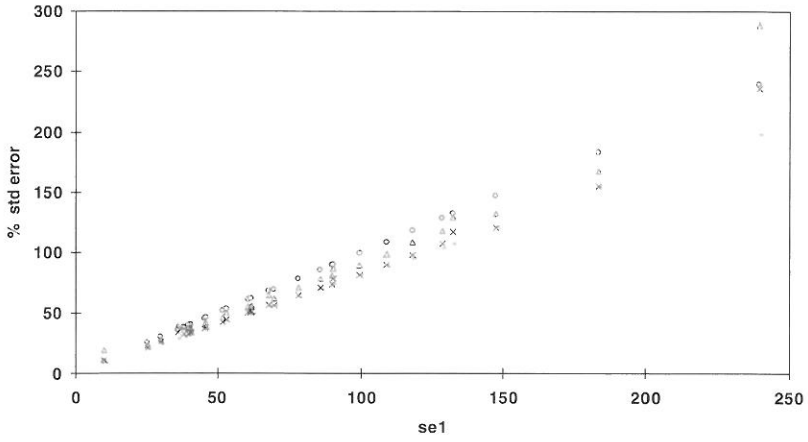

Data set 1

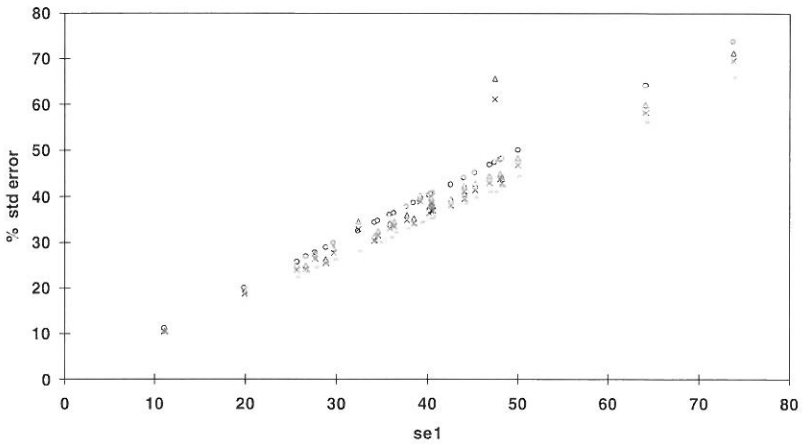

Data set 2

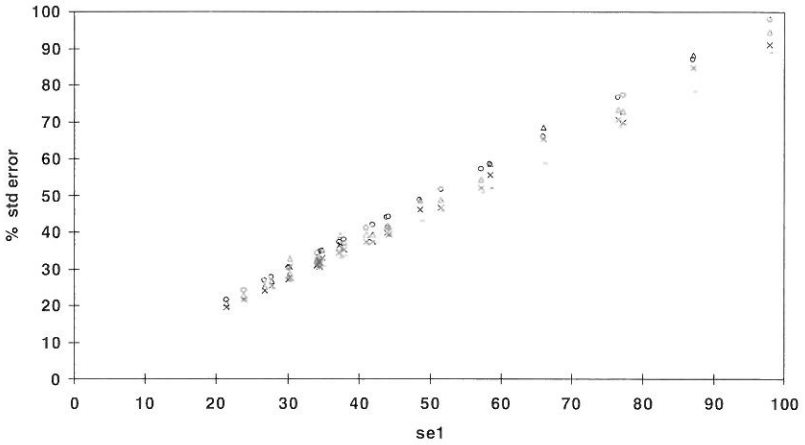

Data set 3

○ se1 △ se2 - ns1 × ns2

Figure 5-1: Variation of se_1, se_2, se_3 and se_4 with se_1 obtained using the OLS Method.

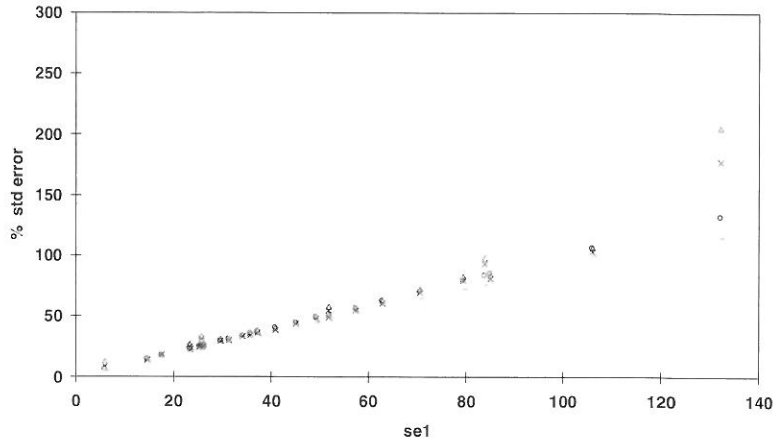

Data set 1

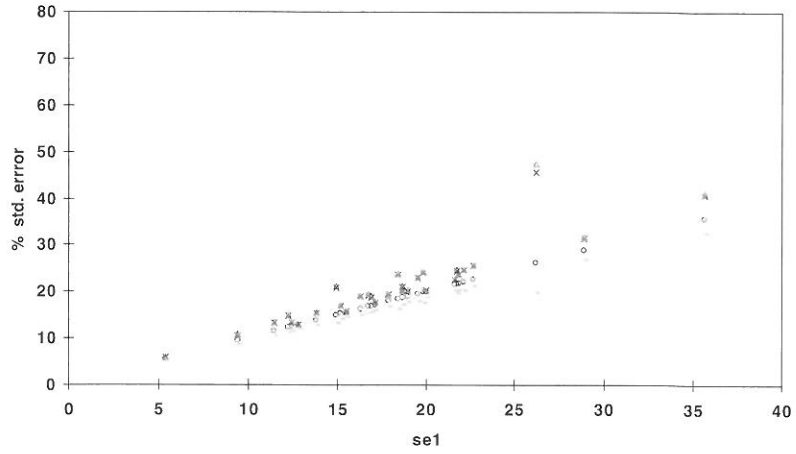

Data set 2

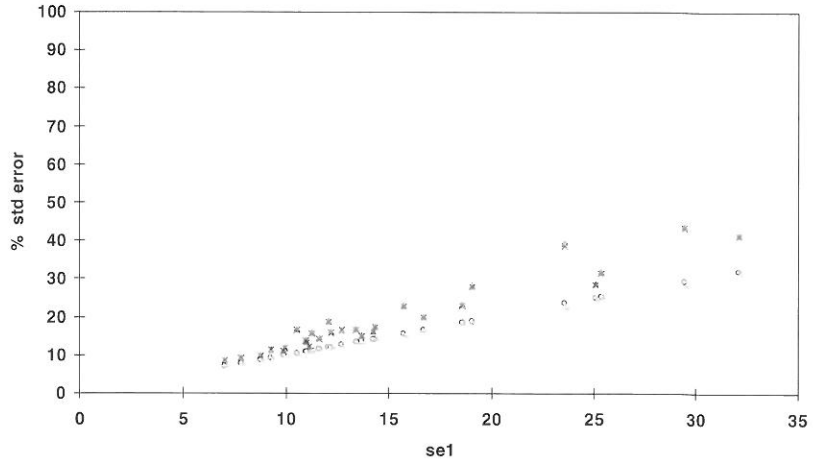

Data set 3

o se1 △ se2 ns1 × ns2

Figure 5-2: Variation of se_1, se_2, se_3 and se_4 with se_1 when the WLS method is used.

The average and the range of the differences between n'_{se1} and $n'_{..}$ for all data sets are given in Table 5-1. It is clear that se_2 is better than NS1 and NS2 when the OLS method is used. This is apparent across all three data sets. However, such a definite statement cannot be made about any estimator when the WLS method is used.

Table 5-1: The average differences between n'_{se1} and $n'_{...}$ when OLS and WLS methods are used.

	Data set 1		Data set 2		Data set 3	
	average	range	average	range	average	range
$n'_{se1}-n'_{se2}$	.14 *.22*	.54-.00 *1.6-.00*	.08 *.74*	.34-.00 *2.8-.02*	.14 *.43*	.05-.00 *1.8-.03*
$n'_{se1}-n'_{seNS1}$	.44 *.45*	1.6-.02 *1.7-.02*	.20 *.59*	.61-.02 *1.7-.02*	.44 *.07*	.01-.00 *.37-.00*
$n'_{se1}-n'_{seNS2}$	.36 *.19*	1.3-.00 *.96-.00*	.13 *.68*	.46-.00 *2.6-.00*	.36 *.42*	.09-.00 *1.8-.03*

(note- The figures in italics are those obtained using the WLS method)

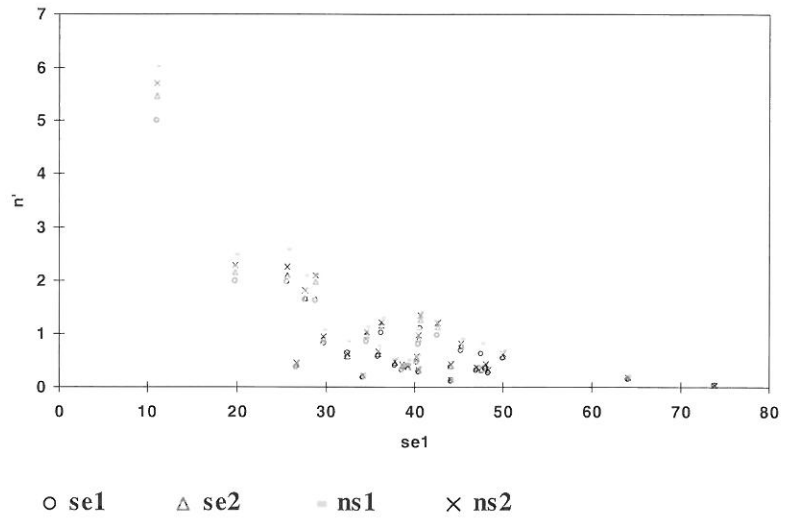

Figure 5-3: Variation of n′ with se_1 using the OLS method - Data set 2.

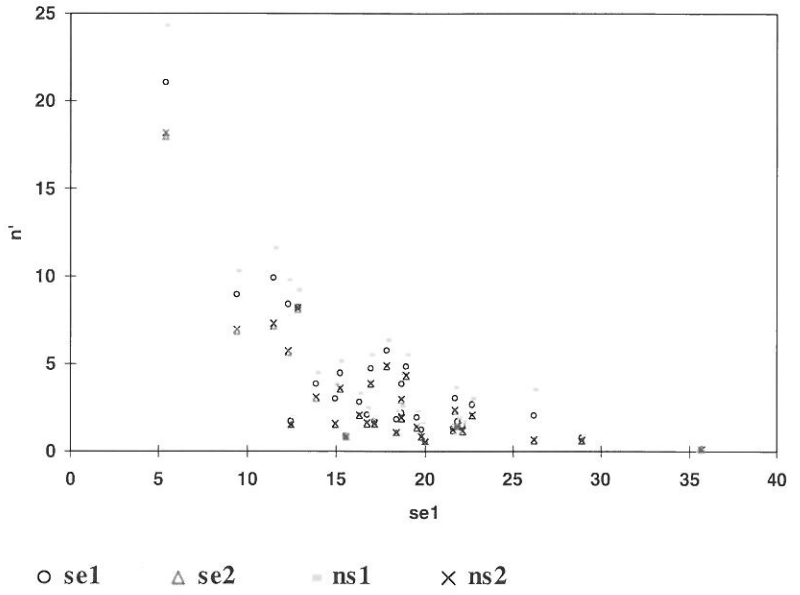

Figure 5-4: Variation of n′ with se_1 when WLS method us used - Data set 2.

6 CONCLUSIONS

The estimates of standard error produced by the four different estimators differ by little as .1% when se_1 is 10% of $\overline{Q}$ and increases up to 28% when se_1 is 240% of $\overline{Q}$ with the OLS method. Table 6-1 shows the maximum differences observed when both the OLS and WLS methods are used.

Table 6-1: The differences shown by se_2, se_{NS1} and se_{NS2} with se_1.

	OLS Method	WLS Method
se_2	15.0%	14.0%
se_{NS1}	28.0%	8.0%
se_{NS2}	9.0%	15.0%

The difference in years of the relative worth of the regression estimates of $\overline{Q}$ calculated using the four different estimators are as per Table 6-2.

Table 6-2: The differences shown by n'_{se2}, n'_{seNS1} and n'_{seNS2} with n'_{se1}.

	OLS Method	WLS Method
se_2	0.54	2.77
se_{NS1}	1.60	1.74
se_{NS2}	1.28	2.65

The four procedures differ by a maximum of 1.60 years in OLS method and 2.77 years in WLS method, when the standard error of the estimated $\overline{Q}$ is high. Therefore the estimators should be used with caution when the estimated standard error of $\overline{Q}$ is high, and are reliable when the estimated standard error of $\overline{Q}$ is low.
The WLS method leads to better estimation of parameters in the regression relationship than OLS method and should be used whenever possible.

REFERENCES

Draper, N. R. and Smith, H. (1981): Applied regression analysis. B John Wiley & Sons., New York.

NERC (1975): Flood Studies Report, Vol1, Chapter 4, National Environment Research Council, UK..

Hardison, C.H. (1971): Prediction error of regression estimates of streamflow characteristics at un-gauged sites. U.S. geological survey professional paper 750-C, C236-C288.

Hebson, C.S. and Cunnane, C. (1987): Assessment of use of At-site and Regional flood Data for Flood Frequency Estimation. Proc. Int. Sympos. On Flood Frequency and Risk Analysis, Baton Rouge, USA. Ed. V.P. Singh. Ridel Publishing. 433-448.

Kumar, V. (1988): Some simulation comparison of flood frequency estimation methods. M.Sc. Thesis, Dept. of Engineering Hydrology, UCG, Ireland.

Nash, J.E. and Shaw, B.L. (1965): Flood frequency as a function of catchment characteristics. Inst. of Civil Engineers, Symp. On River Flood Hydrology (Published 1966), UK. 115-136.

Senaratne, S. and Cunnane, C. (2002): Weighted Least Squares Method –Improved estimates when Index Flood Method is used with annual maximum floods. IAHS Publ. 271,

Senaratne, S. (1998): Flood Frequency Analysis in Ungauged Catchments, PhD dissertation, National University of Ireland, Galway, Ireland.

RELEVANCE OF THE SEASONALITY OF PRECIPITATION AND FLOODS

Andreas Steinbrich, Stefan Uhlenbrook, Sabriye Sancak, Christian Leibundgut

Institute of Hydrology University of Freiburg, Fahnenbergplatz, D-79098 Freiburg, Germany,
Andreas.Steinbrich@hydrology.uni-freiburg.de

SUMMARY

Directional statistics were used to investigate the seasonality of precipitation and floods of different magnitudes for 215 catchments (10 to 954 km^2) in southwest Germany. Distinct patterns of seasonality of floods and precipitation were found. In general, the seasonality of precipitation was less pronounced then the seasonality of floods, and in most catchments floods occurred not at the same time as the extreme rainfall. A change of the seasonality of floods from west to east was found for the investigated area, which might be due to the change from more oceanic to more continental climate. However, this is superimposed by the influence of the topography, what is the first order control of the seasonality of floods. For more extreme floods a more distinct spatial seasonality pattern was observed and more catchments showed summer seasonality. Summer seasonality is mainly caused by convective storms with limited spatial extent and could be found only for small catchments. Winter seasonality is often the result of advective precipitation events that might be very expanded and more frequent in winter times. As a consequence all catchments with an area larger than 450 km^2 showed winter seasonality.
It could be shown, that homogenous regions are more distinct with increasing extremity of the flood events. This reveals the suitability of the seasonality to define homogenous regions for flood frequency analysis because these regions are defined by the same dominating processes controlling especially extreme flood events.

Keywords: Seasonality, floods, precipitation, recurrence intervals, regionalization, Southwest Germany

1 INTRODUCTION

In many regions floods do not appear equally distributed all over the year and the probability of floods is more distinct for different seasons (Magilligan & Graber, 1996; Burn, 1997; Black & Werrity, 1997; Blöschl et al., 1999; Haupt et al., 1999; Merz et al., 1999; Uhlenbrook et al., 2001). This fact is relevant for estimating the recurrence interval of floods. The probability that a given flood level is exceeded might differ substantially for different seasons. Furthermore the seasonal behavior of precipitation and runoff in a catchment might give information about the major processes generating floods in these catchments (Blöschl & Sivapalan, 1997). As the seasonality is linked to the meteorological and hydrological processes generating floods, it provides valuable information for identifying regions that are homogenous in their flood frequency behaviour (Magilligan & Graber, 1996; Black & Werrity, 1997; Piock-Ellena et al., 1999; Haupt et al., 1999).
In a previous investigation the significance of meteorological input and physiographic basin properties for generating extreme floods, defined as floods with a recurrence interval greater than 10 years, were investigated for 29 mesoscale catchments in southwest Germany (Uhlenbrook et al., 2002). Precipitation was found to be the most significant factor whereas digitally available physiographic characteristics were less significant. A distinct seasonality for the occurrence of extreme floods and a less strong seasonality of precipitation events were found. In addition, different recurrence intervals for precipitation events were calculated for different seasons.
The present study focuses on the distribution of seasonality of floods and precipitation in the southwest of Germany. Therefore, an enlarged data set of 215 catchments was investigated in order to gather more dense information about the seasonality of floods in this area and to learn which processes are the major controls of the peculiarity and the timing of flood seasonality. An additional objective is to examine the relationship between the extremity and the seasonality of observed floods of different magnitude.

2 THE INVESTIGATION AREA

The state of Baden-Württemberg is located in the southwest of Germany, surrounded by France, Switzerland, Bavaria and Hessen (Figure 2-1). The relief is dominated by the mountain ranges Black Forest, Schwäbische Alb and Odenwald. South of Baden-Württemberg the Alps build a high barrier that is aligned in direction west to east. Between the mountain ranges lower areas with little relief are situated.

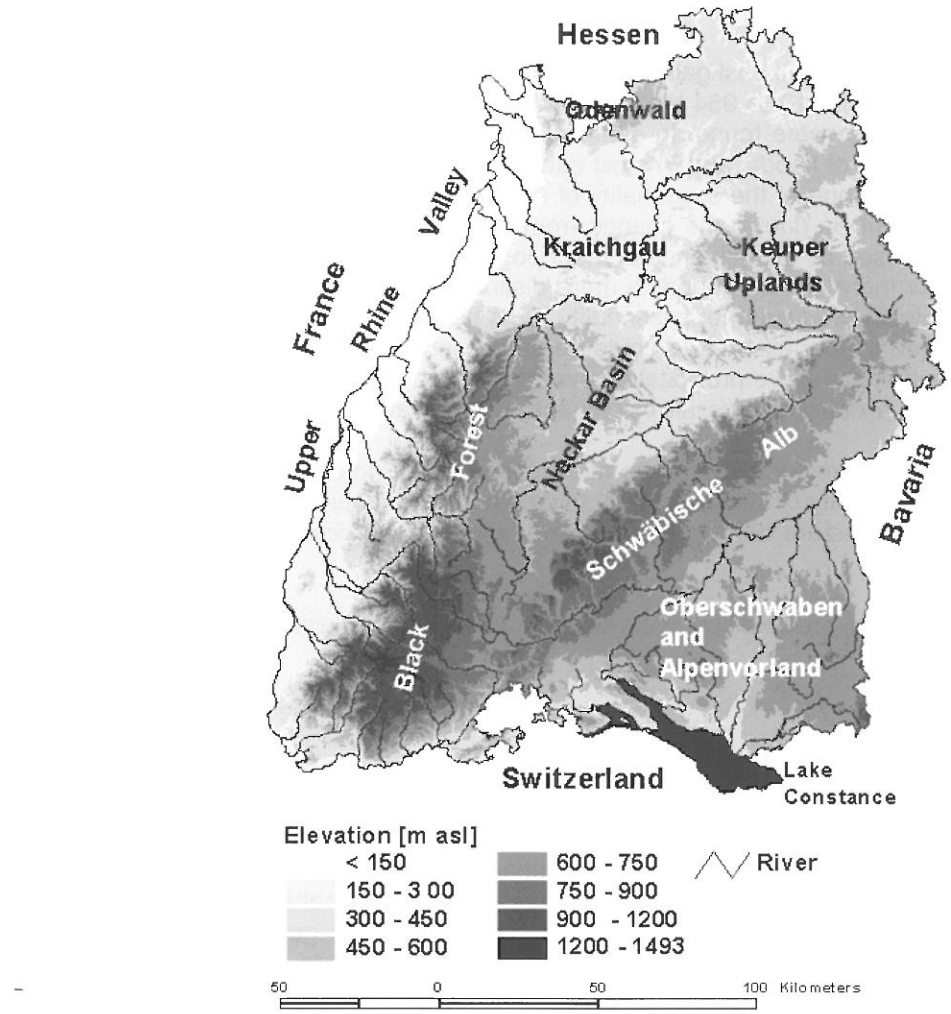

Figure 2-1: The state of Baden-Württemberg and its main landscape units.

3 DATA AND METHODS

3.1 Data base

Daily runoff data of 215 gauging stations in Baden-Württemberg were used to investigate the seasonality of floods. The minimum and maximum record length was 20 and 84 years, respectively. The a priori assumption of trend free seasonality is confirmed by investigations of Eisele et al. (2001). Therefore, no standard period was established because that would have decreased the number of test sites. The catchment areas varied from 10 to 954 km^2.
Daily catchment precipitation was calculated from a 7 x 7 km^2 grid of regionalized precipitation data (DWD, 1999) for the period 1931–1997 in order to investigate the seasonality of the daily rainfall. It has to be noted, that only falling precipitation was considered and no snowmelt model was applied. Measures of catchment altitude and slope were calculated from a digital elevation model with a cell size of 50 x 50 m^2.

3.2 Seasonality of precipitation and floods

The seasonality of precipitation and floods were investigated applying circular statistics modified after Magilligan & Graber (1996) (Figure 3-1). The ratio of actual vector length and maximum possible vector length is a measure for the peculiarity of seasonality. The direction of the resultant vector represents the mean time of the year when the floods occured. The closer the ratio of actual vector length and maximum possible vector length to one, the more events occurred in the same season. A ratio of one would indicate, that all events happened on the same day in the respective years. In the following 'vector length' will be used for the ratio of actual vector length and maximum possible vector length.
The investigation was done for different extents of extremity. As thresholds the values of the 95% 99%, 99.1%, 99.2%, 99.3%, 99.4%, 99.5%, 99.6% and 99.7% quantils of the distribution of daily records for discharge and precipitation were determined, respectively. At the 99.7%-threshold eight catchments had less then five flood events. Thus, this was the highest threshold. A comparison of the 99.7%-thresholds with estimated recurrence intervals (calculated for several basins of different sizes and with different available record lengths) showed that this threshold equals a recurrence interval of about two years. The recurrence interval of the 95%-threshold corresponds roughly to the one year flood. High discharge values that were connected to other events were excluded from the investigation.

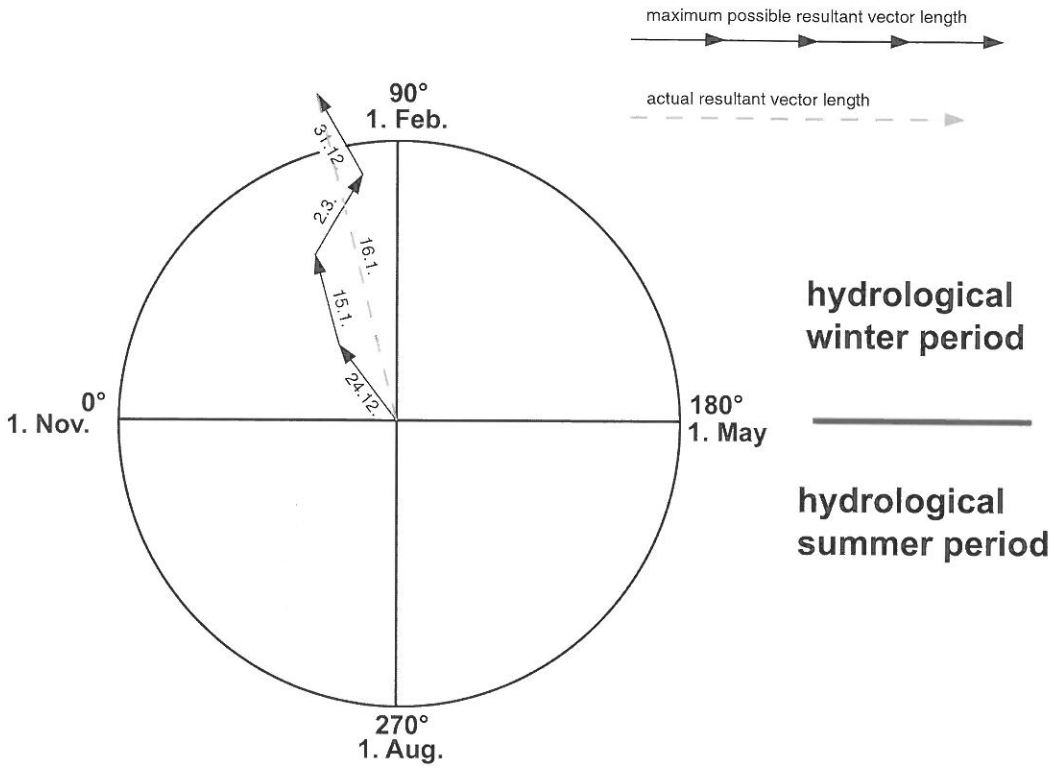

Figure 3-1: Visualizing the seasonality of flood events and precipitation events by estimation of the resultant mean vector by adding together the individual vectors for each flood event. The direction of the arrow of an event represents the date of the flood, the arrow length of the resultant vector indicate the peculiarity of seasonality.

The peculiarity and timing of the seasonality of floods was also determined using the maximum of the regime of normalized mean monthly highest discharge values (according to Pardé, 1947). In order to compare the highest mean monthly values with the seasonality vectors of floods, vectors were calculated for the highest mean monthly discharge values. The length of each vector was determined by the normalized mean monthly highest value and the direction by the 15st of the respective month.

4 RESULTS AND DISCUSSION

4.1 Visualization of the seasonality and statistical investigations

The seasonality vectors of floods show a distinct pattern in direction (date of occurrence) and length (peculiarity) for the southwest of Germany (Figure 4-1-a). The seasonality of the daily catchment precipitation (Figure 4-1-b) is generally less strong and more homogeneous than the seasonality of floods. Similar differences between the patterns of seasonality for precipitation and floods were found by Merz et al. (1999) for Austria. This seems to be caused by the influence of differing catchment storage characteristics (i.e. snow storage, interplay of soil and vegetation storage, or artificial reservoirs). The majority of catchments are characterized by a summer seasonality of precipitation, but most floods occurred in the winter season. Uhlenbrook et al. (2001) showed, that during summer times, when the catchments water storage filling is low, even extreme rainfall events could lead to only moderate floods. In winter season with filled reservoirs and sometimes snow coverage even moderate rainfall events were able to cause extreme floods. Therefore, regions with summer seasonality of precipitation and winter seasonality of floods can occur. In regions with winter seasonality of precipitation, flood seasonality falls into the winter season too, observed for the Black Forest and the Odenwald. These are the only regions, where winter seasonality of precipitation was found. In both regions the flood occurred mainly in the early winter, while for the rest of the investigated area most floods occurred in late winter or early spring. Floods in the hydrological summer period were found only for a few catchments.
In the regions of the Black Forest and the Odenwald is a direct link between the seasonality of precipitation and the seasonality of floods, while this is not the case for the rest of the area. This is also corroborated by the results of a regression analysis. No correlation was found between length or direction of the seasonality vectors of floods and precipitation. This is caused by the heterogeneity of the over all relation between precipitation seasonality and flood seasonality.

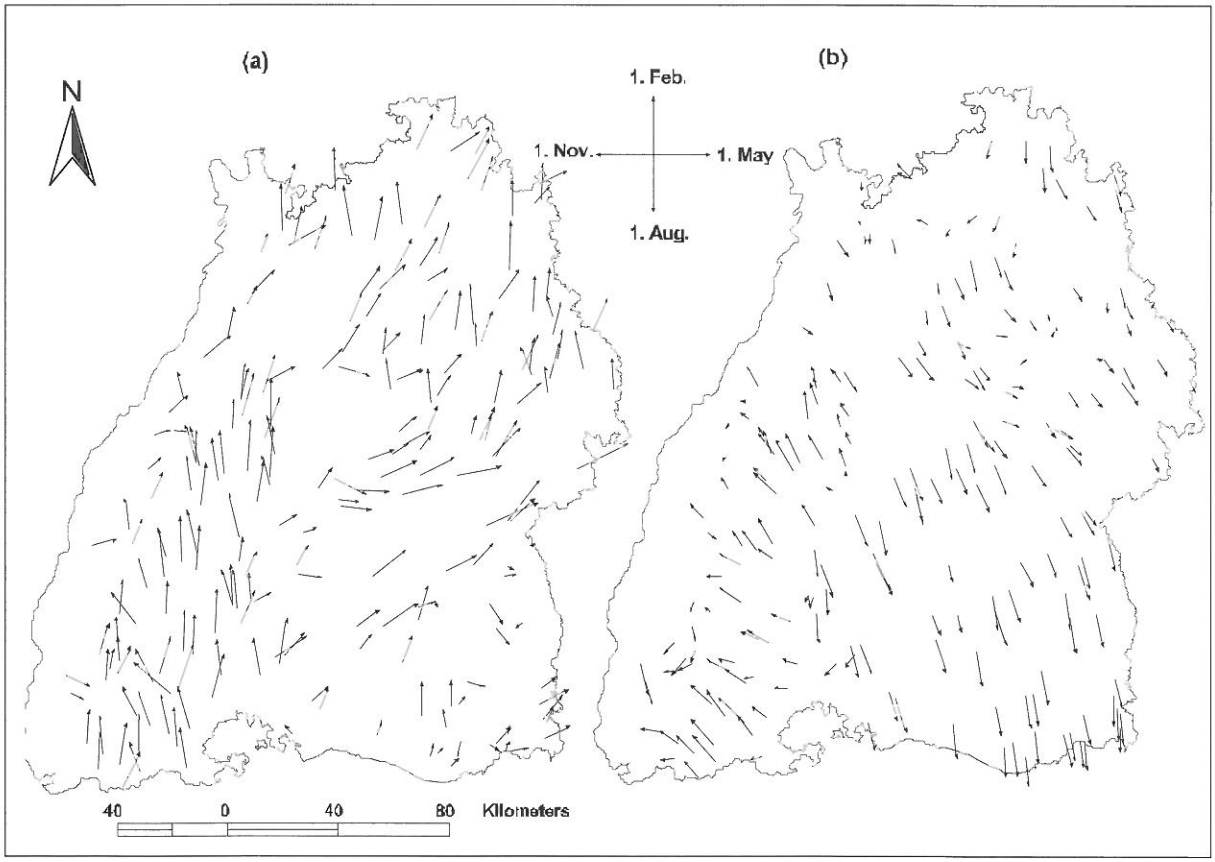

Figure 4-1: Seasonality of floods (a) and precipitation (b) of events that exceed the 99.6%-threshold (cf. Figure 3-1).

Between the seasonality of the normalized mean monthly highest discharge values and the seasonality of floods a linear relationship could be found (Figure 4-2). The seasonality of floods can be expressed partly by the normalized highest mean monthly discharge values (r = 0.7). Nevertheless, there are catchments where flood seasonality differs from the seasonality of highest mean monthly discharge (Figure 4-2).

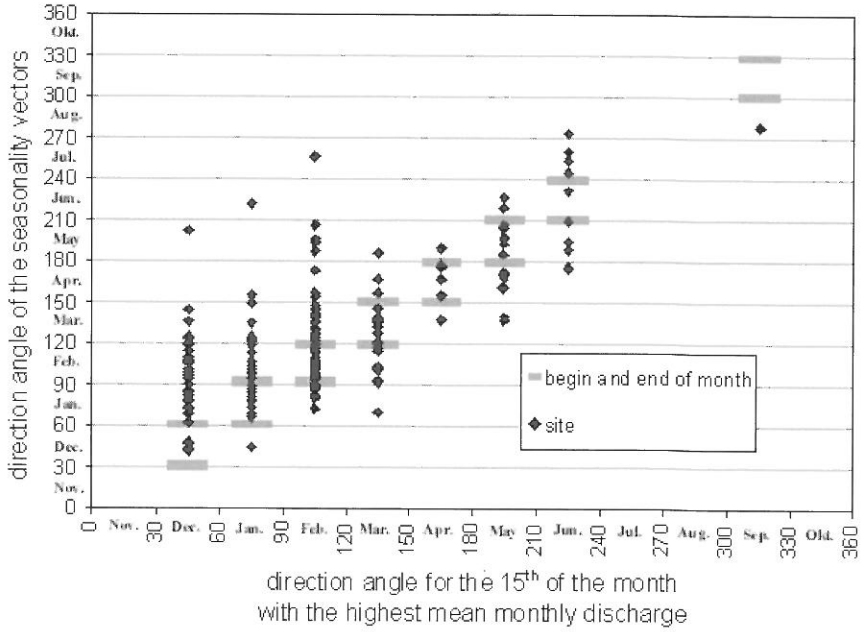

Figure 4-2: Relationship between the seasonality of floods (99.6%-threshold) and the maximum of the regime of normalized mean monthly highest discharge values.

The peculiarity of seasonality (expressed by the length of vectors) and the date of occurrence (expressed by the direction of vectors) of floods were investigated in relation to an increasing extremity for events exceeding the 95%-threshold (Figure 4-3-a) up to events exceeding the 99.7%-threshold (Figure 4-3-b). It can be seen, that with increasing extremity of floods more catchments with seasonality vectors longer then 0.7 occurred. To test if the number of events in the data sets for different thresholds affects the length of vectors, the data sets of all events exceeding the 95%-threshold was divided randomly in subsets of different sizes. Therefore, a large subset with 100 events was investigated, what is close to the mean event number for the 95%-threshold, down to the smallest subset with five events, what is less then the mean event number for the 99.7%-threshold. New vector lengths were calculated for each subset. In deed it was found, that the number of events influences the mean vector lengths. With decreasing number of events, the mean vector length was increasing. Consequently, the increasing length of vectors is not only a result of increasing extremity but also a consequence of decreasing number of events.
In addition Figure 4-3 shows that for more extreme events the temporal variability of seasonality is higher than for less extreme events. More catchments with summer seasonality of floods were observed with increasing extremity of the events. When estimating the seasonality of events that exceed the 95%-threshold, it was found that nearly the whole area is dominated by winter seasonality. Using only the events exceeding the 99.7%-threshold a considerable number of catchments with summer seasonality became obvious.
The relatively wide range of catchment area sizes in the data set allowed to examine the influence of scale on flood seasonality. There was no catchment with an area greater than 450 km^2 with summer seasonality (Figure 4-4-a). This was also found including less extreme events. For the catchments that are smaller then 450 km^2, floods occurred nearly all over the year. Therefore, no statistical correlation between catchment area and angle of seasonality vector could be found.
A similar situation was found by plotting the catchment sizes versus the length of seasonality vectors for events exceeding the 99.7%-threshold (Figure 4-4-b). There is a wide variability of seasonality of catchments with an area less then 450 km^2. With two exceptions all catchments greater than 450 km^2 are characterized by strong seasonality. However, this tendency was not found for the set of events exceeding the less extreme 95%-threshold. The two catchments that have no distinct seasonality but are much larger then 450 km^2 are situated in very southeast of the investigated area. Here a region

with weak seasonality was found (Figure 4-1-a). The wide variation of vector length among the smaller catchments hinder an over all significant correlation between catchment size and peculiarity of seasonality.

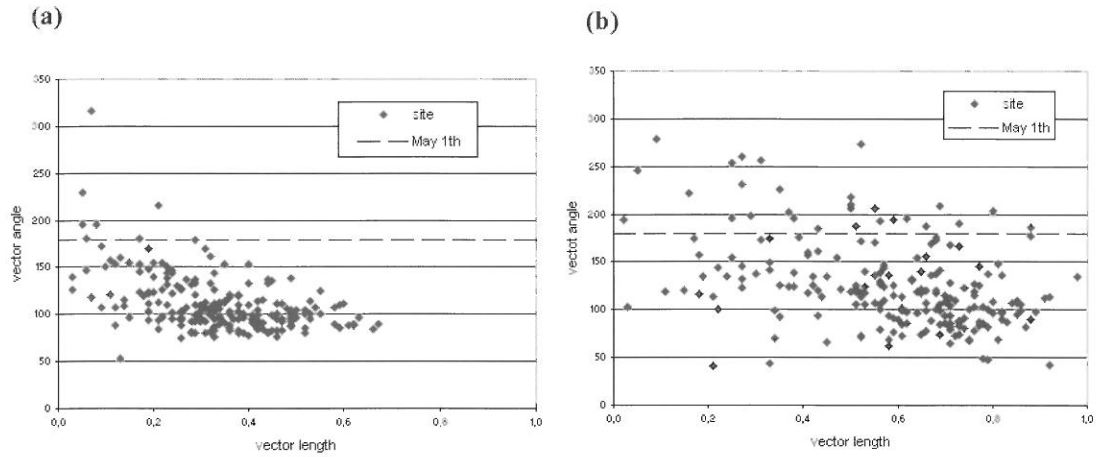

Figure 4-3: (a) Mean vector angle versus mean vector length for events exceeding the 95%-threshold and (b) for events exceeding the 99.7%-threshold.

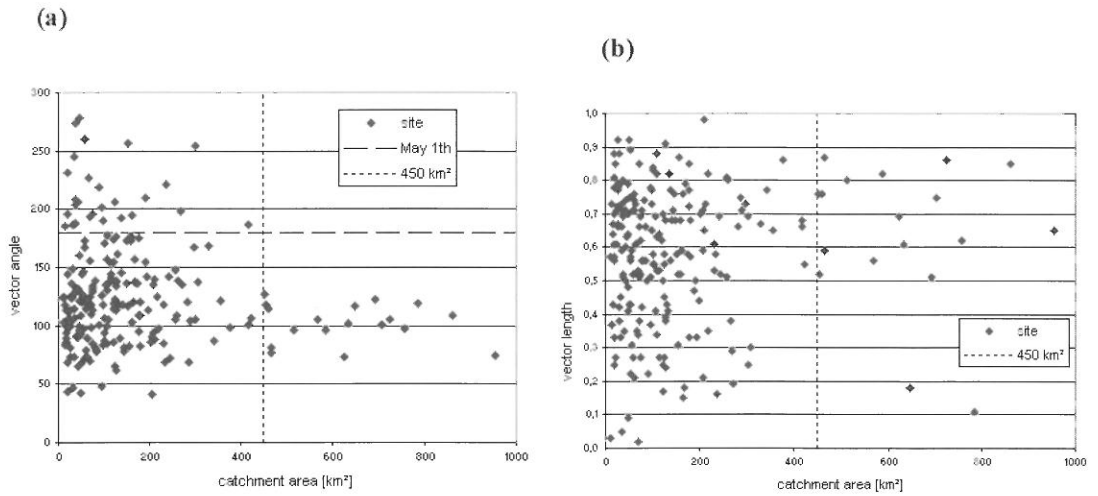

Figure 4-4: (a) Influence of catchment size on the angle of the seasonality vectors and (b) on the length of the seasonality vectors for flood events exceeding the 99.7-threshold.

Only weak correlations were found between the altitude above sea level (r = -0.25) or the mean slope (r = -0.23) and the mean timing of floods (seasonality vector angle). No correlation was found between measures of altitude or slope and the seasonality vector length. The differences of altitudes in Baden-Württemberg are not as high, as for instance in Austria or Switzerland where a more pronounced influence of the altitude on the seasonality was found (Piock-Ellena et al., 2000). No correlation was also found between geographic position and the length or direction of seasonality vectors.

4.2 Regions with similar seasonality

In a first step different attempts were made to identify homogenous seasonality regions, using several cluster analyses and different sets of variables. The results were not satisfying, because most clusters did not form geographic regions. In a next step, an alternative approach was made to extract homogeneous regions. As a threshold to separate the data the angle of the seasonality vector to May 1st was chosen, because this date separates the hydrological winter from the hydrological summer season. To separate the data with respect to the peculiarity of seasonality two additional thresholds were used. The first is the vector length value of 0.4, assuming that a shorter vector length indicates no distinct seasonality. As second threshold value the vector length of 0.7 was used to identify catchments

with a strong seasonality, as they have longer vector lengths. If that value is exceeded, all flood events were observed within three months. The chosen thresholds separate the data into the three classes with "weak or no seasonality", "moderate seasonality" and "strong seasonality".
The flood events that exceed the 99.6%-threshold were used for defining homogenous regions for two reasons. First, it was found that with increasing extremity of flood events the spatial seasonality pattern becomes more obvious. By using the 95%-threshold only weak and moderate winter seasonality was found for most of the catchments. With every step to more extreme thresholds the regional pattern, as shown in Figure 6-4, became more distinct. Second, the number of events that defines the seasonality should be as height as possible to be representative. The data set of floods that exceed the 99.6%-threshold offers a sufficient number of events for almost all sites (Figure 4-5).

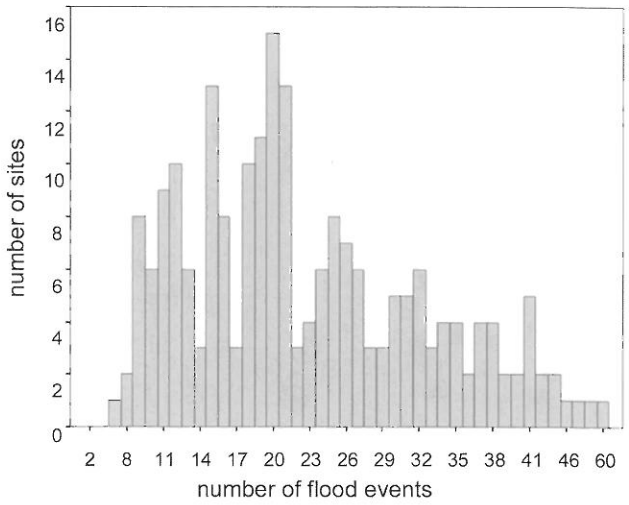

Figure 4-5: Distribution of the frequency of flood events exceeding the 99.6%-threshold.

In Figure 4-6 the result of the grouping procedure is shown. It can be seen, that there is a correlation between the topography (Figure 2-1) and seasonality. In general, homogenous seasonality regions in the investigated area are not as well separated as in the more mountainous countries Austria and Switzerland (Piock-Ellena et al., 2000), what confirms the effect of the relief on the seasonality. Strong winter seasonality appears in catchments that are situated at the east and south slopes of the mountain ranges. There are two catchments (in Figure 4-6 marked by an arrow) with strong winter seasonality that on the first sight seem to be located at the northwest slopes of the Schwäbische Alb. However, the two catchments divide the ridge of the Schwäbische Alb parallel to its alignment into two ridges and therefore are situated at the southeast slope of one of the two ridges, respectively.
The catchments situated in the Black Forest and Odenwald are characterized by moderate or strong winter seasonality; most flood events occurred in the early winter (see Figure 4-1-a). It can be assumed that the southwest circulation, what occurs while west cyclonic and southern west circulation patterns, plays a key role of the early winter seasonality in this regions. It often carries moist and warm air masses into that regions during that time of the year and leads to snow melt accompanying intense rainfall.
The influence of the southwest circulation decreases from west to east and in the lee of mountain ranges. The catchments located at the Schwäbische Alb that are shielded from the southwest circulation by the Black Forest are characterized by late winter seasonality (Figure 4-1-a). The frequent appearance of floods in March and April here seems to be the result of snowmelt at the end of winter.
The Keuper Upland and the area east of the Odenwald show moderate winter seasonality. The flood appearance varies from catchment to catchment from February to March. Both, snowmelt at the end of winter and the influence of the southwest circulation might play a key role here.
The Kraichgau, Neckar Basin as well as Oberschwaben and Alpenvorland are very heterogeneous. A reason might be that the topography is very smooth in theses regions and therefore, a mix of various factors are influencing the seasonality. A summer seasonality of precipitation (Figure 4-1-b) and an influence of snowmelt in late winter might balance each other widely.

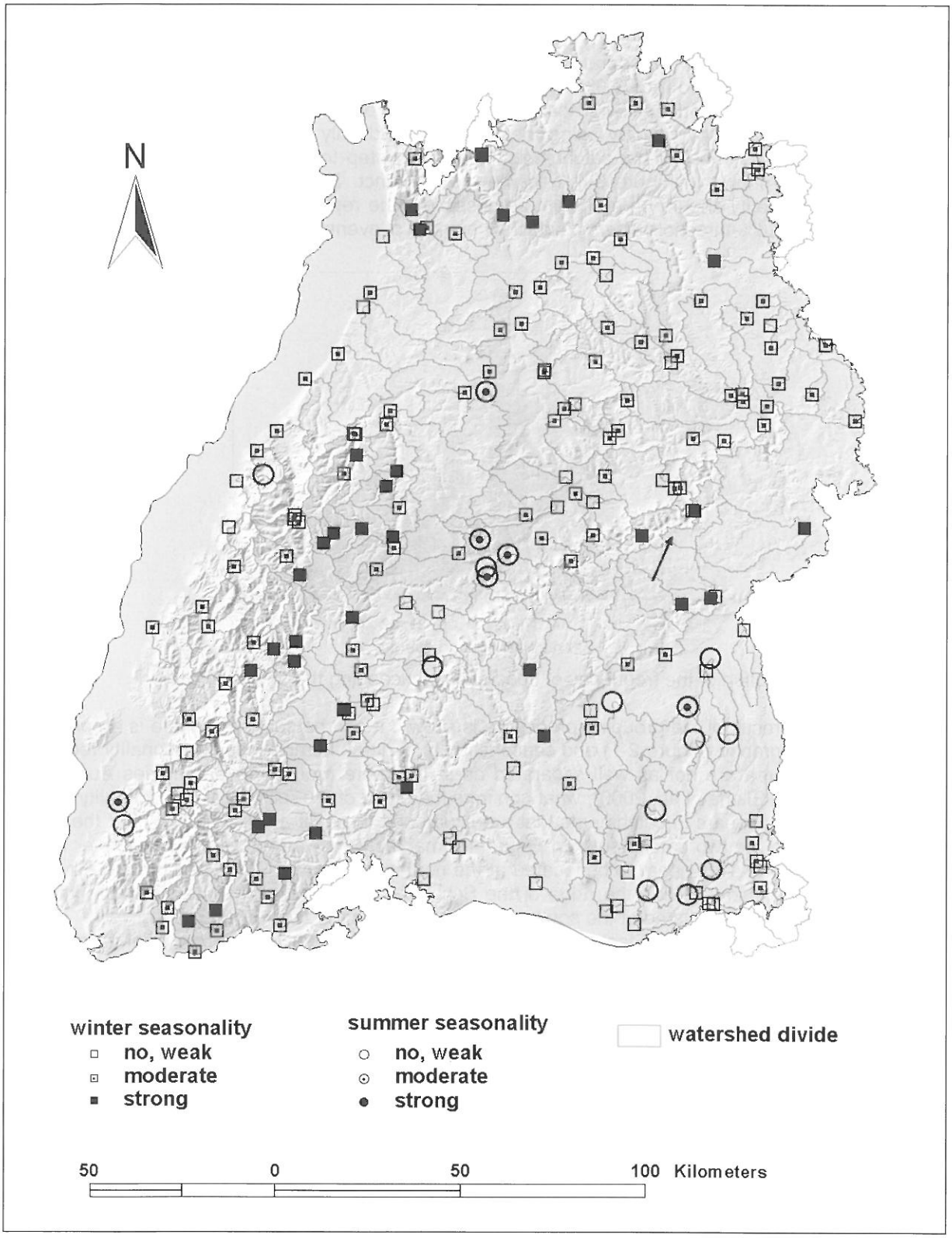

Figure 4-6: Grouping of the catchments due to the seasonality of floods that exceed the 99.6%-threshold.

Summer seasonality is found only in small catchments (Figure 4-4-a) located in the regions of Oberschwaben and Alpenvorland, Neckar Basin, Kraichgau and the steep west slopes of the Black Forest. It is supposed, that convective rainfall events cause the most extreme floods in these catchments. The reason why only small catchments show summer seasonality is the limited spatial extent of convective cells. The location of these catchments is also suitable to confirm the assumption that convective rainfall events are the main flood producing processes in these catchments, because they are located

in regions where the topography support the formation of convective cells. The steep west orientated slopes of the Black Forest can cause considerable differences of air temperature compared with the surrounding areas when in summer afternoons the sun shines with an optimal angle for convection. The five catchments with summer seasonality of floods in the Neckar Basin (in the center of Baden-Württemberg) are located at or close to the steep west slope of the Schwäbische Alb. The catchments in Oberschwaben and Alpenvorland are close to the edge of the Alps, where convective rainfall events occur frequently. From Figure 4-1-b it can be seen, that the Kraichgau, Neckar Basin as well as Oberschwaben and Alpenvorland are characterized by a considerably seasonality of rainfall, and the most extreme daily rainfall events occurred in June. The two catchments with catchments size greater than 450 km^2 and weak seasonality (Figure 4-4-b) are situated in the Oberschwaben and Alpenvorland region, where convective rainfall events are likely an important factor of flood generation. However, such events affect only small areas, thus they would not be able to cause summer seasonality for that large catchments but are effective enough to hinder winter seasonality.

5 CONCLUDING REMARKS

- The seasonality of floods is more distinct then the seasonality of precipitation and shows a more heterogeneous spatial pattern, what reveals the influence of differing catchment characteristics on the seasonality.
- For most catchments differ the time when the most extreme floods occurred considerably from the time, when most extreme precipitation events were observed. This can be explained by different fillings of the hydrological reservoirs of the catchments in winter and summer season.
- The topography in interaction with typical atmospheric circulation patterns in southwest Germany is the most important controls on the seasonality of floods.
- There was no statistical significant effect of the geographic position of the catchments on seasonality. However, a shift in the temporal occurrence of floods from early winter to late winter from west to east became obvious. This suggests an influence of the more oceanic to the more continental climate type. But this influence is superimposed by the stronger influence of the topography.
- Larger catchments (> 450 km^2) are all characterized by winter seasonality and stronger seasonalities. Here the most important flood generating processes are advective rains and snow melt events, that are more frequent in the winter season. Convective summer events usually are not able to cause extreme floods in larger catchments, due to their limited spatial extent. They affect in particular small catchments, where the only summer seasonality of floods could be observed.
- The increasing clearness of seasonality patterns with increasing extremity of floods reveals the suitability of seasonality in applied hydrological studies, e.g. to define homogenous regions for flood frequency analysis.
- The strong influence of the west cyclonic and southern west circulation patterns on winter seasonality of floods in the Black Forest and Odenwald is of particular interest in relation to climate change. It was shown by Caspary & Bardossy (1995), that the frequency of the circulation type west cyclonic in winter season is increasing since the early seventies in southwest Germany. According to Caspary & Bardossy (1995) this is a reason to fear an increased flooding risk in the winter season in these regions.

Future investigations will concentrate to determine the influence of snow on the seasonality of floods. In current project of the German Weather Survey the differentiation of fallen precipitation and snowmelt is examined for the whole area of Baden-Württemberg on a daily base for the last decades. This will be the base to gain further insights into the importance of snow melt for flood generation and its spatial and temporal varying significance.

6 ACKNOWLEDGEMENTS

This study was partly sponsored by the KLIWA-Project A 2.1.6 and the BWPLUS-Project BWC 99011. The following authorities made data records available: Institution for Environmental Protection Baden-Württemberg (Landesanstalt für Umweltschutz Baden-Württemberg, LfU) and the German Weather Survey (Deutscher Wetterdient Offenbach).

7 REFERENCES

Black, A.R., Werritty, A. (1997): Seasonality of flooding: a case study of North Britain. Journal of Hydrology 195, 1-25. Amsterdam.

Blöschl, G., Sivapalan M. (1997): Process controls on regional flood frequency: Coefficient of variation and basin scale. Water Resources Research 12 2967-2980. Washington DC.

Blöschl, G. et al. (1999): Prozessorientierte Regionalisierung von Hochwässern. Schriftenreihe des Fachgebietes Wasserbau und Wasserwirtschaft der Universität Kaiserslautern.

Burn, D.H. (1997): Catchment similarity for regional flood frequency analysis using seasonality measures. Journal of Hydrology 202, 212-230. Amsterdam.

Caspary, H.J., Bardossy, A. (1995): Markieren die Winterhochwasser 1190 und 1993 das Ende der Stationarität in der Hochwasserhydrologie infolge von Klimaänderungen? Wasser & Boden 47, Jahrgang 3/95. Berlin.

DWD (1999): Bereitstellung von langen Reihen interpolierter Gitterpunkte des Niederschlags (Tageswerte) mit Hilfe des Verfahrens BONIE für Baden-Württemberg. Bericht des KLIWA-Projektes A1.1.1/BW. Berlin.

Eisele, M. et al. (2001): Einzugsgebietsbezogene Bewertung der Abfluss- und Stoffdynamik als Grundlage eines Bewertungsverfahrens „Hydrologische Güte" zum operationellen Einsatz im nachhaltigen Flussgebietsmanagement. Abschlussbericht des Projektvorhabens BWC 99011, Umweltforschungszentrum Karlsruhe, Projektträger BWPLUS, Institute of Hydrology, University of Freiburg, Germany.

Haupt, R. et al. (1999): Saisonalität und Regionalisierung von Hochwaserscheiteldurchflüssen in Mecklenburg-Vorpommern. Wasserwirtschaft 89 (1999) 7-8, 388-394. Wiesbaden.

Magilligan, F.J., Graber, B.E. (1996): Hydroclimatological and geomorphic controls on the timing and spatial variability of floods in New England, USA. Journal of Hydrology 178, 159-180. Amsterdam.

Merz, R. et al. (1999): Seasonality of flood processes in Austria. In: IAHS Publ. No. 255, 273-278. Wallingford.

Pardé, M. (1947): Fleuves et Rivieres, sec. Edn. Colin, Paris.

Piock-Ellena et al. (1998): On the regionalisation of flood frequencies-Catchment similarity based on seasonality measures. Paper submitted to Theme E.d of the 28th Biennial IAHR Congress, Graz, Austria.

Piock-Ellena et al. (2000): Saisonalitätsanalyse als Basis für die Regionalisierung von Hochwässern. Wasser, Energie, Luft – eau, enerie, air 92. Jahrgang, 2000, Heft 1/2 Baden, Schweiz.

Uhlenbrook S. et al. (2001): Regional Analysis of the Generation of Extreme Floods. IAHS Publication, in press. Amsterdam.